EFFECTS OF MDGA2 REDUCTION ON SYNAPTIC DEVELOPMENT AND DEPRESSION IN *MUS MUSCULUS*: AN AUTISM SPECTRUM DISORDER MODEL

Katherine Andrec

A THESIS SUBMITTED TO THE FACULTY OF GRADUATE STUDIES IN PARTIAL FULFILLMENT OF THE REQUIREMENTS FOR THE DEGREE OF MASTER OF SCIENCE

GRADUATE PROGRAM IN BIOLOGY

YORK UNIVERSITY

TORONTO, ONTARIO

JANUARY 2026

Abstract

MDGA2, an autism-linked synapse organizer, restricts excitatory synaptogenesis by inhibiting neurexin-neuroligin adhesion complexes and BDNF/TrkB signaling. *Mdga2*$^{+/-}$ mice, modeling autism-associated mutations, show increased excitatory synapse density and hyperexcitation in adulthood, resulting in altered hippocampus-dependent cognition and plasticity. Despite the critical role of synapse organizers in development, the effects of Mdga2 reduction on synaptogenesis, synaptic pruning, and long-term depression (LTD) remain unclear. To address this gap, this study investigated synaptic weakening via LTD induction, spine development across postnatal stages via Golgi-Cox staining, and proteomic alterations in the hippocampus of *Mdga2*$^{+/-}$ mice. Results reveal that Mdga2 reduction induces premature synapse maturation and enhanced synaptogenesis in the dorsal hippocampus, alongside deficits in NMDAR-dependent LTD. Proteomic analyses uncovered dysregulation of signaling, ion homeostasis, ubiquitination, translation, oxidative stress, and neuroinflammation pathways. These findings suggest that Mdga2 loss disrupts early synaptic development and circuit refinement, contributing to autism-like phenotypes and persistent alterations in synaptic signaling.

Acknowledgements

I would like to sincerely thank my supervisor, Dr. Steven Connor, for the continued support, guidance, and mentorship throughout all my experiments and troubleshooting, and my advisor, Dr. Georg R Zoidl, for the insight and feedback relating to this project. Thank you to the current and past members of the Connor lab – Kyle Patel, Samuel Holm, Zahra Ghasemi, Parisa Tari, Rani Shouk, Jie Jang, and Georg S. Zoidl – for your continued encouragement and aid. A very special thank you to Rani Shouk for your collaboration in the Golgi-staining experiments; It was a privilege to be your mentor, and your help was invaluable. For all the emotional support throughout my graduate school experience and for acting as my thesis editor, thank you to my soon-to-be husband, Shawn McGlashon.

Statement of Contribution

Golgi-Cox staining experiments were run in collaboration with Rani Shouk. Experimental design and piloting were completed by Katherine Andrec. Production of Golgi-Cox slides and images was jointly completed by Rani Shouk and Katherine Andrec. To maintain blinding, measurements were conducted by Rani Shouk, and statistical analyses presented here were run by Katherine Andrec.

Table of Contents

List of Tables

List of Figures

(B) P21, (C) P28, and (D) P42.

Figure 4.6. Significantly enriched gene ontology (GO) biological process associated with differentially phosphorylated proteins in *Mdga2*$^{+/-}$ ventral CA1 tissue relative to *Mdga2*$^{+/+}$ ventral CA1 tissue at (A) P14, (B) P21, and (C) P42.

Chapter 1: General Background

1.1 Introduction

Autism spectrum disorder (ASD) is a highly heterogeneous neurodevelopmental disorder characterized by impaired social interactions, communication deficits, sensory sensitivities, stereotypy, and/or restricted interests (Landa, 2008; Public Health Agency of Canada, 2016; L. Wang et al., 2023). There has been a notable increase in the prevalence of autism spectrum disorder in Canadian children, rising from just 0.1% reported in the country's first epidemiological study in 1988 to 2.0% by 2019 (Bryson et al., 1988; Public Health Agency of Canada, 2022). Worldwide, the pooled point-prevalence of ASD increased from approximately 0.25% (1994–1999) to nearly 1% by 2023, with higher rates reported in high-income countries where access to diagnostic services is greater (Talantseva et al., 2023). This increase in prevalence is driven primarily by broader diagnostic criteria, improved screening and earlier identification, and increased awareness and reduced stigma rather than a true rise in the number of new autism cases or an epidemic caused by environmental or genetic changes (Pearson, 2025; Zeidan et al., 2022). This makes research, policy, and healthcare surrounding ASD critically important because early identification and intervention can significantly improve developmental outcomes and quality of life for individuals with autism.

The highly heterogeneous nature of ASD adds complexity to ASD research; there is a lack of a clear unifying cause of ASD, with a multitude of potential environmental and genetic contributing factors, including approximately 1000 identified risk genes associated with ASD in the Simons Foundation Autism Research Initiative gene database as of 2021 (Sauer et al., 2021). A growing body of research suggests that mutations in genes encoding synapse organizer proteins (SOPs), which play crucial roles in synapse development, differentiation, and support

(Siddiqui & Craig, 2011), contribute to the development of syndromic ASD in part by disrupting the excitation-inhibition (E/I) ratio of synaptic activity (Bourgeron, 2009; J. Chen et al., 2014; E. Lee et al., 2017). Recent advancements in genetic mouse models of ASD have greatly enhanced our understanding of the disorder's potential underlying pathology. These models involve targeted mutations in genes known to be associated with ASD, allowing the study of how the reduction or elimination of their associated proteins impacts brain development, neural circuitry, and behavior. In addition, they provide construct validity by replicating genetic risk factors identified in humans and face validity through exhibiting ASD-relevant behaviors such as social deficits, indicated by sniffing and social grooming behaviors, and repetitive actions, such as rearing and self-grooming (Kazdoba, Leach, & Crawley, 2016; Kazdoba, Leach, Yang, et al., 2016). As an early-onset neurodevelopmental disorder, exploring the effects of mutations in ASD risk genes during post-natal neural development in animal models is critical to investigate how they disrupt key processes, such as synapse formation and neural circuit maturation/refinement, which can have both immediate and long-lasting effects on cognition and behaviour. This approach offers valuable insights into identifying the best timing for interventions and targeting therapies that address the fundamental causes of ASD, rather than merely managing symptoms later in life.

1.2 Critical Periods and Plasticity in Neurodevelopment

The developing brain undergoes dynamic phases in which neural circuits are highly sensitive to environmental input and internal firing patterns. These critical periods mark windows of heightened plasticity where sensory and cognitive networks are sculpted through both genetic instructions and experience-dependent mechanisms. Disruptions during these developmental windows can have lasting consequences for circuit structure and function. One of

the hallmark features of critical periods is the rapid formation and refinement of synaptic connections; During early development, synaptogenesis involves the overproduction of synapses, with excessive potential connections. Following this phase, activity-dependent mechanisms guide the pruning of excess synapses, leaving behind more refined and efficient networks that reflect meaningful patterns of activity and experience. This balance ensures the efficient wiring of sensory and cognitive circuits and is critical in developing the proper excitation/inhibition (E/I) balance (Tau & Peterson, 2010).

In humans, synaptogenesis rapidly occurs in gestation, with a peak growth spurt occurring at approximately 36-40 weeks in gestation with overall peak synaptic density peaking around 2 years of age, with areas used for advanced cognitive processes, such as the prefrontal cortex (PFC), peaking slightly later in infancy and early childhood. Pruning and circuit refinement occur most rapidly between 2-16 years of age, with pruning continuing into the mid-20s in the PFC as complex behaviours and cognitive processes continue to develop (Semple et al., 2013; Tau & Peterson, 2010). Mice, on the other hand, have a peak brain growth spurt around post-natal day (P) 7-10, with the peak synaptic density occurring at approximately P20-P21. Synaptic pruning then follows until approximately P35-49 (Semple et al., 2013; Tau & Peterson, 2010). Mice have a much more condensed neural developmental time-line, making them an ideal model system to study this entire process in a relatively short amount of time. This makes murine genetic models of neurodevelopmental disorders, such as ASD, especially useful as researchers can track interaction between the genetic mutation of interest and time through development.

Closely tied to pruning is circuit refinement, a process that integrates both activity-dependent mechanisms and inhibitory signaling to fine-tune connections. Through this

refinement process, redundant or noisy inputs are eliminated while meaningful circuits for perception, cognition, and behavior are strengthened. The principal mechanism through which circuits are refined is synaptic plasticity, the capacity of synapses to strengthen or weaken in response to activity which is often referred to as Hebbian plasticity. In 1949, the Canadian psychologist Donald Hebb introduced a transformative theory of synaptic plasticity and proposed that when the axon of one neuron (cell A) is close enough to activate another neuron (cell B) and consistently participates in triggering it, a growth process or metabolic change occurs in one or both cells. This change increases the efficiency of cell A in activating cell B (Hebb, 1949). About two decades later, in 1973, neuroscientists Tim Bliss and Terje Lømo experimentally confirmed Hebb's theory by showing that brief high-frequency stimulation of neurons can induce a sustained increase in synaptic excitability in the dentate area of an anesthetized rabbit, a phenomenon now known as long-term potentiation (LTP) (Bliss & Lomo, 1973). LTP enhances synaptic strength, typically by stimulating N-methyl-D-aspartate receptors (NMDARs) to allow the rapid influx of calcium. The increase in intracellular calcium triggers a signaling cascade involving various kinases (CaMKII, PKA) and cyclic adenosine monophosphate (cAMP) that leads to increased α-amino-3-hydroxy-5-methyl-4-isoxazolepropionic acid receptor (AMPAR) expression in the post-synaptic membrane, enhancing post-synaptic ionic current in response to the same pre-synaptic release of glutamate (Lüscher & Malenka, 2012). In 1978, Thomas Dunwiddie and Gary Lynch first discovered activity-dependent long-term depression (LTD), the counter of LTP, in which they were able to reduce synaptic efficacy in the Schaeffer-collateral pathway within hippocampal slices from a rat by applying 1Hz low-frequency stimulation (LFS), while high frequency stimulation (HFS) of 5-100Hz resulted in potentiation (Dunwiddie & Lynch, 1978). Although they did not know it at the time, the LTD they discovered as a result

of 1Hz LFS was also a result of NMDAR activation, a fact that would not be discovered until around two decades later (Dudek & Bear, 1992). LFS results in a more prolonged and reduced flux of calcium through NMDARs compared to HFS and activates a different signaling cascade involving calcium-calmodulin complexes and various phosphatases (PP1, PP2B) resulting in AMPAR internalization from the post-synaptic membrane as opposed to insertion (Pinar et al., 2017). During development, LTP-like processes are known to drive the transformation of immature, NMDA-receptor-based synaptic contacts into mature, conducting AMPAR/NMDAR synapses (Durand et al., 1996), increase formation of dendritic spines, and enlarge/strengthen existing synapses (Watson et al., 2016), all of which act in a competitive mechanism to selectively stabilize synapses (De Roo et al., 2008a). On the other hand, immature synapses that experience relatively lower firing rates or lower coincidence rates with synaptic partners undergo LTD-like processes making them likely targets for synaptic pruning. In fact, LTD and synaptic pruning share common molecular pathways, ultimately resulting in the phosphorylation and internalization of AMPARs with LTD being a potential initial step in activity-dependent synaptic pruning (Heynen et al., 2003; Piochon et al., 2016). Therefore, during critical periods, the balance between LTP and LTD is crucial; disruptions in plasticity at this stage can encode maladaptive patterns of connectivity, effectively "locking in" aberrant circuit structures that persist into adulthood.

1.3 The Role of Synapse Organizer Proteins

Synapse organizer proteins (SOPs) play a central role in the formation, maturation, and specialization of chemical synapses during brain development. These proteins function as molecular bridges that span the synaptic cleft as adhesion complexes, connecting presynaptic and postsynaptic membranes, or as secreted factors that enhance synaptogenesis by activating

intracellular signaling cascades (Siddiqui & Craig, 2011). In an adhesion complex, the extracellular domains of pre- and post-synaptic proteins bind together to provide structural stability and bidirectional signaling required for synaptic differentiation. There are a vast number of SOPs expressed throughout the brain that often have multiple isoforms and binding partners, which determine the strength and type of synapse that will develop (Table 1.1, Figure 1.1).

Table 1.1 Major synapse organizer proteins and binding partners. Adapted from A. K. Lee et al., 2020, and Siddiqui & Craig, 2011.

Synapse Organizer	Function	Major Binding Partners
EphrinB–EphB complex	Bidirectional signaling molecules controlling dendritic spine morphogenesis and synaptic maturation	PDZ-domain scaffolds, syntenins, CASK
Cerebellin 1 (Cbln1)	Secreted synaptic organizers connecting presynaptic NRXN and postsynaptic GluD2 receptors in cerebellum and cortex	NRXNs, GluD2, PSD-95 via GluD2
Synaptic Cell Adhesion Molecules (SynCAMs)	Homophilic immunoglobulin-like adhesion molecules mediating excitatory synapse formation, specifically post-synaptic differentiation, as well as axon guidance and myelination	SynCAMs (homophilic), MUPP1, CASK, syntenins
Pre-synapic		
Neurexins (NRXN)	Organize both excitatory and inhibitory synapses by forming trans-synaptic complexes; regulate neurotransmission and synaptic structure	NLGNs, LRRTMs, Cbln, GluD2
Leukocyte Common Antigen-Related Receptor Tyrosine Phosphatase (LAR-RPTPs; LAR, PTPσ, PTPδ)	Presynaptic receptor phosphatases binding multiple postsynaptic partners; organize both excitatory and inhibitory synapses	NGL-3, TrkC, Slitrks, Interleukin-1 receptor accessory protein (IL1RAPL1, IL1RAcP)
Post-synaptic		
Neuroligins (NLGN)	Postsynaptic adhesion molecules that induce presynaptic differentiation; specify synapse type (e.g., NLGN1 at excitatory, NLGN2 at inhibitory synapses)	NRXN, MAGUK Scaffolds, Gephyrin

Leucine-rich Repeat Transmembrane Neuronal Proteins (LRRTMs)	Promote excitatory synapse formation via trans-synaptic signaling; regulate AMPAR recruitment	NRXN, MAGUK Scaffolds, AMPARs
Netrin-G Ligands (NGL)	Postsynaptic adhesion molecules mediating bidirectional signaling during synaptogenesis	LAR-RPTPs, MAGUK Scaffolds
Slit and Trk-like family (Slitrks)	Postsynaptic organizers of inhibitory (Slitrk1-3) and excitatory (Slitrk1/2) synapses	LAR-RPTPs (PTPσ/δ)
Membrane-Associated Guanylate Kinase Homologs Scaffolds (MAGUK; PSD-95, SAP97, PSD-93)	Postsynaptic scaffold proteins anchoring receptors and adhesion molecules; organize postsynaptic density (PSD)	NMDARs, AMPARs, NLGNs, LRRTMs, Shank, Homer

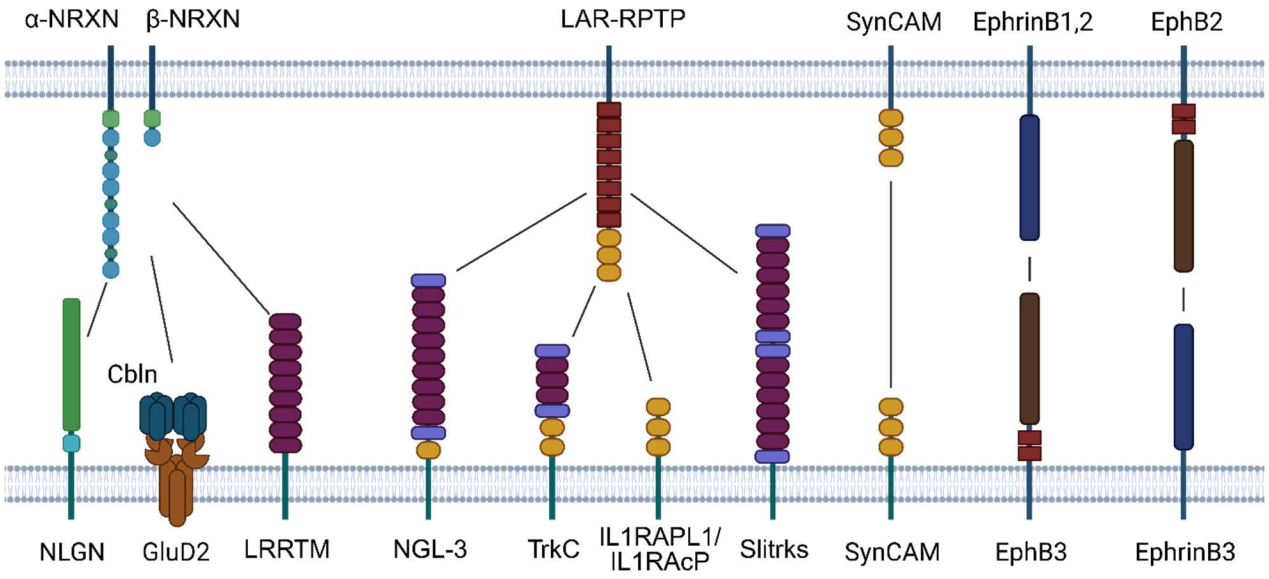

Figure 1.1. Major synaptic adhesion complex pre- and post-synaptic binding partners. Adapted from Siddiqui & Craig, 2011, and Lee et al., 2020. Symbols show the extracellular domains and binding partners of synapse organizer proteins that form synaptic adhesion complexes. Abbreviations: NRXN, neurexin; LAR-RPTP, leukocyte common antigen-related receptor tyrosine phosphatase; SynCAM, synaptic cell adhesion molecules; EphB, ephrin type-B receptor; NLGN, neuroligin; GluD2, glutamate receptor, ionotropic, delta-2; LRRTM, leucine-rich repeat transmembrane protein; NGL, netrin-G ligand; TrkC, tropomyosin receptor kinase C/neurotrophic receptor tyrosine kinase 3; IL1RAPL1, interleukin 1 receptor accessory protein-like 1; IL1RAcP, interleukin 1 receptor accessory protein; Slitrks, slit and TRK-like family. Made with Biorender.com.

Presynaptic differentiation is locally triggered by presynaptic organizers, including neurexins (NRXNs) and leukocyte common antigen-related receptor tyrosine phosphatases (LAR-RPTPs). These proteins, along with synaptic adhesion partners, aggregate on axonal surfaces to nucleate protein-protein interaction networks that recruit and assemble synaptic vesicles and active zone machinery. NRXNs cluster on presynaptic membranes and mediate intracellular interactions with active zone proteins, such as calcium/calmodulin-dependent serine protein kinase (CASK) and MINT (Munc 18 interacting protein), and members of the actin-nucleating Arp2/3 complex. These interactions coordinate the assembly of neurotransmitter release sites and drive cytoskeletal remodeling essential for synaptic vesicle clustering and stable neurotransmission (Chia et al., 2013; Y. Jin & Garner, 2008; H. Y. Kim et al., 2021; A. K. Lee et al., 2020; Schaan Profes et al., 2024). Similarly, LAR-RPTPs promote presynaptic differentiation by interacting with intracellular scaffolding proteins such as liprin-α, which functions as a pivotal organizer of presynaptic architecture required for neurotransmitter release (Bomkamp et al., 2019; Chia et al., 2013; Y. Jin & Garner, 2008; A. K. Lee et al., 2020). These protein complexes collectively establish the molecular framework essential for synaptic vesicle trafficking, vesicle docking, and regulated neurotransmitter release at developing synapses. This recruitment is driven primarily by high-affinity binding interactions rather than enzymatic catalysis (Siddiqui & Craig, 2011). Postsynaptic differentiation similarly relies on aggregation of postsynaptic organizers such as neuroligins (NLGNs), leucine-rich repeat transmembrane neuronal proteins (LRRTMs), and netrin-g ligands (NGLs), which recruit core scaffold proteins (PSD-95, Shank, Homer) and glutamate or GABA receptor subunits. These organizers often terminate in PDZ domain binding sites, enabling stable binding in the postsynaptic region (Siddiqui & Craig, 2011). Together, adhesion complexes and scaffolding organizers orchestrate synapse formation, maturation, and the reliable transmission of neuronal signals.

SOPs, particularly NRXN, NLGN, LRRTMs, and SHANK (SH3 and multiple ankyrin repeat domains protein) family scaffolds, are key determinants of synapse formation, function, and plasticity, and their disruption has been strongly linked to ASD. Human genetic studies have identified rare, highly penetrant mutations in genes encoding NRXN1, NLGN3, NLGN4X, SHANK2, and SHANK3 in individuals diagnosed with ASD (Bucan et al., 2009; J. Chen et al., 2014). For example, deletions or loss-of-function point mutations in NRXN1 have been repeatedly observed in ASD patients, with deletion carriers exhibiting profound synaptic deficits, neurodevelopmental delay, and social impairment (Onay et al., 2016). Similarly, missense mutations in NLGN3 (such as R451C) and NLGN4X (such as R87W or frameshifts) have been identified in cases of ASD and X-linked intellectual disability, with mouse models recapitulating these mutations exhibiting alterations in inhibitory or excitatory synaptic transmission, impaired social interaction, and repetitive behaviors (El-Kordi et al., 2013; Etherton et al., 2011; Fuccillo et al., 2014; Jamain et al., 2003, 2008). SHANK family mutations, especially in SHANK3, are associated with Phelan-McDermid syndrome and ASD, producing synaptic spine abnormalities and perturbed glutamatergic signaling (X. Wang et al., 2011). Additional variants in genes encoding LRRTMs (LRRTM3 and LRRTM4), CNTNAP2 (contactin-associated protein-like 2, another neurexin superfamily member), and other synaptic organizers have also been implicated in ASD (Bucan et al., 2009; Wright & Washbourne, 2011; J. Chen et al., 2014). These findings support the notion that synapse organizer protein dysfunction disrupts neuronal circuit development and synaptic homeostasis, leading to the core cognitive, social, and behavioral symptoms characteristic of autism.

1.4 The Role of MDGA Proteins

In 2001, a novel brain-derived immunoglobulin protein was first identified by differential display polymerase chain reaction (PCR) screen used to investigate secreted transmembrane proteins in the basilar pons of rat, and was dubbed 1g6M as it contained six immunoglobulin

domains and a single meprin, A-5 protein, receptor protein-tyrosine phosphatase mu (MAM) domain (Gesemann et al., 2001). A year later, the genetic organization of the gene encoding this Ig6M protein in humans was characterized and was found to contain a glycosylphosphatidylinositol (GPI) anchor in addition to a MAM domain, and was thus referred to as a GPIM protein, although the function of the protein was still unknown (De Juan et al., 2002). Finally, in 2004, this novel protein, previously referred to as Ig6M and GPIM, was cloned by the same group that initially conducted the differential display PCR, and referred to the protein by its current name, MAM domain-containing GPI anchor 1 protein (MDGA1) (Litwack et al., 2004). Interestingly, the same study identified a second closely related homologue, MDGA2; MDGA1 and MDGA2 share the same structural organization with 40% identical amino acids and 85% conserved amino acids, and were both confirmed to contain six Ig domains, one fibronectin type III (FnIII) type domain, one MAM domain, and a GPI anchor (Figure 1.2). (Litwack et al., 2004). MDGA protein expression was found to be specific to the central and peripheral nervous system during embryonic and early post-natal development (examined to P7) with the authors suggesting the proteins having a role in developmental processes such as cell migration, and axon outgrowth and guidance (Litwack et al., 2004). Further studies supported this idea, suggesting a role of MDGA proteins in initial brain development including in neuronal migration, cortical lamination, and cell adhesion (Ishikawa et al., 2011; Joset et al., 2011; Takeuchi et al., 2007). Even before the specific protein-protein interactions and cellular mechanisms of MDGA proteins were elucidated, *MDGA1/2* mutations began to be implicated in neurological disorders; *MDGA1* was identified as a risk gene for schizophrenia and bipolar disorder (Kähler et al., 2008; J. Li et al., 2011), and in 2009, Bucan and colleagues classified *MDGA2* as an ASD risk gene after identifying truncation loss-of-function mutations in eight unrelated cases of ASD (Bucan et al., 2009). It was not until 2013

that Lee and colleagues published their findings that MDGA1 and MDGA2 specifically bind to NLGN2 via their three terminal Ig domains, inhibiting the formation of NLGN-NRXN adhesion complexes, thereby negatively regulating inhibitory synapse formation and function (K. Lee et al., 2013). One limitation of this study was that surface binding assays, overexpression assays, and artificial synapse-formation assays were conducted exclusively with MDGA1 and not MDGA2 proteins or manipulations, leading to a generalization of MDGA protein functions. It was later shown that both MDGA proteins can bind to all NLGNs with different affinities with the binding site I of MDGA proteins overlapping with the NLGN-NRXN interface, preventing their interaction via steric hindrance and forming a tetrameric MDGA-NLGN complex (Figure 1.2) (Connor et al., 2016; Elegheert et al., 2017; J. A. Kim et al., 2017);. MDGA1 preferentially binds NLGN2 to repress inhibitory synapse development, and MDGA2 preferentially binds NLGN1 and NLGN2; however, the localization of MDGA2 has been a bit more contentious with conflicting reports from various model types, including *in vivo* reduction (*Mdga2*$^{+/-}$), reduction and overexpression in culture, and co-expression models (Bemben et al., 2023; Connor et al., 2016; Loh et al., 2016; Pettem et al., 2013; D. Zhao et al., 2025).

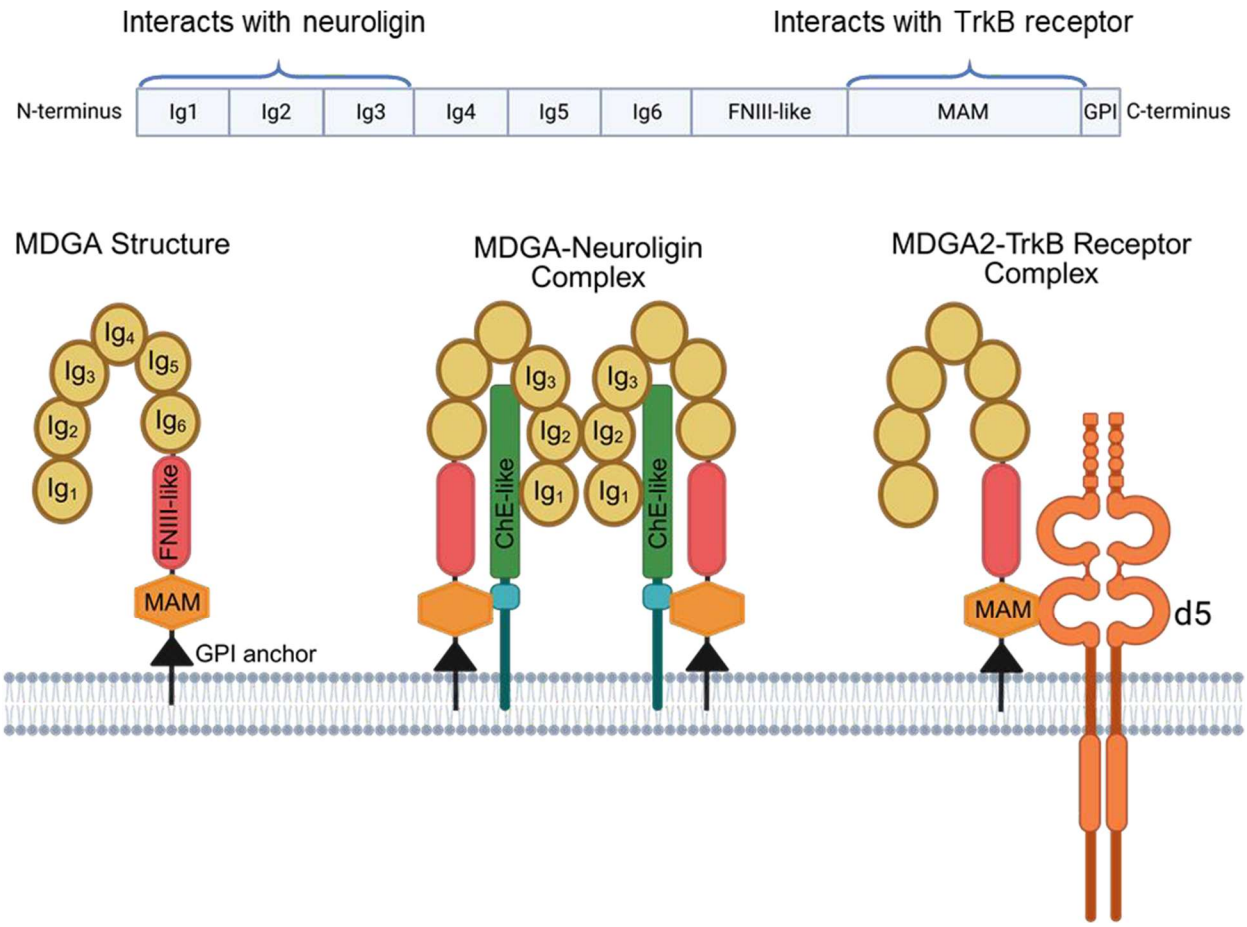

Figure 1.2. MDGA protein structure and interactions. MDGA proteins contain six immunoglobulin (Ig) domains, a fibronectin type III (FnIII) domain, a meprin, A-5 protein, receptor protein-tyrosine phosphatase mu (MAM) domain, and a C-terminus glycosylphosphatidylinositol (GPI) anchor. The three terminal Ig domains of bind the cholinesterase-like (ChE-like) domain of post-synaptic neuroligins to prevent the formation of transynaptic neuroligin-neurexin adhesion complexes. The MAM domain of MDGA2 proteins binds to the IgG2/d5 domain of tropomyosin receptor kinase B (TrkB) competitively with brain-derived neurotrophic factor (BDNF) to reduce TrkB-BDNF signaling. Together, these interactions repress synapse formation and development.

The current working model is that MDGA2 acts to repress both excitatory and inhibitory synaptic development and the observation that a reduction of MDGA2 *in vivo* (*Mdga2*$^{+/-}$ mice) still leads to reported normal levels of inhibitory synaptic activity and development (Connor et al., 2016), may be due to the ability of MDGA1 to compensate for the reduction in MDGA2, although this hypothesis requires additional exploration (Connor et al., 2016, 2019). Taken with the fact that MDGA protein expression peaks at approximately P14 (Toledo et al., 2022; Zhao et al., 2025), the MDGA shielding of Nlgn suggests that during the stage of neurite extension, MDGAs act to prevent early axon-dendrite contact and excess synaptogenesis.

Very recently, MDGA2 has been found to also bind to competitively with tropomyosin receptor kinase B (TrkB) receptors. Immunoprecipitation assays confirmed the binding of TrkB receptor's IgG2/d5 domain with MDGA2's MAM domain with the removal of either domain abolishing this interaction (D. Zhao et al., 2025). In culture, neurons with a reduction or knockout of MDGA2 have increased phosphorylation of TrkB receptors when induced by BDNF in a dose dependent manner, providing functional evidence that MDGA2 suppresses BDNF signaling (D. Zhao et al., 2025). TrkB-BDNF signaling drives neuronal development through three key pathways: MAPK/ERK, PI3K-AKT, and PLCγ-Ca^{2+}/CaMKII, which regulate survival, differentiation, and synaptic plasticity (W. Jin, 2020; Schirò et al., 2022). Upon BDNF binding, TrkB autophosphorylation recruits adaptor proteins to activate MAPK/ERK, enhancing CREB-dependent transcription for neurogenesis and dendrite arborization (Pradhan et al., 2019; Revest et al., 2014; Schirò et al., 2022), while PI3K-AKT promotes neuronal survival and axon growth (W. Jin, 2020). PLCγ triggers intracellular Ca^{2+} release, activating CaMKII which phosphorylates CREB and modulates synaptic strength (Pradhan et al., 2019; Schirò et al., 2022), with TrkB also regulating presynaptic glutamate release and postsynaptic receptor clustering (e.g., AMPARs/NMDARs) to stabilize neural circuits (Pradhan et al., 2019; C. S.

Wang et al., 2022). Therefore, similar to its interaction with NLGN, MDGA2 reduces TrkB-BDNF signaling to repress these effects, providing a second mechanism of synaptic development repression.

1.5. *Mdga2*$^{+/-}$ Mouse Model of ASD

To model the truncation loss-of-function mutation of MDGA2 found in various ASD cases (Bucan et al., 2009), *Mdga2*$^{+/-}$ mice were developed and used to investigate the effects of Mdga2 reduction on neurophysiology and behavior (Connor et al., 2016; Fertan et al., 2021). Two key types of validity are essential for effective animal models: face validity and predictive validity. Face validity concerns how well the animal's behavioral symptoms and neurological markers mimic those seen in human disorders, ensuring superficial similarity. Predictive validity assesses the model's ability to accurately predict the response to treatments or interventions used in humans (Belzung & Lemoine, 2011; van der Staay et al., 2009). Currently, the *Mdga2*$^{+/-}$ model demonstrates high face validity, and although some studies have shown potential rescue of certain phenotypes, its predictive validity has yet to be established. In 2016, Connor and colleagues first demonstrated the electrophysiological and behavioural implications of a heterozygous loss-of-function mutation in *Mdga2* with the *Mdga2*$^{+/-}$ mouse model (Connor et al., 2016). First, they confirmed that in co-immunoprecipitation assays, NLGN2 co-precipitated with MDGA1, while both NL1 and NL2 co-precipitated with MDGA2, suggesting MDGA2 would suppress both inhibitory and excitatory synaptic transmission as previously discussed.

This was confirmed as overexpression of MDGA2 in culture resulted in reduced inhibitory and excitatory synaptic density and signaling. Interestingly, in adult *Mdga2*$^{+/-}$ mice, only excitatory synapses showed changes in activity, density, and structure, while inhibitory synapses remained unchanged compared to wild-type (WT) mice. This included an increased density of asymmetric (excitatory) synapses in the hippocampal Cornu Ammonis 1 (CA1) region; elevated

levels of excitatory synaptic proteins such as post-synaptic density protein 95 (PSD-95) in both the PFC and CA1, and neuroligin-1 (NL1) specifically in CA1; higher amplitude and frequency of miniature excitatory post-synaptic currents (mEPSCs); and an increased ratio of AMPA receptor to NMDA receptor-mediated currents (Connor et al., 2016), which have since been confirmed by other groups (X. Wang et al., 2024; D. Zhao et al., 2025). This is supported by findings that *Mdga2*$^{+/-}$ mice exhibit enhanced excitatory synaptic transmission driven by abnormal activation of BDNF/TrkB signaling, as evidenced by increased levels of BDNF, elevated phosphorylation of TrkB receptors, and hyperphosphorylation of downstream signaling molecules detected in hippocampal synaptoneurosomes. Collectively, these processes drive increased AMPA receptor-mediated excitatory activity and disrupt neural circuit balance (D. Zhao et al., 2025). In addition, *Mdga2*$^{+/-}$ hippocampal slices have altered LTP profiles with enhanced early LTP (E-LTP), which is protein-synthesis independent, and impaired late LTP (L-LTP), which is protein-synthesis dependent (Baltaci et al., 2019; Connor et al., 2016). Therefore, although Mdga2 appears to repress both inhibitory and excitatory synaptic development, a reduction of Mdga2 in this model only affects excitatory synaptic development, indicating that Mdga1 expression is sufficient to maintain normal inhibitory synapse density and signaling when Mdga2 is reduced. Hyperexcitability is known to be a neurological biomarker of ASD, and an increase in excitatory synaptic density and signaling without any change in inhibitory signaling would result in an elevated E/I ratio, demonstrating how a reduction of MDGA2 could contribute to hyperexcitability-related ASD phenotypes such as social deficits, repetitive behaviors, and impaired cognitive function.

ASD diagnosis is based on behavioral symptoms such as persistent deficits in social communication and interaction, restricted, repetitive patterns of behavior, interests, or activities—such as stereotyped movements – sensory responses, and difficulties with learning

and memory. Although biomarkers such as alterations in E/I balance, neurotransmitter imbalance, neuroinflammation, and oxidative stress have been supported, only behavioural symptoms are used in diagnostics (American Psychiatric Association, 2013; DiCicco-Bloom et al., 2006; Goldani et al., 2014; Landa, 2008). Therefore, to have face validity, ASD animal models must display behavioural phenotypes akin to ASD symptoms. Altered behaviour in *Mdga2*$^{+/-}$ pups can be seen as early as P3-P21; pups have an earlier onset of the acoustic startle response, and reduced ultrasonic vocalizations, open-field activity, and exploration behaviour (Fertan et al., 2023). In adulthood, *Mdga2*$^{+/-}$ mice display behavioral phenotypes akin to ASD symptoms, including increased repetitive behaviours (ex., grooming), deficits in memory, and decreased social affiliation, sociability, and social novelty preference (Connor et al., 2016; Fertan et al., 2021; X. Wang et al., 2024; D. Zhao et al., 2025). The alterations in E/I ratio and behavioural phenotypes validate *Mdga2*$^{+/-}$ mice as a model of ASD, making them a valuable tool to probe the potential mechanisms and development for therapeutics related to ASD pathology.

To have predictive validity, the *Mdga2*$^{+/-}$ model must accurately predict the response to treatments or interventions in humans. Although predictive validity has not yet been established, Zhao and colleagues, and Huo and colleagues have successfully attenuated ASD-like behavioural phenotypes in *Mdga2*$^{+/-}$ mice by targeting two distinct mechanisms. Published in the same report that first described the interaction between Mdga2 and TrkB receptors, Zhao and colleagues demonstrated that bilateral injection of an MDGA2-derived peptide containing part of the MAM domain (MDGA2-P2) into the hippocampus reduced sociability and social novelty deficits by binding TrkB receptors *in vivo* (D. Zhao et al., 2025). This demonstrated that blocking BDNF-TrkB interaction may have therapeutic benefits in ASD caused by a reduction in MDGA2; however, it is important to note that MDGA2-P2 administration did not improve repetitive self-

grooming or novel location recognition, which were used as measures of repetitive behaviour/stereotypy and cognitive function, respectively (D. Zhao et al., 2025). Huo and colleagues took a different approach; instead of introducing an MDGA2 alternative peptide, they elucidated and targeted the lysosomal pathway that degrades MDGA2 proteins. They discovered that the lysosomal degradation pathway was mediated by sortilin 1 (SORT1) and that ribosomal protein S23 retrogene 1 (RPS23RG1) prevents this degradation by competing with SORT1 for MDGA2 binding (Huo et al., 2025). A knockdown of SORT1 increased MDGA2 levels, while loss of RPS23RG1 decreased MDGA2 and lead to ASD-like behaviours in mice, such as social deficits and increased repetitive behaviors (Huo et al., 2025), similar to those seen in *Mdga2*$^{+/-}$ mice (Connor et al., 2016; X. Wang et al., 2024; D. Zhao et al., 2025). Based on these interactions, Huo and colleagues developed and intravenously administered a peptide derived from the extracellular domain of RPS23RG1 (RPS23RG1-P2) that binds to MDGA2. RPS23RG1-P2 was able to restore MDGA2 levels and mEPSC frequency and amplitude in *Mdga2*$^{+/-}$ mice to WT levels, and rescue social affiliation, sociability, and social novelty preference deficits (Huo et al., 2025); however, similarly to the MDGA2-P2 peptide, the RPS23RG1-P2 peptide was unable to attenuate repetitive grooming behaviours. Taken together, targeting the overactive pathways and degradation pathways shows immense potential as therapeutics in cases of ASD related to a reduction of MDGA2.

1.6 Review of the Hippocampus

The hippocampus is a brain structure within the limbic system located within the medial temporal lobe in humans, best known for its roles in forming and retrieving memories, emotional processing, and spatial navigation (Knierim, 2015). Structurally, the hippocampus is composed of several interconnected regions forming the classic trisynaptic circuit first described by Santiago Ramón y Cajal in his 1893 work and later in his 1911 book (Cajal, 1911): the dentate

gyrus (DG), cornu ammonis 3 (CA3), and cornu ammonis 1 (CA1). The granule cells of the DG received input mainly by from layer II of the entorhinal cortex (EC) through the perforant pathway (synapse one) and sends projections to the pyramidal neurons of the CA3 via the mossy fiber pathway (synapse two). The CA3 then projects to other pyramidal neurons of the CA1 (synapse three) to complete the trisynaptic circuit as well as sending projections to other CA3 pyramidal neurons. The CA1 completes the circuit loop with outputs projecting back to layers V/VI of the EC (Figure 1.3) (Basu & Siegelbaum, 2015). In additional to the principal excitatory neurons, there are many classes of inhibitory interneurons which regulate activity both locally (within the same hippocampal region) and from long-range, such as inhibitory projections from the DG to CA3 and reciprocal inhibitory connections between the CA1 and EC (Basu & Siegelbaum, 2015). The EC acts as the principal integrative hub for the hippocampus, serving as both its major input and output gateway. Layer II and III neurons of the EC receive highly processed, multimodal sensory and associative information from the perirhinal and postrhinal cortices, parahippocampal regions, olfactory cortex, amygdala, and subcortical structures like the thalamus and septum. After processing within the hippocampus, the EC redistributes this hippocampally processed information to widespread cortical and subcortical targets, including sensory, associative, and limbic areas (Hernández-Frausto & Vivar, 2024).

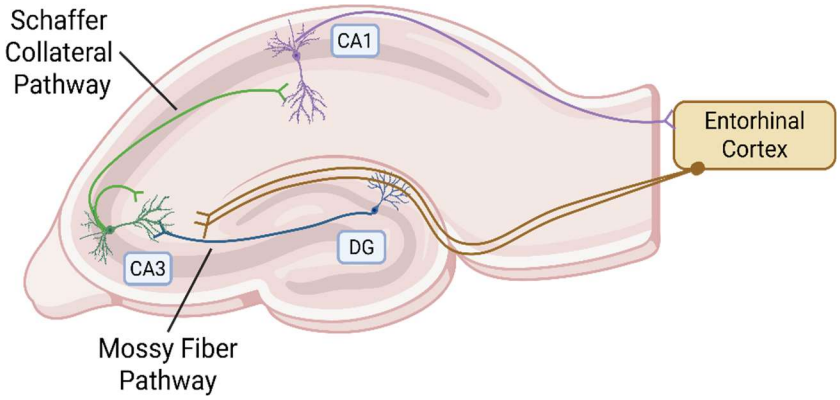

Figure 1.3. The Trisynaptic circuit of the hippocampus. Adapted from Neves et al., 2008. Abbreviations: DG, Dentate Gyrus; CA, Cornu Ammonis. Made with Biorender.com.

The hippocampus is essential for forming, organizing, and retrieving memories, as well as converting short-term experiences into long-term declarative memory. One of the landmark studies involving hippocampal function in humans involves the case of patient H.M., who experienced severe memory loss following surgical removal of his hippocampi in 1953 in an attempt to treat drug-resistant epilepsy. Following the surgery, H.M. experienced severe anterograde amnesia, in which he was unable to form new episodic memories, but his capacity for motor and semantic learning, and recalling older, long-term memories was spared (Scoville & Milner, 1957; Squire, 2009). This emphasized the hippocampus's critical role in episodic memory formation rather than procedural memory, along with introducing the concept of systems consolidation—the gradual process through which memories initially dependent on the hippocampus become increasingly stabilized in neocortical networks over time. Through this consolidation process, older memories eventually rely less on the hippocampus and more on distributed cortical storage sites, allowing them to persist even after hippocampal damage (McClelland et al., 1995; Müller & Pilzecker, 1900; Scoville & Milner, 1957; Squire et al., 2015). In addition, the hippocampus plays a critical role in emotional processing by interacting closely with structures like the amygdala and anterior cingulate cortex to connect memories with emotional responses. It helps to recall emotional memories and regulate emotions, particularly in social and affective contexts, by supporting the integration of episodic memory with emotional salience and self-related processing (Brown et al., 2015; Zhu et al., 2019). The hippocampus is also strongly involved in spatial navigation, supported by the discovery of "place cells" in 1971 by John O'Keefe and John Dostrovsky in the hippocampus of rats (O'Keefe & Dostrovsky, 1971). Place cells refer to pyramidal neurons that fire selectively when an animal occupies a specific location, forming a map-like representation of the environment known as a cognitive map. These cells are primarily located in the CA1 and CA3

regions and are sensitive to local and distal spatial cues, such as visual landmarks, olfactory signals, and boundaries (O'Keefe & Dostrovsky, 1971; O'Keefe & Conway, 1978; Humphreys et al., 1998). Functional imaging experiments and lesion studies have confirmed the role of the hippocampus in spatial navigation and memory in humans, supporting the work done in rats (Maguire, Burke, et al., 1996; Maguire, Frackowiak, et al., 1996; Kessels et al., 2001). Overall, the hippocampus serves as a crucial brain structure for forming and consolidating new declarative memories, integrating spatial and emotional information to create a cohesive representation of experience, while supporting memory retrieval and navigation within contextual environments.

Plasticity in the hippocampus is fundamental for learning and memory because it allows the strength and efficacy of synaptic connections between neurons to be dynamically modified in response to experience, and for this reason, the hippocampus is one of the most plastic regions in the brain with plasticity persisting beyond development and into adulthood (Leuner & Gould, 2010). For this reason, many plasticity studies use the hippocampus to investigate LTP and LTD, including the pioneering work of Bliss and Lømo in 1973 regarding LTP, and of Dunwiddie and Lynch in 1978 regarding LTP and LTD (see section 1.2 Critical Periods and Plasticity in Neurodevelopment). LTP and LTD serve as the cellular basis for learning and memory and forgetting respectively, which was directly demonstrated by Nabavi and colleagues in 2014 when they successfully engineered the deactivation and subsequent reactivation of a fear conditioned memory through optical delivery of LTD and LTP (Nabavi et al., 2014). This dynamic capacity for synaptic change and circuit remodeling underlies the hippocampus's crucial role in acquiring, storing, and adapting memories throughout life (Leuner & Gould, 2010).

The hippocampus is anatomically and behaviorally divided along its dorsal-ventral

(posterior-anterior in primates) axis. The dorsal hippocampus (posterior in primates) is especially important for spatial memory and navigation, is rich in place cells and specialized for processing cognitive maps, and for episodic memory. The ventral hippocampus (anterior in primates) is more involved in regulating emotional memory and cognition (Broadbent et al., 2004; A.-R. Lee et al., 2017; Okuyama et al., 2016; Phillips et al., 2019; Harland et al., 2021). The magnitude of synaptic plasticity also exhibits regional heterogeneity along the dorsal-ventral axis. Transient heterosynaptic depression, in which activation of one group of synapses leads to a transient reduction in the efficacy of neighboring, inactive synapses, and group I metabotropic glutamate receptor (mGluR) dependent LTD is enhanced in the ventral region of the hippocampus, while NMDAR LTD is not significantly different between the dorsal and ventral regions (Tidball et al., 2017; Dubovyk & Manahan-Vaughan, 2018; Trompoukis & Papatheodoropoulos, 2020). On the other hand, LTP is enhanced and the degree and range of paired-pulse facilitation – a short-term synaptic plasticity phenomenon where the second of two closely spaced synaptic stimuli produces a larger postsynaptic response than the first – was larger in the dorsal hippocampus (Maruki et al., 2001; Kouvaros & Papatheodoropoulos, 2016; Papatheodoropoulos & Kouvaros, 2016; Dubovyk & Manahan-Vaughan, 2018). Counterintuitively, there is an inverse relationship between the magnitude of synaptic plasticity and the expression levels of plasticity-related neurotransmitter receptors along the hippocampal dorsoventral axis. Although the ventral hippocampus shows higher expression of receptors such as NMDA (GluN2B, GluN1), metabotropic glutamate, $GABA_B$, and dopamine D1 receptors, the capacity for synaptic plasticity is elevated in the dorsal hippocampus, where these receptor levels are lower (Dubovyk & Manahan-Vaughan, 2018). Therefore, in assays of synaptic plasticity, it may be beneficial to distinguish between the dorsal and ventral hippocampus during analysis. Taken together, the features discussed highlight the hippocampus as a structurally and functionally heterogeneous

brain region whose specialized circuitry and plasticity mechanisms support a wide array of cognitive and emotional processes, making it a highly useful region to investigate plasticity and development. For this reason, along with MDGA2 having high expression in this region, all assays in this thesis were conducted in the CA1 region of the hippocampus.

1.7 Objectives and Hypotheses

Critical periods in brain development, such as those marked by synaptogenesis and synaptic pruning, are crucial for the establishment of appropriate neural circuits and the balance of E/I activity. Synaptic plasticity plays a pivotal role during these periods, allowing for activity-dependent refinement of circuits through mechanisms like LTP and LTD (Stampanoni Bassi et al., 2019). While alterations in LTP have been observed in adult *Mdga2*$^{+/-}$ mice, the impact of MDGA2 reduction on LTD and synaptic development during critical periods remains unexplored. Altered LTD is a common theme in mouse models of ASD, with alterations observed in models such as *Fmr1* KO, *Nlgn3* KO, *Syngap*$^{+/-}$, *Tsc2*$^{+/-}$, and eIF4E transgenic mice, which has renewed interest in potential dysregulation of synapse maturation and pruning in ASD models (Baudouin et al., 2012; Piochon et al., 2016). LTD and synaptic pruning share common molecular pathways, ultimately resulting in the phosphorylation and internalization of AMPARs with LTD being a potential initial step in activity-dependent synaptic pruning (Heynen et al., 2003; Piochon et al., 2016). Moreover, when synaptic density is observed to be altered in adulthood in a genetic ASD model, it cannot be determined if it is due to alterations in synaptogenesis or synaptic pruning processes; therefore, it is vital to conduct time-course experiments during critical periods of development. This can provide insight into the origin of synaptic density changes in adulthood and can suggest ideal times and targets for therapeutic intervention. Thus, I aimed to probe the development of excitatory synaptic spines in the CA1 region of the hippocampus by investigating potential alterations in NMDAR and mGluR

mediated LTD using *Mdga2*$^{+/-}$ mice during the critical period of synaptic pruning (P28-P42) (Chapter 2) and analyzing spine morphology and density during periods of synaptogenesis and synaptic pruning (P14-P42) (Chapter 3). In addition, I probed alterations in protein expression and phosphorylation states in hippocampal synaptoneurosomes preparations to elucidate dysregulated pathways or processes that may be involved in synaptic development and plasticity (Chapter 4). The hypothesis posits that MDGA2 reduction will impair LTD due to premature synapse maturation, reducing the susceptibility of synapses to activity-dependent weakening. Furthermore, it is hypothesized that the disinhibition of excitatory synapse development by a reduction of Mdga2 will lead to excessive synaptogenesis and/or impaired synaptic pruning leading to elevated excitatory post-synaptic density in adolescence. This work will help create an early neurodevelopmental profile in *Mgda2*$^{+/-}$ mice, which may provide insights into the development of adult phenotypes and targets for early-life therapeutic intervention.

Chapter 2: The Effect of Mdga2 Reduction on Synaptic Long-Term Depression

2.1. Introduction

2.1.1. Overview

Synaptic LTD in the hippocampus plays a crucial role in maintaining synaptic balance and supporting information storage by selectively weakening specific synaptic connections in an activity-dependent manner. This process is important for preventing the saturation of synaptic potentiation produced by LTP, thereby enabling continued learning and new memory formation and ensuring proper E/I balance. LTD is not merely a passive counterpart to LTP but has distinct physiological relevance: it enables the fine-tuning of neural circuits underlying spatial learning and contributes to the pruning of less active or unreliable synapses (Shinoda et al., 2010; Piochon et al., 2016; Stacho & Manahan-Vaughan, 2022). At the cellular level, LTD involves receptor trafficking (such as AMPAR endocytosis) and structural remodeling, leading to activity-dependent weakening or elimination of depressed synapses, allowing for the stabilization of more persistent connections (Lüscher et al., 1999; Nägerl et al., 2004; Zhou et al., 2004). In fact, LTD is believed to be a critical first step in synaptic elimination (pruning), which is an essential process during post-natal development to refine neural circuits, as repetitive induction of LTD leads to synaptic shrinkage and loss (Shinoda et al., 2010; Henson et al., 2017; Piochon et al., 2016). Overall, LTD is critical for multiple processes in the hippocampus, including synaptic and circuit refinement, learning and memory, and maintaining proper E/I balance.

2.1.2. Molecular Pathways of LTD

Post-synaptic LTD can be induced in distinct ways in CA1 pyramidal neurons (Oliet et al., 1997); the most studied, as previously mentioned, is NMDAR-dependent and was described in the early work of Thomas Dunwiddie and Gary Lynch (Dunwiddie & Lynch, 1978). This form of LTD relies on persistent, moderate calcium influx into the post-synapse through

NMDARs. This leads to the formation of calcium-calmodulin complexes, which activate the phosphatases calcineurin/protein phosphatase 2B (PP2B) and protein phosphatase 1 (PP1). PP1 dephosphorylates the subunit GluA1, which causes the lateral diffusion and endocytosis of the AMPA receptor (Figure 2.1) (Pinar et al., 2017). Conversely, Group I metabotropic glutamate receptor (mGluR)-dependent LTD at Schaffer collateral (CA3)–CA1 synapses is a postsynaptic form of plasticity mediated by group 1 mGluR (mGluR1 and mGluR5) activation. Upon stimulation, these Gq-coupled receptors activate phospholipase Cβ (PLCβ), leading to the production of inositol 1,4,5-trisphosphate (IP_3) and diacylglycerol (DAG). IP_3 induces the release of calcium from internal stores, while DAG activates protein kinase C (PKC) and other downstream signaling cascades (Figure 2.1) (Lüscher & Huber, 2010; Pinar et al., 2017). This moderate, localized calcium elevation and PKC activation trigger dephosphorylation of the GluA2 subunit of AMPA receptors through the striatal-enriched protein tyrosine phosphatase (STEP), promoting AMPA receptor internalization and diminishing synaptic strength (Y. Zhang et al., 2008; Pinar et al., 2017). In hippocampal CA1 neurons, mGluR-LTD also requires rapid local dendritic protein synthesis and activation of the mitogen-activated protein kinase kinase (MEK1/2) - extracellular signal-regulated kinase (ERK1/2) pathway which promotes phosphorylation of transcription factors such as cyclic AMP-responsive element-binding protein (CREB) and ETS transcription factor (Elk-1), driving immediate early gene expression (ex. Arc/Arg1.3) required for LTD expression (Huber et al., 2000; Y. Wang et al., 2009; Mango & Ledonne, 2023).

Concurrently, phosphoinositide 3-kinase (PI3K) – protein kinase B (Akt) – mammalian target of rapamycin (mTOR) pathway signaling enhances dendritic translation of plasticity-related proteins, supporting sustained AMPA receptor removal and structural remodeling (Figure 2.1) (Hou & Klann, 2004; Mango & Ledonne, 2023). mGluR-LTD requires this local protein

synthesis for maintenance beyond its initial induction, distinguishing it from NMDA receptor-dependent LTD, which usually does not require new protein synthesis for early phases. Ultimately, both NMDAR and mGluR pathways involve clathrin-mediated endocytosis of AMPARs, but there are pathway specific triggers (Anggono & Huganir, 2012). Therefore, although the end result is similar, it is possible that the intracellular signalling cascades are affected differently by Mdga2 reduction. On the other hand, it is possible that the reduction of Mdga2 could cause increased AMPAR-PSD-95 anchoring (Connor et al., 2016; D. Zhao et al., 2025), leading to impairments in AMPAR internalization in both pathways.

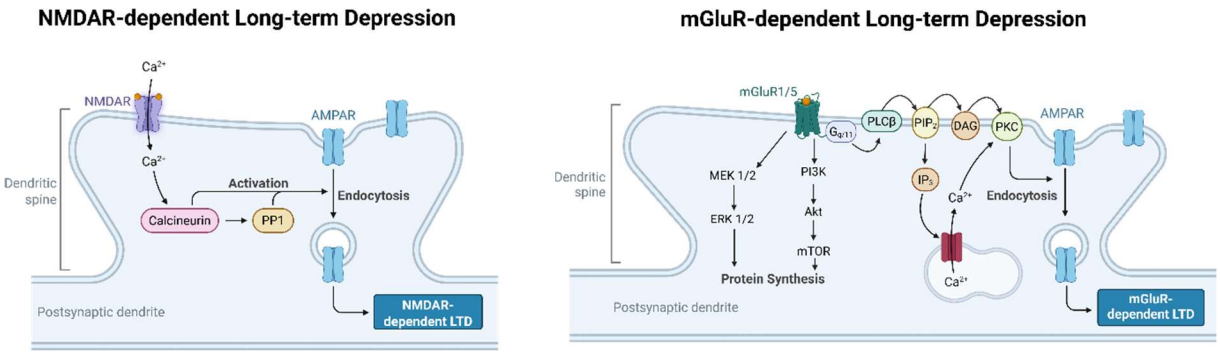

Figure 2.1. Simplified schematic of NMDAR-dependent and mGluR-dependent LTD pathways. Adapted from Pinar et al., 2017, and Mango & Ledonne, 2023. NMDAR-dependent LTD is triggered by a moderate, prolonged increase in intracellular calcium, leading to the activation of calcineurin and protein phosphatase 1 (PP1), which ultimately causes the phosphorylation and internalization of AMPARs from the post-synaptic membrane. mGluR-dependent LTD is triggered by the activation of group 1 mGluRs (mGluR1/5), resulting in the activation of several pathways. Phospholipase C beta (PLCβ) activates the phosphatidylinositol 4,5-bisphosphate (PIP_2)- inositol trisphosphate (IP_3)- diacylglycerol (DAG) pathway, leading to the release of calcium from internal stores and the activation of protein kinase C, and AMPAR internalization. The activation of mGluR1/5 also activates several pathways that lead to protein synthesis, including the mitogen-activated protein kinase kinase (MEK1/2)- extracellular signal-regulated kinase (ERK1/2), and the phosphoinositide 3-kinase (PI3K) – protein kinase B (Akt) – mammalian target of rapamycin (mTOR) pathway, which are critical for mGluR-LTD expression. Made with Biorender.com.

2.1.3 LTD Diminishes with Synapse Maturity

Although plasticity in the hippocampus is critical for learning and memory beyond the period of synaptic pruning and maturation, it becomes considerably more difficult to induce LTD in mature synapses. Mature synapses demonstrate a reduced capacity for plasticity, partially predicated on a lower proportion of NR2B/GluN2B-containing receptors, which alters the temporal dynamics of calcium influx required for NMDAR-dependent LTD induction (X. Zhao et al., 2009; Brigman et al., 2010; Cui et al., 2013). Mature synapses also have larger, more stable postsynaptic densities (PSDs) with increased concentrations of scaffolding proteins like PSD-95, which anchor AMPA receptors more firmly, limiting their lateral mobility and internalization during LTD induction (X. Chen et al., 2015; Kaizuka & Takumi, 2024). The coupling efficiency between mGluRs or NMDARs and downstream signaling pathways, including phosphatase activation and receptor endocytosis machinery, also diminishes with maturity, raising the threshold for LTD induction (Lohmann & Kessels, 2014). Taken altogether, while NMDAR- and mGluR-dependent LTD share a common outcome—activity-dependent AMPAR internalization—the molecular pathways leading to this depression are distinct and are influenced by synaptic maturity in the hippocampus.

2.1.4. Link to Hippocampal-Dependent Cognitive Processes and ASD

NMDAR- and mGluR-dependent LTD in the hippocampus are also implicated in behavioral/cognitive functions such as novelty detection, spatial learning, and memory flexibility (Kemp & Manahan-Vaughan, 2004; Ashby et al., 2021; Stacho & Manahan-Vaughan, 2022). Together, LTD and LTP interplay allow for the flexible updating of neural representations during novelty detection and spatial navigation. LTD acts as a system for resolving conflicting information by weakening older synaptic traces, which is essential for learning new environments and behavioral flexibility, while LTP is able to form new traces representing the updated information (Stacho & Manahan-Vaughan, 2022; Hagena & Manahan-Vaughan, 2024).

Overall, NMDAR and mGluR LTD pathways maintain synaptic homeostasis and fine-tune circuit plasticity, supporting the hippocampus' role in learning-dependent behavioral adaptations and episodic memory formation. These processes have significant implications for ASD; Disruptions in LTD can lead to impaired spatial and social learning and memory, which have been observed in models of ASD alongside alterations in LTD profiles (Table 2.1). Therefore, disruptions in LTD can have significant implications for both circuit regulation and cognitive function.

Table 2.1. Autism spectrum disorders with altered LTD profiles and associated behaviours. Several animal models of ASD have alterations in NDMAR or mGluR-dependent LTD that co-occur with alterations in hippocampal LTD-dependent cognitive processes.

Model	NMDAR-LTD	mGluR-LTD	Linked Behaviour	Reference
Nlgn1$^{+/-}$	Impaired	Enhanced	Deficits in contextual fear memory; impaired social memory	(Dang et al., 2018)
Fmr1 KO	Impaired or no change	Enhanced	Impairments in cognitive flexibility	(Huber et al., 2002; Tian et al., 2017)
Shank3 mutants (R87C, R375C, InsG)	No change	Impaired	Impaired spatial memory	(K. Lee et al., 2019)
Tsc2$^{+/-}$	No change	Impaired	Impaired contextual fear conditioning	(Auerbach et al., 2011)

2.1.5 Objective and Hypothesis

Although LTP has been studied in *Mdga2*$^{+/-}$ mice, LTD has yet to be studied. Therefore, the objective of this chapter is to investigate the potential effect of Mdga2 reduction on synaptic LTD in the Shaffer-Collateral pathway terminating in the CA1 of the hippocampus. There are several points of evidence in the synaptic physiology of *Mdga2*$^{+/-}$ mice that indicate there may be potential disruptions in synaptic LTD. NMDAR-mediated E-LTP is enhanced in the CA1 of adult *Mdga2*$^{+/-}$ mice (Connor et al., 2016), which may suggest a potential shift in NMDAR-

mediated LTP-LTD balance. Moreover, *Mdga2*$^{+/-}$ adult mice have increased PSD-95 expression, which may limit the mobility and internalization of AMPAR as previously discussed (Connor et al., 2016; D. Zhao et al., 2025). From a theoretical standpoint, the interactions between Mdga2 and Nlgn, and Mdga2 and TrkB receptors are known to repress synaptic development, therefore a reduction of Mdga2 would likely result in disinhibition of excitatory synaptic development and maturation during early postnatal development critical periods such as synaptogenesis and synaptic pruning surrounding the time when Mdga2 expression peaks (~P14) (Connor et al., 2016; D. Zhao et al., 2025). It is hypothesized that this disinhibition will lead to early synapse maturation, increased recruitment of PSD proteins, and potential biases towards LTP over LTD, resulting in LTD deficits during postnatal neural development. It is predicted that NMDAR-dependent LTD and/or mGluR-dependent LTD will be impaired in the CA1 in *Mdga2*$^{+/-}$ mice relative to WT controls aged P28-P42.

2.2 Materials and Methods

2.2.1 Mice

The mutant *Mdga2* allele was generated by replacing exon 1 with a *LacZ-pA-PGK-Neo-pA* cassette, preventing transcription of the *Mdga2* mRNA, as described in Connor et al., 2016 (Connor et al., 2016). Mice were harem bred in-house on a C57BL/6J background by breeding an *Mdga2*$^{+/-}$ (HET) male with two *Mgda2*$^{+/+}$ C57BL/6J wild-type (WT) females to produce HET and WT littermates. The female breeders were either bred in-house in a pure C57BL/6J line or obtained from Jackson Laboratories. Pups were weaned at P28 ± 1 day unless used for experimentation before that date. Ear notches were taken to be used as identifiers and to conduct genotyping via polymerase chain reaction (PCR) and gel electrophoresis. Same-sex littermates were housed together after weaning on a 12-hour light/dark cycle and were provided food and water *ad libitum*

2.2.2 Slice Preparation

WT and HET mice were selected between P28-P42. Following swift cervical dislocation and decapitation, the brains were removed from the skull and submerged in 4ºC artificial cerebrospinal fluid (aCSF) (Table 2.2). Brains were hemi-dissected, and the hippocampi were removed and sliced in 400µm thick transverse sections using a manual tissue chopper. Four slices were taken from each ventral and dorsal end, for a total of 16 slices per animal (Figure 2.2A). For NMDAR LTD experiments, slices recovered on a nylon mesh within an interface recording chamber heated to 30-31ºC for at least two hours before recording. For mGluR LTD experiments, the CA3 region was removed before slices were transferred to a submerged recovery chamber with RT oxygenated aCSF. The temperature of the aCSF was gradually increased to 30.5ºC over 30 minutes, and the slices were left to recover for at least two hours before recording.

Table 2.2. Artificial cerebrospinal fluid for hippocampal slice preparation and electrophysiological recordings. The following components were dissolved in double-distilled water to achieve an osmolality of 300-320, and then bubbled with 95% O_2/5% CO_2 to adjust the pH to 7.4.

Component	Molarity (mM)	Molecular Weight (g/mol)	Amount per 1L ddH_20 (g)
NaCl	124	58.44	14.5
KCl	4.4	74.55	0.656
$MgSO_4$	1.3	120.37	0.312
NaH_2PO_4	1.0	119.98	0.240
$NaCHO_3$	26.3	84.01	4.42
$CaCl_2$	2.5	110 (1M solution)	2.5ml
D-glucose	10	180.16	3.6

2.2.3 Electrophysiology Rig Set-up

For all recordings, slices were held in a dual interface and submerged chamber (Scientific Systems Design Inc, BSC1-2) and continually perfused with oxygenated aCSF through gravity-fed lines. A nylon mesh was inserted into the chamber to convert from submerged recording to interface recording. Extracellular excitatory postsynaptic fields were elicited by applying a 100μs current from a constant current isolated stimulator (Digitimer Ltd, model DS3) through a bipolar nichrome stimulation electrode. Cellular responses were recorded with a glass microelectrode filled with aCSF (R=1-4MΩ). Excitatory post-synaptic field potentials (fEPSPs) were recorded using an Axon Instruments Axon™ Digidata®1550 digitizer and MultiClamp 700B amplifier with Clampex 11.3 and MultiClamp 700B Commander software.

2.2.4 NMDAR LTD Recording

Electrodes were placed on the surface of the CA1 stratum radiatum (SR) for interface recording to record fEPSPs from the Schaffer-Collateral pathway (Figure 2.2B). The aCSF flow rate was set to 2-3mL/min. The stimulus intensity was set to elicit 50-60% of the maximum fEPSP, which was required to have a minimum amplitude of 1.0mV. To obtain a baseline, fEPSPs were recorded once per minute for 20 minutes (total of 20 sweeps) prior to LTD induction. NMDAR LTD was induced by 15 minutes of 1Hz low-frequency stimulation (LFS) (total of 900 sweeps). Following induction, recordings were taken once per minute for 60 minutes to determine the degree and maintenance of LTD. A maximum of one ventral and one dorsal recording was taken from each animal.

2.2.5 mGluR LTD Recording

Following recovery, a single hippocampal slice was transferred from the recovery chamber to a submerged recording chamber and was held in place with a harp. The stimulation and recording electrodes were embedded into the SR of the CA1 (Figure 2.2B). The flow rate of aCSF was set to 2mL/min. The stimulus intensity was set to elicit 50-60% of the maximum

fEPSP, which was required to have a minimum amplitude of 1.0mV. Ten minutes before the start of baseline recording, 50μM DL-2-Amino-5-phosphonopentanoic acid (AP5) (HelloBio, batch E2043-2-8) was bath applied to the slice to block NMDARs. AP5 was continuously applied during the baseline recording of one stimulation per minute for 20 minutes (total of 20 sweeps) before LTD induction. Following the 20-minute baseline, 100μM of S-3,5-dihydroxyphenylglycine (DHPG) (HelloBio, batch E1163-5-4) was bath applied for 5 minutes at a rate of 2mL/min (total of 10mL) while the slice was continually stimulated once per minute. The DHPG was then washed out, and recordings continued at one sweep per minute for 60 minutes.

2.2.6 Statistical Analysis

WinLTP 3.00 Reanalysis(W. W. Anderson & Collingridge, 2007) was used to measure the slope of the recorded fEPSPs (Figure 2.2C). Statistical analyses using T-tests and ANOVAs were conducted using GraphPad Prism 9, and linear mixed-effect models were conducted using RStudio (Posit team, 2025).

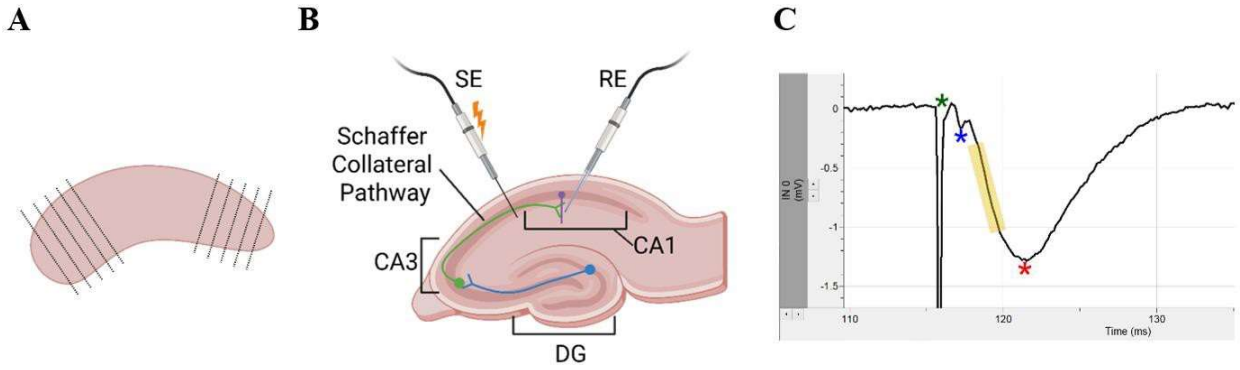

Figure 2.2. Representative images of hippocampal preparation and recording.

(A) Representative image of hippocampus sectioning. A small amount of tissue was removed from each end of the hippocampus before four 400 µm-thick transverse sections were taken. Four slices were taken from the dorsal (left) end and four from the ventral (right) end. Created with BioRender.com.

(B) Representative illustration of electrode placement in the Schafer collateral pathway and CA1 region. For NMDAR LTD experiments, the electrodes were placed at the surface for interface recording. For mGluR LTD experiments, electrodes were embedded into the tissue for submerged recordings. RE: recording electrode. SE: stimulating electrode. DG: dentate gyrus. Created with BioRender.com.

(C) Example excitatory post-synaptic field potential (fEPSP) recording. A 100µs current is applied, resulting in a stimulation artifact (*) followed by the presynaptic fiber volley (*) and the post-synaptic field potential (*). The highlighted yellow area represents the slope of the fEPSP measured for analysis. The y-axis represents the potential in millivolts (mV) and the x-axis represents time in milliseconds (ms).

2.2.6.1 Linear Mixed Effect Modeling

The last 10 minutes of the 60-minute post-stimulation recordings for both NMDAR-dependent and mGluR-dependent LTD were analyzed using a linear mixed effects model implemented in R (version 4.5.0) with the packages lmerTest, emmeans, ggplot2, and dplyr. The model tested the fixed effects of Genotype (WT, HET), Region (Dorsal, Ventral), Time (continuous), and their interactions on the fEPSP slope, while accounting for repeated measurements within a single recording/slice via a random intercept for SliceID [i.e., (1 | SliceID)] to account for its random effect.

```
model <- lmer(fEPSP ~ Genotype * Region * Time + (1| SliceID), data=ImportedCSV)
```

Model parameters were estimated using restricted maximum likelihood (REML). A model summary was generated to provide estimates, standard errors, degrees of freedom, t-values, and p-values for fixed effects. To further evaluate the overall significance of fixed effects and their interactions, a Type III analysis of variance (ANOVA) table based on Satterthwaite's approximation was generated. This ANOVA partitioned the variation explained by each fixed effect term and tested whether the variability attributed to these terms was statistically significant when accounting for random effects (i.e. variation within a single recording). Estimated marginal means (EMMs) for the genotype-by-region interaction were computed to facilitate pairwise post hoc comparisons within and between groups using the Sidak method for multiple comparisons. Predictions and confidence intervals from the fixed effects were generated over the observed time range and visualized using ggplot2. Residual diagnostics included residual scatterplots and histograms to visualize the fit of the model.

2.3. Results

2.3.1. NMDA Receptor-Dependent Long-Term Depression Induction and Maintenance Are Impaired in the Hippocampus of Mdga2$^{+/-}$ Mice

Recording from the CA1 of acute hippocampal slices from WT and HET mice

was conducted to investigate the effects of Mdga2 reduction on NMDAR-dependent LTD (Figure 2.3). Following induction of LTD via 1Hz LFS, the degree of LTD was evaluated at two time points – the first 10 minutes following LFS, representing the induction phase, and the last 10 minutes of the 60-minute post-stimulation recording, representing the maintenance phase. In both the induction and maintenance phases, there were no significant differences in the fEPSP slopes between the dorsal and ventral slices within either genotype, suggesting LTD induction and maintenance are not dependent on hippocampal region in either genotype. However, the average fEPSP slopes in both the induction and maintenance phases were significantly higher in HET slices, indicating impairments in NMDAR-dependent LTD following stimulation (First 10 minutes, WT dorsal 67.38%±4.23%, WT ventral 61.94%±5.26%, HET dorsal 82.28%±2.52%, HET ventral 78.96%±1.64%; Two-way ANOVA, region $F_{(1,28)}$=1.405 and p=0.8745, genotype $F_{(1,28)}$=18.68 and p=0.0006, interaction $F_{(1,28)}$=0.08261 and p=0.8572; WT dorsal-WT ventral and HET dorsal-HET ventral p>0.80, WT dorsal-HET dorsal p=0.0139, WT ventral-HET ventral p=0.0075, by Tukey's multiple comparisons test; n=8 per group; Last 10 minutes, WT dorsal 57.52%±3.88%, WT ventral 68.52%±5.52%, HET dorsal 83.39%±3.52%, HET ventral 84.75%±2.37%; Two-way ANOVA, region $F_{(1,28)}$=0.02540 and p=0.2458, genotype $F_{(1,28)}$=15.14 and p=0.0002, interaction $F_{(1,28)}$=0.03300 and p=0.7759; WT dorsal-WT ventral and HET dorsal-HET ventral p>0.30, WT dorsal-HET dorsal p=0.0081, WT ventral-HET ventral p=0.0029, by Tukey's multiple comparisons test; n=8 per group) (Figure 2.3A-C).

T-tests and ANOVAs are commonly used to analyze electrophysiological experiments with an ongoing time component, such as LTD and LTP experiments, by averaging data points across time points for each experiment to produce a single data point per experiment. While this is a powerful analysis to determine overall changes in fEPSP size or slope, it removes the time component of the experiment from the analysis. Additionally, it does not consider variation

between measurements in the overall recording, which can represent the stability of the recording, or any changes in field size as a function of time, which can represent growing or decaying synaptic responses. Therefore, an additional analysis using a linear mixed effect model (LMM) was conducted in addition to the ANVOA for the last 10 minutes of the 60-minute post stimulation recording (Figure 2.3D-E). An LMM allows the analysis to incorporate both fixed effects—such as genotype and region, which reflect systematic differences between groups—and random effects, such as variation between slices, which account for repeated measures and random variation in the field size within a recording. By modeling these repeated measurements within the same slice as random effects, the LMM corrects for non-independence and retains all information about how the data change over time and between groups (Yu et al., 2022) (refer to the Methods section for information regarding the model).

In the fixed effects estimates, the genotype HET coefficient indicated an estimated increase in fEPSP slope of 11.14% compared to WT (REML; estimate =11.14, t = 1.95, p = 0.061). The Genotype-by-Time interaction also showed a trend towards increasing slope over time in HET slices (REML, t = 1.96, p = 0.051), however it is worth noting that this change was very marginal at 0.3832% per minute. The ANOVA with Satterthwaite's method revealed a significant effect of genotype (Type III ANOVA; genotype F=8.6772, p=0.006247). There was no significant main effect of region or time, nor were there any significant interactions. Post hoc EMM testing revealed trending higher fEPSP slopes in HET compared to WT in the dorsal region (estimate = 12.9, p = 0.060 with Sidak's method) and a significant difference in the Ventral region (estimate = 13.4, p = 0.049, Sidak's method) (Figure 2.3D-E). For the full output of the NMDAR-dependent LTD LMM see Appendix A. Taken together with the results of the two-way ANOVA, it can be concluded that a reduction of Mdga2 impairs the induction and maintenance phase of NMDAR-dependent LTD in a manner which is independent of CA1

location along the dorsal-ventral axis.

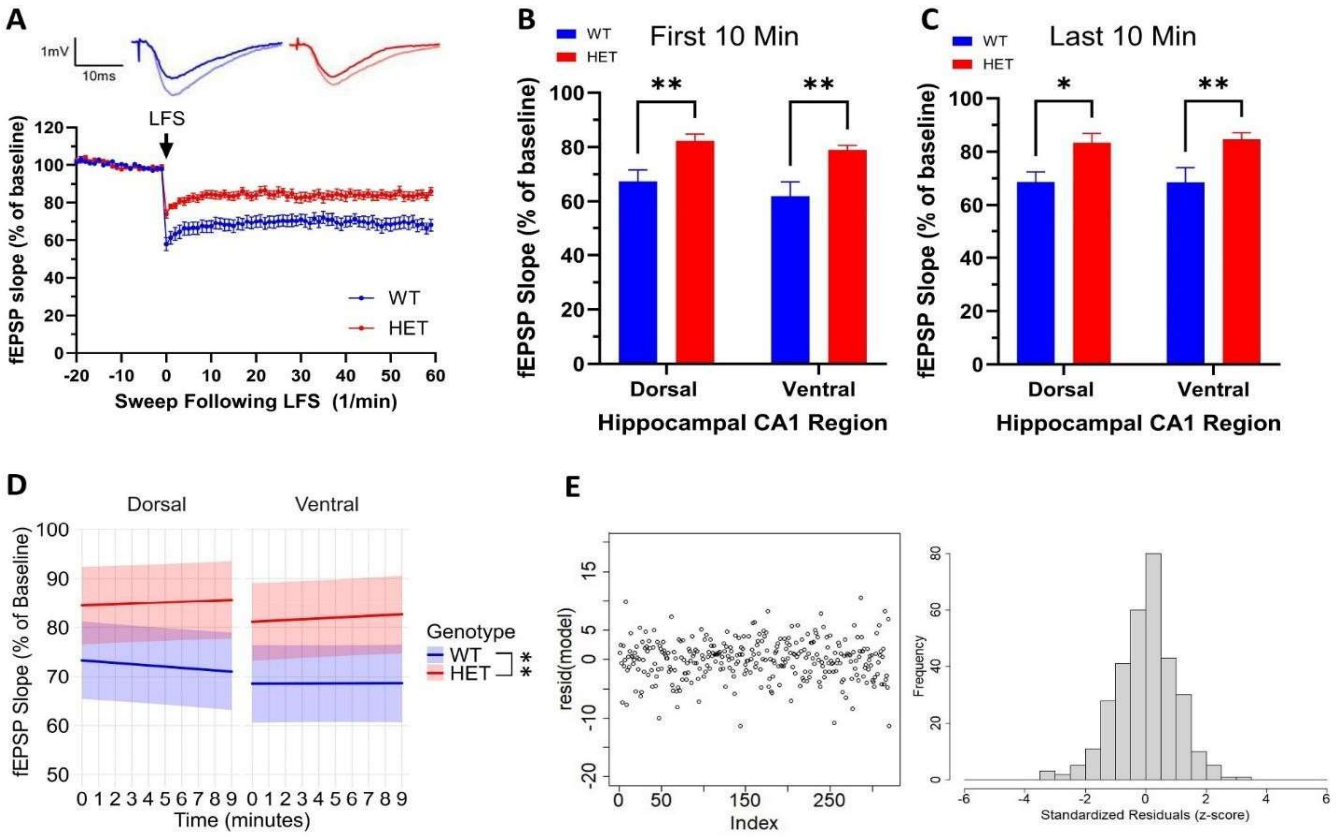

Figure 2.3. NMDAR-dependent LTD induction and maintenance are impaired in *Mdga2*$^{+/-}$ (HET) slices compared to *Mdga2*$^{+/+}$ wild-type (WT) controls.

(A) fEPSP slopes (% of baseline) 20 minutes before and 60 minutes following LTD induction via low frequency stimulation (LFS; 1Hz for 15mins) in HETS and WT controls. Data represent pooled dorsal and ventral slices (n=16). Inset traces represent example fEPSPs showing the degree of depression (darker trace) relative to baseline (lighter trace) in the last ten minutes of the one-hour post-stimulation recording.

(B) There is a strong main effect of genotype, and no effect of hippocampal CA1 region, nor any interaction between factors during the induction phase (first 10 minutes) following stimulation (WT dorsal 67.38%±4.23%, WT ventral 61.94%±5.26%, HET dorsal 82.28%±2.52%, HET ventral 78.96%±1.64%; Two-way ANOVA, region $F_{(1,28)}$=1.405 and p=0.8745, genotype $F_{(1,28)}$=18.68 and p=0.0006, interaction $F_{(1,28)}$=0.08261 and p=0.8572; **p<0.01 by Tukey's multiple comparison test).

(C) There is a strong main effect of genotype, and no effect of hippocampal CA1 region, nor any interaction between factors during the maintenance phase (last 10 minutes) following stimulation (WT dorsal 57.52%±3.88%, WT ventral 68.52%±5.52%, HET dorsal 83.39%±3.52%, HET ventral 84.75%±2.37%; Two-way ANOVA, region $F_{(1,28)}$=0.02540 and p=0.2458, genotype $F_{(1,28)}$=15.14 and p=0.0002, interaction $F_{(1,28)}$=0.03300 and p=0.7759; *p<0.05, **p<0.01 by Tukey's multiple comparison test).

(D) Linear mixed effect modeling of the last 10 minutes (minutes 50-60) following 15 minutes of LFS demonstrating a main effect of genotype on fEPSP slope independent of

hippocampal CA1 location along the dorsal-ventral axis. Highlighted area represents 95% confidence intervals (Type III ANOVA; genotype F=8.6772, **p=0.006247).

(E) Residual plot (left) and histogram of z-score standardized residuals (right) showing a normal distribution of residuals with a majority of residuals within 2-3 standard deviations, indicating that the linear mixed effect model is a good fit.

Error bars indicate SEM.

2.3.2. NMDAR Activation Via Low-Frequency Stimulation Does Not Depress Mdga2$^{+/-}$ Synapses to Wild-Type Levels

To further investigate the impairment of NMDAR-dependent LTD in HET slices, the responses during the 15-minute 1Hz LFS were analyzed. Both groups showed the initial rapid potentiation during the first minute, followed by progressive depression over the course of the LFS (Figure 2.4). When binned into one-minute intervals, it was found that the average fEPSPs were significantly higher in the HET group starting at minute two, with the difference in magnitude continuing to grow until minute 15 (Multiple unpaired t-tests with two-stage step-up Benjamini, Krieger, and Yekutieli method, FDR(Q)=0.05, min 1-6 #q<0.05, min 7-15 ##q<0.01; n=16) (Figure 2.4B). To ensure that any effect was not lost due to averaging over large, 1-minute bins (60 sweeps), analysis was also run with 5-second bins (5 sweeps) (Figure 2.4A, C-E). It was found that there was no significant difference in the maximum potentiation between WT and HET slices (WT, 117.5% ± 1.67%, HET, 121.3% ± 3.76%; Welch's t-test, $t_{20.6}$=0.909, p=0.374; n=16) (Figure 2.4C). The fEPSPs plateaued 17.03% ± 5.65% higher in the HET slices by the end of the LSF relative to WT slices (WT, 70.1% ± 4.76%, HET, 87.1% ± 3.05%; Welch's t-test, $t_{25.5}$=3.01, p=0.0058; n=16) (Figure 2.4D) and the overall depression of the fEPSPs from peak potentiation to the plateau was 13.26% ± 5.23% lower in HET slices (WT, 47.4% ± 4.72%, HET 34.2% ± 2.26%; Welch's t-test, $t_{21.5}$=2.53, p=0.0191; n=16) (Figure 2.4E). Both the 1-minute and 5-second bins confirm that both WT and HET slices potentiate initially to the same degree, but the HET slices show impaired depression during the 15-minute 1Hz LFS, indicating that it is an induction deficit causing impairments in NMDAR-dependent LTD.

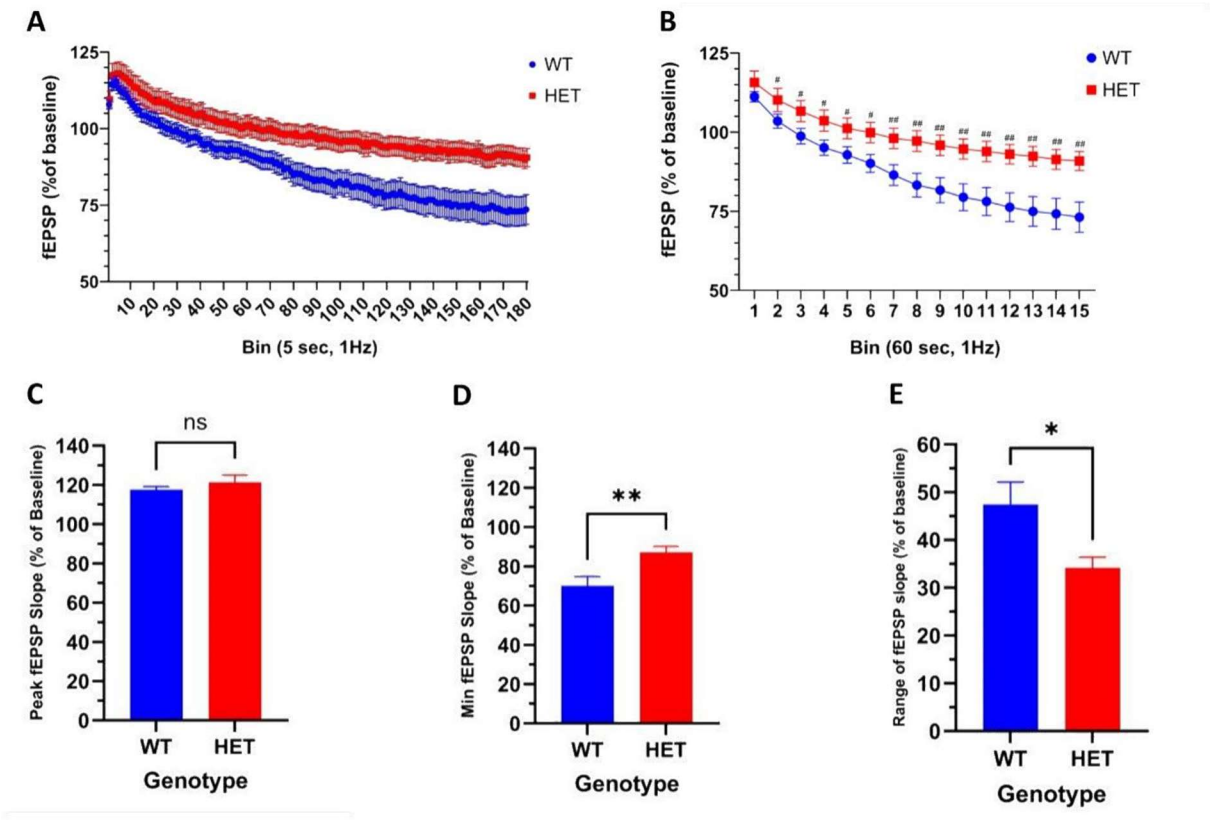

Figure 2.4. 15 min 1Hz low frequency stimulation to activate NMDA receptors does not depress synapses in *Mdga2*$^{+/-}$ (HET) slices to the same level as *Mdga2*$^{+/+}$ (WT) slices.

(A) fEPSP slopes (% of baseline) in 5-second bins during the 15 minutes of 1Hz LFS in HETs and WT controls. Data represent pooled dorsal and ventral slices (n=16).

(B) *Mdga2* HETs display larger fEPSP slopes during 15 minutes of 1Hz LFS from minute 2-15. Each data point represents the mean of 1-minute bins (60 sweeps) from each animal. (Multiple unpaired t-tests with two-stage step-up Benjamini, Krieger, and Yekutieli method, FDR(Q)=0.05, #q<0.05, ##q<0.01; n=16).

(C) The peak of the fEPSP slopes (% of baseline) did not differ between WT and HET 5-second bins (WT, 117.5% ± 1.67%, HET, 121.3% ± 3.76%; Welch's t-test, $t_{20.6}$=0.909, p=0.374; n=16).

(D) The minimum (trough) of the fEPSP slopes (% of baseline) is significantly larger in the HET group than the WT group (5-second bins) during 15 minutes of 1Hz LFS, indicating that the HET synaptic responses do not decay to the same level as WT (WT, 70.1% ± 4.76%, HET, 87.1% ± 3.05%; Welch's t-test, $t_{25.5}$=3.01, **p=0.0058; n=16).

(E) The total range of the fEPSP slopes (% of baseline) from the maximum to the minimum is significantly smaller in the HET group than the WT group (5-second bins) during the 15 minutes of 1Hz LFS (WT, 47.4% ± 4.72%, HET 34.2% ± 2.26%; Welch's t-test, t21.5=2.53, *p=0.0191; n=16).

2.3.3. mGluR-dependent LTD Remains Intact in Mdga2$^{+/-}$ Slices but Reduced Dorsal-Ventral Distinction in the Maintenance Phase

To determine if the deficits observed in NMDAR-dependent LTD in *Mgda2*$^{+/-}$ slices is pathway specific or if LTD deficits were universal and independent from induction pathway, mGluR LTD was tested via application of 100μm S-DHPG (Figure 2.5). Similar to the analysis of the NMDAR-dependent LTD, the degree of mGluR-dependent LTD was evaluated at two time points – the first 10 minutes following the 5-minute application of S-DHPG and a 5-minute washout, representing the induction phase, and the last 10 minutes of the 60-minute recording following S-DHPG application, representing the maintenance phase. In line with previously established patterns, mGluR-dependent LTD was significantly enhanced in WT ventral slices relative to WT dorsal slices in both the induction and maintenance phases (Tidball et al., 2017). Interestingly, this pattern was observed only in the induction phase of HET slices, with no significant difference in field size between HET dorsal and HET ventral slices during the maintenance phase. Unlike the NMDAR-dependent LTD, there was no difference in LTD induction or maintenance between genotypes within each region (First 10 minutes, WT dorsal 78.88%±2.48%, WT ventral 57.66%±3.83%, HET dorsal 72.17%±3.52%, HET ventral 58.19%±5.58%; Two-way ANOVA, region $F_{(1,28)}$=19.24 and p=0.0001, genotype $F_{(1,28)}$=0.5947 and p=0.4471, interaction $F_{(1,28)}$=0.8147 and p=0.3744; WT dorsal-WT ventral p=0.0008, HET dorsal-HET ventral p=0.0202, WT dorsal-HET dorsal p=0.2465, WT ventral-HET ventral p=0.9266, by Tukey's multiple comparisons test; n=8 per group; Last 10 minutes, WT dorsal 77.52%±1.89%, WT ventral 63.48%±3.36%, HET dorsal 72.27%±3.00%, HET ventral 65.46%±3.26%; Two-way ANOVA, region $F_{(1,28)}$=12.60 and p=0.0014, genotype $F_{(1,28)}$=0.3111 and p=0.5815, interaction $F_{(1,28)}$=1.515 and p=0.2286; WT dorsal-WT ventral p=0.0021, HET dorsal-HET ventral p=0.1123, WT dorsal-HET dorsal p=0.2164, WT ventral-HET ventral p=0.6377, by Tukey's multiple comparisons test; n=8 per group) (Figure 2.5A-C). The results of the LMM analysis were consistent with the two-way ANOVA analysis; In the fixed effects

estimates, the coefficient for region indicated a significant decrease in fEPSP slope in ventral slices compared to dorsal (REML; estimate = -12.80, t = -2.96, p = 0.0057). There was no significant effect of genotype, time, or any interaction terms on fEPSP slope. The coefficient for the genotype HET was not significant, showing a small estimated decrease of 4.17 percent compared to WT (REML; t = -0.96, p = 0.34). The Genotype-by-Region interaction term also failed to reach significance (REML; t = 1.04, p = 0.31). The ANOVA with Satterthwaite's method revealed a significant effect of region (Type III ANOVA; region F = 9.89, p = 0.0035), confirming that fEPSP slopes were different between ventral and dorsal slices. Genotype, time, and all interaction terms were not significant in the ANOVA. Post hoc EMM testing found a significant difference in fEPSP slope between WT slices in the dorsal and ventral regions (estimate = 14.04, p = 0.0043 with Sidak's method), while the HET ventral versus HET dorsal comparison was not significant (estimate = -6.81, p = 0.21, Sidak's method) (Figure 2.5D-E).

For the full output of the mGluR-dependent LTD LMM, see Appendix B. Overall, it can be concluded that mGluR-LTD is not impaired when Mdga2 is reduced. However, the regional difference in LTD seen in WT slices—with stronger depression in ventral than dorsal hippocampus—appears to be diminished in *Mdga2*$^{+/-}$ slices during the maintenance phase. These findings indicate that, unlike NMDAR-dependent LTD, mGluR-dependent LTD does not exhibit genotype-dependent deficits, but may display subtle alterations in the pattern of regional synaptic plasticity when Mdga2 is reduced.

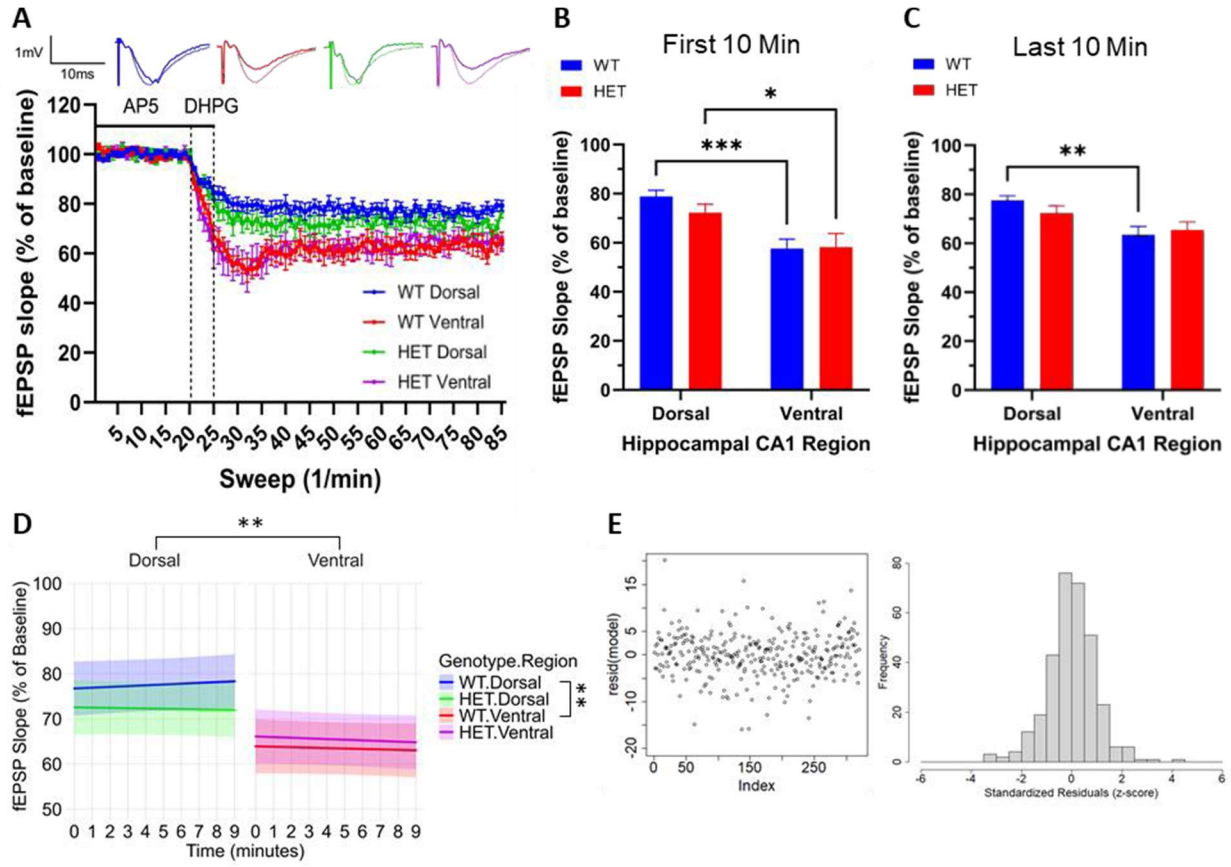

Figure 2.5. mGluR-dependent LTD is intact in *Mdga2*$^{+/-}$ (HET) slices, but loses distinction in amplitude between dorsal and ventral regions in the maintenance phase.

(A) fEPSP slopes (% of baseline) 20 minutes before and 60 minutes following LTD induction via 100µm S-DHPG in the dorsal and ventral region of WT and HET hippocampal slices. Inset traces represent example fEPSPs showing the degree of depression (darker trace) relative to baseline (lighter trace) in the last ten minutes of the one-hour post-drug administration recording.

(B) There is a main effect of CA1 hippocampal region (dorsal vs ventral) but no main effect of genotype nor any interaction between factors during the induction phase (first 10 mins following 5 min washout) following drug application. (WT dorsal 78.88%±2.48%, WT ventral 57.66%±3.83%, HET dorsal 72.17%±3.52%, HET ventral 58.19%±5.58%; Two-way ANOVA, region $F(1,28)=19.24$ and $p=0.0001$, genotype $F(1,28)=0.5947$ and $p=0.4471$, interaction $F(1,28)=0.8147$ and $p=0.3744$; *p=0.0202, ***p=0.0008, n=16)

(C) There is a main effect of CA1 hippocampal region (dorsal vs ventral) but no main effect of genotype nor any interaction between factors during the maintenance phase (last 10 minutes) of recording following drug application (WT dorsal 77.52%±1.89%, WT ventral 63.48%±3.36%, HET dorsal 72.27%±3.00%, HET ventral 65.46%±3.26%; Two-way ANOVA, region $F(1,28)=12.60$ and $p=0.0014$, genotype $F(1,28)=0.3111$ and $p=0.5815$, interaction $F(1,28)=1.515$ and $p=0.2286$; **p=0.0021, n=16).

(D) Linear mixed effect modeling of the last 10 minutes (minutes 50-60) following 15 minutes of LFS. Highlighted area represents 95% confidence intervals (ANOVA with Sidak

method; **p<0.01).

(E) Residual plot (left) and histogram of z-score standardized residuals (right) showing a normal distribution of residuals with a majority of residuals within 2-3 standard deviations, indicating that the linear mixed effect model is a good fit.
Error bars represent SEM.

2.4. Discussion

Overall, NMDAR-dependent LTD induction is impaired in the CA1 of *Mdga2*$^{+/-}$ acute slices. In contrast, mGluR-dependent LTD induction via DHPG remains intact, but with a potential loss of the dorsal-ventral distinction in the amplitude of LTD maintenance. The WT controls showed a robust increase in the degree of mGluR-dependent LTD in the ventral CA1 relative to the dorsal CA1, demonstrating that the loss of dorsal-ventral distinction in the *Mdga2*$^{+/-}$ slices was due to the reduction of Mdga2 and not the slicing, induction, or recording methodology.

The deficit in NMDAR-LTD induction but not mGluR-LTD induction or expression indicates that a reduction in Mdga2 selectively impairs NMDAR-related activity or intracellular signaling and does not reflect an overall inability of the synapses to undergo activity-dependent weakening or associated AMPAR internalization. Taken together with enhanced NMDAR-dependent E-LTP in acute hippocampal slices from *Mdga2*$^{+/-}$ mice (Connor et al., 2016), impaired NMDAR-LTD is likely due to a shift in NMDAR LTD-LTP balance rather than a global decrease in NMDAR activity or signaling. Both NMDAR-LTD and LTP are driven by an increase in post-synaptic intracellular calcium concentrations ($[Ca^{+2}]_i$); however, the temporal dynamics and amplitude of $[Ca^{+2}]_i$ dictate the direction of plasticity (Mizuno et al., 2001), Brief, high-amplitude $[Ca^{+2}]_i$ transients favor activation of calcium/calmodulin-dependent protein kinase II (CaMKII) and other kinases that promote AMPAR insertion and LTP induction. In contrast, prolonged but moderate $[Ca^{+2}]_i$ elevation activates protein phosphatases such as calcineurin and PP1, leading to AMPAR dephosphorylation and internalization underlying LTD (Mulkey et al., 1993; Cummings et al., 1996; S.-N. Yang et al., 1999). This is mimicked in most electrical stimulation induction protocols of early LTD and LTP, with high-frequency stimulation of 50-100Hz for 1 minute being commonly used to induce LTP and low-frequency stimulation of 1-3Hz for 5-15 minutes being used to induce LTD (Lüscher & Malenka, 2012).

In *Mdga2*$^{+/-}$ mice, alterations in NMDAR subunit composition — particularly increasing GluN2A-containing NMDARs — likely change calcium influx profiles. GluN2B-containing receptors, which have slower deactivation kinetics and higher calcium permeability, are critical for the prolonged $[Ca^{+2}]_i$ elevations needed for LTD induction, whereas GluN2A-containing receptors exhibit fast activation and deactivation kinetics, leading to brief but high-amplitude calcium influx into postsynaptic neurons, primarily associated with LTP induction (Bartlett et al., 2007; L. Liu et al., 2004; Iacobucci & Popescu, 2018). An increased GluN2A/GluN2B ratio could favor faster but shorter calcium transients, thus biasing synapses towards LTP over LTD, which is consistent with the finding that cultured hippocampal slices lacking Mdga2 and acute hippocampal slices from *Mdga2* cKO mice have an increased expression of GluN2A subunits with no change in GluN2B subunits (S. Kim et al., 2024). This potential mechanism is consistent with mGluR-LTD remaining intact in the presence of the NMDA antagonist AP5; in contrast to NMDAR-LTD, mGluR-LTD does not rely on extracellular influx of calcium, but on the release of calcium from intracellular stores such as the endoplasmic reticulum (Pinar et al., 2017). Therefore, changes in ionotropic receptor kinetics would have minimal effects on the induction or maintenance of NMDAR-independent mGluR-LTD. To test this new hypothesis and to serve as a potential rescue, experiments involving non-saturating levels of a GluN2A antagonist, such as NVP-AAM077, could be used during NMDAR-LTD experiments to determine if partial blockage of GluN2A restores NMDAR-LTD in *Mdga2*$^{+/-}$ slices to WT levels.

Hippocampal-dependent behaviours observed in *Mdga2*$^{+/-}$ mice can also be linked to impairments in NMDAR-LTD. NMDAR-LTD is critical for the consolidation, but not the initial acquisition, of contextual fear conditioning (X. Liu et al., 2014). This is consistent with the observed impairments in *Mdga2*$^{+/-}$ mice during foot-shock contextual fear conditioning tasks,

where the initial learning of the foot-shock and location pairing is intact, but deficits in contextual fear memory are evident 24 hours later and persist up to seven days after training (Connor et al., 2016; X. Wang et al., 2024). NMDAR-LTD, but not LTP, is critical for spatial memory consolidation in the Morris water maze test (Ge et al., 2010). Although *Mdga2*$^{+/-}$ mice can improve latency to a hidden platform within a few trials, this spatial memory is impaired when probed three days after training (Connor et al., 2016). Overall, *Mdga2*$^{+/-}$ hippocampal slices from both the dorsal and ventral region demonstrate deficits in NMDAR-LTD induction which may contribute directly to select cognitive impairments and is consistent with enhanced NMDAR-dependent E-LTP observed in *Mdga2*$^{+/-}$ mice.

mGluR-LTD can be robustly induced by DHPG in both dorsal and ventral CA1 regions in *Mdga2*$^{+/-}$ mice, indicating normal function of group I mGluR signaling and core downstream effectors; however, the regional difference is abolished in the maintenance phase, with the dorsal CA1 of *Mdga2*$^{+/-}$ mice having slightly, but not significantly, enhanced mGluR LTD than WT controls. Although there was a significant difference between the dorsal and ventral regions in *Mdga2*$^{+/-}$ slices in the induction phase, this difference was abolished in the maintenance phase. In WT animals, the ventral hippocampus has a significantly higher expression of mGluR1, but not mGluR5, in both the SR and the stratum lacunosum-moleculare (SLM) (Dubovyk & Manahan-Vaughan, 2018). It is possible that a reduction in Mdga2 could result in this difference being abolished as excitatory synaptic development is disinhibited, or that there is an effect on intracellular signaling cascades or protein translation pathways required for mGluR-LTD. However, it is worth noting that there is a higher level of variance in experiments from ventral slices of *Mdga2*$^{+/-}$ mice relative to other groups, and it is possible that this increase in variance is occluding a potential true difference between regions in *Mdga2*$^{+/-}$ slices. It may be beneficial to increase the sample sizes in each group before making definitive conclusions.

Chapter 3: Characterization of Hippocampal CA1 Synaptic Spine Density and Morphology Through Postnatal Development

3.1 Introduction

3.1.1 Biological Function, Structure, and Development of Synaptic Spines

Most excitatory inputs onto pyramidal neurons in the hippocampal CA1 are located on small protrusions of dendrites called synaptic/dendritic spines (Megías et al., 2001; von Bohlen Und Halbach, 2009). Synaptic spines were first identified as a structure on neurons by Santiago Ramon y Cajal in 1888 by utilizing the Golgi staining technique developed by Camillo Golgi, which contributed to Cajal and Golgi receiving the Nobel Prize for Physiology and Medicine in 1906 (García-López et al., 2007; *Nobel Prize in Physiology or Medicine 1906*, n.d.). Since their discovery, an abundance of research has been conducted relating to the function and dynamic modulation of synaptic spines, along with their connection to functional and structural plasticity.

Synaptic spines are actin-rich protrusions that are generally composed of a head region containing the post-synaptic density (PSD) and a narrow neck region that connects to the dendritic shaft allowing for a greater area on the dendrite for synaptic input and for the compartmentalization of biochemical and electrical signals within individual synapses (Figure 3.1)(Nimchinsky et al., 2002; Arellano et al., 2007). This structural compartmentalization allows individual excitatory synapses to undergo plasticity independently, which supports the fine-tuning of synaptic strength and input specificity during integration (Yuste & Denk, 1995; Nimchinsky et al., 2002). In contrast, inhibitory synaptic inputs are often located directly on dendritic shafts or the soma in CA1 pyramidal neurons (Megías et al., 2001), where they can exert shunting or hyperpolarizing effects that influence the integration of multiple excitatory inputs by reducing membrane resistance or directly opposing depolarization (Villa & Nedivi, 2016; Boivin & Nedivi, 2018). The balance and interaction between excitation on spines and inhibition on shafts allow neurons to integrate and filter synaptic inputs with high spatial and

temporal precision, shaping synaptic plasticity and modulating neuronal output in a branch-specific manner to maintain circuit stability and support complex computations (Villa & Nedivi, 2016; Boivin & Nedivi, 2018; Horton et al., 2024).

During development, dendritic spine morphology undergoes significant changes that reflect the maturation of synaptic circuits. In the early postnatal period, neurons predominantly display dendritic filopodia, which are thin, highly dynamic protrusions lacking a defined spine head that actively sample the local environment for presynaptic partners. These filopodia frequently transform into immature spines upon establishing contact with axonal boutons, initiating synaptogenesis (Ziv & Smith, 1996; Fiala et al., 1998). As synaptic spines continue to mature and develop, they begin to retract close to the dendritic shaft and form a well-defined head and narrow neck (Zito et al., 2009; Gipson & Olive, 2017). The classification of spines according to their length and head width is commonly used to gauge their maturity; spine types range from least to most mature as filopodia, thin, stubby, mushroom, and branched spines, respectively (Nimchinsky et al., 2002; Risher et al., 2014) (Figure 3.1). During dendritic spine maturation, immature filopodia-like protrusions transform into stable, mushroom-shaped spines through coordinated signaling that reorganizes the actin cytoskeleton and expands the PSD by recruiting and clustering scaffolding proteins (e.g., PSD-95), receptors (AMPA and NMDA), and signaling complexes (Nimchinsky et al., 2002; Ethell & Pasquale, 2005; Nourbakhsh & Yadav, 2021). In addition to changes during development, synaptic spines exhibit dynamic morphological changes that correspond closely with both LTP and LTD. During LTP, spine heads typically undergo rapid expansion and enlargement, accompanied by actin polymerization and increased PSD size (Lin et al., 2005; Y. Yang et al., 2008). Conversely, LTD is associated with spine shrinkage or reduction in spine volume through the depolymerization of filamentous actin and autophagy-mediated degradation of PSD-95 (Zhou et al., 2004; Compans et al., 2021).

Overall, synaptic spines are highly dynamic structures whose morphology and molecular composition closely correlate with development and plasticity. Their maturation involves coordinated extracellular signaling, intracellular cascades, actin remodeling, and expansion of the postsynaptic density, all of which contribute to spine growth and stabilization. These processes enable individual spines to independently regulate synaptic strength, supporting the fine-tuning of neuronal circuits essential for learning, memory, and cognitive flexibility.

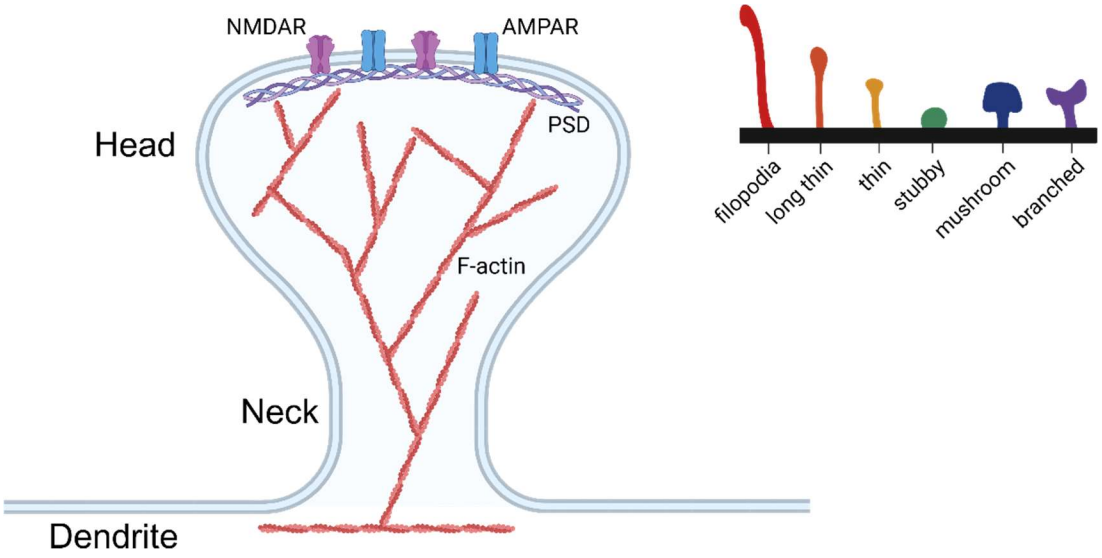

Figure 3.1. Illustration of a synaptic spine and the different subcategories. Synaptic spines typically consist of an actin-rich bulbous head region connected to the dendrite by a narrow neck, allow for chemical and electrical compartmentalization. The head region contains the post synaptic density (PSD) which includes various scaffolding proteins which anchor post-synaptic receptors and proteins like AMPAR and NMDARs. As spines mature, their morphology changes as the spine retracts closer to the dendrite, the head width enlarges, and the neck becomes more defined. Synaptic spines are often classified as filipodia, (long) thin, stubby, mushroom, and branched to indicate their gross morphology and maturity. Adapted from Gipson & Olive, 2017 and made with Biorender.com.

3.1.2. Synaptogenesis and Synaptic Pruning

Synaptogenesis and synaptic pruning are fundamental, complementary processes that collectively refine neural circuits by balancing surplus synapse formation with the selective elimination of redundant or weak connections. During early development, the overproduction of synapses generates a surplus of potential connections, providing a scaffold for diverse neural inputs that can be selectively stabilized or removed (Sakai, 2020). Synaptic pruning refines this initially imprecise wiring through activity-dependent mechanisms governed largely by Hebbian plasticity principles (Piochon et al., 2016; Faust et al., 2021), with an initial rapid period of elimination followed by a decrease in elimination rate, which optimizes the efficiency of networks (Navlakha et al., 2015). The interplay of synaptogenesis and pruning enhances circuit specificity, efficiency, and computational capacity by ensuring that only appropriately patterned synaptic connections persist. This refinement improves signal-to-noise ratio within neural networks, promoting functional segregation and integration necessary for precise information processing (Faust et al., 2021).

In the CA1 region of the mouse hippocampus, synaptogenesis begins during the early postnatal period and continues into adolescence. Excitatory synapses begin to rapidly form around P5–7, coinciding with the emergence of dendritic spines on CA1 pyramidal neurons. By P10–P15, the density of spines increases sharply as axons from Schaffer collateral inputs of CA3 neurons establish functional glutamatergic synapses (Collin et al., 1997; Lohmann & Kessels, 2014). During this time, spines are mostly thin and filopodia-like, serving as exploratory structures that sample presynaptic partners (Ziv & Smith, 1996; Zito et al., 2009). Early synapse formation depends on cell-adhesion molecules such as neuroligins, neurexins, and SynCAMs, which align pre- and postsynaptic specializations (Craig & Kang, 2007; Krueger et al., 2012; Qi et al., 2022). Synaptic density peaks at approximately P21, and as spines begin to mature through

P15–P30, there is a transition from motile filopodia to stable, mushroom-shaped spines with expanded PSDs and compartmentalized calcium signaling (Ethell & Pasquale, 2005; Semple et al., 2013; Y. Yang et al., 2024). Maturation involves the coordinated regulation of the actin cytoskeleton by small Rho GTPases such as Rac1, RhoA, and Cdc42, which are activated downstream of NMDARs, TrkB–BDNF signaling, and EphB–ephrinB interactions (Nimchinsky et al., 2002; Ethell & Pasquale, 2005; Nourbakhsh & Yadav, 2021).. These pathways promote the assembly of scaffolding proteins (e.g., Homer, Shank, SAPAP) and receptor clustering, strengthening synaptic transmission and spine stability (Ethell & Pasquale, 2005). Concurrently, glial-derived cues, such as astrocytic thrombospondins and cholesterol, further promote synapse maturation, while microglia begin to survey and refine connections (Akinlaja & Nishiyama, 2024).

Following the burst of synaptogenesis, synaptic pruning refines the CA1 network by eliminating weak or redundant synapses. This process peaks around P30–P45 in mice, coinciding with the end of adolescence, and results in a net decrease in spine density as mature circuitry is established (Semple et al., 2013; Faust et al., 2021). Activity-dependent pruning is largely mediated by microglia through the complement system (C1q–C3–CR3), which tags less-active synapses for removal (Paolicelli et al., 2011; Gomez-Arboledas et al., 2021). NMDAR activity and calcium-dependent phosphatases such as calcineurin contribute to the selective weakening of spines destined for elimination, often through LTD-like mechanisms that cause AMPA receptor internalization and spine shrinkage (Zhou et al., 2004; Ethell & Pasquale, 2005; Piochon et al., 2016). Conversely, spines that experience strong, correlated pre- and postsynaptic activity are stabilized through LTP-dependent signaling, reinforcing Hebbian refinement (De Roo et al., 2008b; Ethell & Pasquale, 2005).

3.1.3. Link to ASD

Human and animal model research increasingly indicates that atypical synaptic density and altered synaptogenesis or synaptic pruning may contribute to the pathophysiology of ASD. Recent studies using advanced brain imaging techniques have revealed that individuals with ASD often exhibit reduced synaptic density across multiple brain regions which correlates strongly with the severity of social and communication deficits characteristic of the disorder (Matuskey et al., 2024). Conversely, postmortem human studies have also demonstrated cases of excessive synaptic density linked to impaired pruning mechanisms mediated by pathways such as mTOR signaling (Tang et al., 2014). The resulting synaptic overabundance or deficit likely alters the E/I balance and impairs circuit refinement, possibly contributing to altered network connectivity and functional hyper- or hypo-connectivity observed in autistic brains (Rubenstein & Merzenich, 2003; Nomi & Uddin, 2015; Canitano & Palumbi, 2021). Alterations in synaptic density and deficits in spine maturation, synaptogenesis, and pruning have been found in a multitude of rodent models of ASD, including *FMR1* KO, *Shank3* InsG3680, *Tsc2*$^{+/-}$, and *Cntnap2* KO, supporting the findings in limited human studies (G. R. Anderson et al., 2012; Comery et al., 1997; C. Huang et al., 2023; Shimada & Yamagata, 2022) . Overall, Disruptions to spine maturation, synaptogenesis, and/or pruning can cause E/I imbalance as a deficit in excitatory spine density can lead to hypo-activity, while an excess of excitatory spine density can cause hyper-activity and an increase noise-to-signal ratios, which is consistent with the neuropathology of ASD (Gatto & Broadie, 2010; Limon & Corona-Moreno, 2025).

3.1.4 Objective and Hypothesis

In the *Mdga2*$^{+/-}$ model of ASD, there is an increase in excitatory synaptic density in the CA1 SR in adulthood but no alterations in spine length, width, or PSD area (Connor et al., 2016; D. Zhao et al., 2025). Interestingly, there is still a selective increase in excitatory synapse density in the stratum oriens (SO), SR, and SLM of the CA1 6-7 weeks following *Mdga2* conditional

knock out in CA1 pyramidal neurons at 5-6 weeks of age suggesting an ongoing role of Mdga2 in maintaining excitatory synaptic density beyond the period of synaptogenesis (X. Wang et al., 2024). This is accompanied by an increase in excitatory signaling in both *Mdga2*$^{+/-}$ and *Mdga2*-cKO models (Connor et al., 2016; X. Wang et al., 2024; D. Zhao et al., 2025), again pointing to hyperactivity contributing to alteration in E/I balance. Studies involving *Mdga2* models provide evidence from adulthood that there is a dysregulation of excitatory synaptic development, however, it is unclear if this is due to excessive synaptic formation or a deficit in synaptic pruning, both of which would contribute to increased synaptic density in adulthood. Moreover, it is possible that although there is no difference in synaptic width or PSD area in adulthood, there are transient differences in spine morphology during development that could indicate pre-mature maturation of spines, which would be consistent with disinhibition of excitatory synaptic development.

Determining the time in development when differences begin to manifest can provide valuable insight into optimal periods for intervention, which is especially useful in neurodevelopmental disorders that manifest early in life, such as ASD. Therefore, the objective of this chapter is to investigate the effect of Mdga2 reduction on synaptic spine density and morphology is the SR of the CA1 throughout the period of synaptogenesis and pruning using Golgi-Cox staining at ages P14, P21, P28, and P42. It is hypothesized that the disinhibition of excitatory synaptic development caused by a reduction in Mdga2 will lead to pre-mature spine maturation, which may lead to deficits in pruning, as well as excessive synaptogenesis. The predictions that accompany this hypothesis include: (a) an increase is spine width and higher proportion of mature spine classifications (mushroom, branched) and less immature classifications (filipodia, thin) early in development (P14-P28); (b) a higher peak synaptic density at P21; (c) a persistent increase in spine density during the period of synaptic pruning

following peak synaptic density (P28-P42); and (d) partial or complete normalization of spine length and width by P42, indicating a shift in maturation as opposed to a global change in spine morphology into adulthood.

3.2 Materials and Methods

3.2.1 Golgi-Cox Preparation

Golgi-cox staining was conducted with HET and WT littermates sacrificed at P14, P21, P28, and P42. Three mice per age and genotype were used, with the three mice per group from different litters to reduce litter effects and maximize genetic diversity. The mice were sacrificed via cervical dislocation and decapitation, followed by rapid removal of the brain. Extracted brains were rinsed and hemi-dissected, with the exception of the P14 brains, which remained intact. The brains were processed as per the instructions of the FD Rapid GolgiStain™ Kit, which included treatment with an impregnation solution containing potassium dichromate, potassium chromate, and mercuric chloride, followed by a tissue-protectant solution. Brains were coated with tissue-freezing medium (TFM^{TM}, Electron Microscopy Sciences) and flash-frozen with -70ºC isopentane and stored at -80ºC until sectioning.

3.2.2 Tissue Sectioning and Slide Preparation

Treated brains were cryosectioned with a Microm HM525 NX cryostat at a chamber temperature of -23°C. Coronal brain sections were cut sequentially from the caudal (posterior) end of the mouse brain, moving rostrally (toward the anterior) with a thickness of 100µm, which facilitates high-quality imaging of neuronal spines. The Allen Mouse Brain Atlas (Allen Institute for Brain Science, 2004) and Allen Reference Atlas – Mouse Brain (Allen Institute for Brain Science, 2011) were used as references to identify slices containing the hippocampus, which were collected and mounted onto gelatin-coated slides (FD Neurotechnologies) (Figure 3.2A). Slides were dried overnight and then stained in accordance with the FD Rapid GolgiStain^{TM} Kit (information regarding the specific chemical identity of the staining solution is

withheld as a trade secret by FD neurotechnologies). Slides were then serially dehydrated with ethanol and cleared with xylene before cover slipping.

3.2.3 Brightfield Microscopy Imaging

Images of secondary and tertiary proximal apical dendrites of CA1 pyramidal neurons were taken via brightfield microscopy with a Zeiss Axio Observer.Z1/7 microscope utilizing an Alpha Plan-Apochromat 100x/1.46 Oil DIC (UV) M27 objective lens. Dendrites were selected if they were attached to an intact primary apical dendrite and soma, and had a minimum length of 30µm (Figure 3.2). Z-stacks were taken of each dendritic segment with an optical slice thickness of 0.500µm, an exposure time of 478ms, and a light intensity of 75.7% from the transmitted light LED source. Images were acquired using an AxioCam MR R3 camera with ZEN 2.6 blue edition software.

3.2.4 Image Analysis

Images were imported into ImageJ as hyperstacks. The brightness and contrast were automatically adjusted by ImageJ, followed by the application of the unsharp mask filter with a radius of 5 pixels and a mask weight of 0.6. Hyperstacks were then converted to RGB color and exported as an image sequence. These image sequences were then imported into Reconstruct 1.1.0.0. A 20-30µm section of dendrite was selected in each sequence, and the spines on the segment were used to evaluate spine morphology and density. Head width (HW) and spine length (SL) were measured to classify spines as described in Risher et al. (2014) (Risher et al., 2014) in hierarchical order as, branched (spine contains two or more heads, manually entered), filipodia (SL>2µm), mushroom (HW>0.6µm), long-thin (SL>1µm), thin (SL/HW>1µm), or stubby (SL/HW≤1) (Figure 3.2B). Five images per animal were analyzed, for a sample size of 15 images per group. Statistical analysis was run in GraphPad Prism 9.

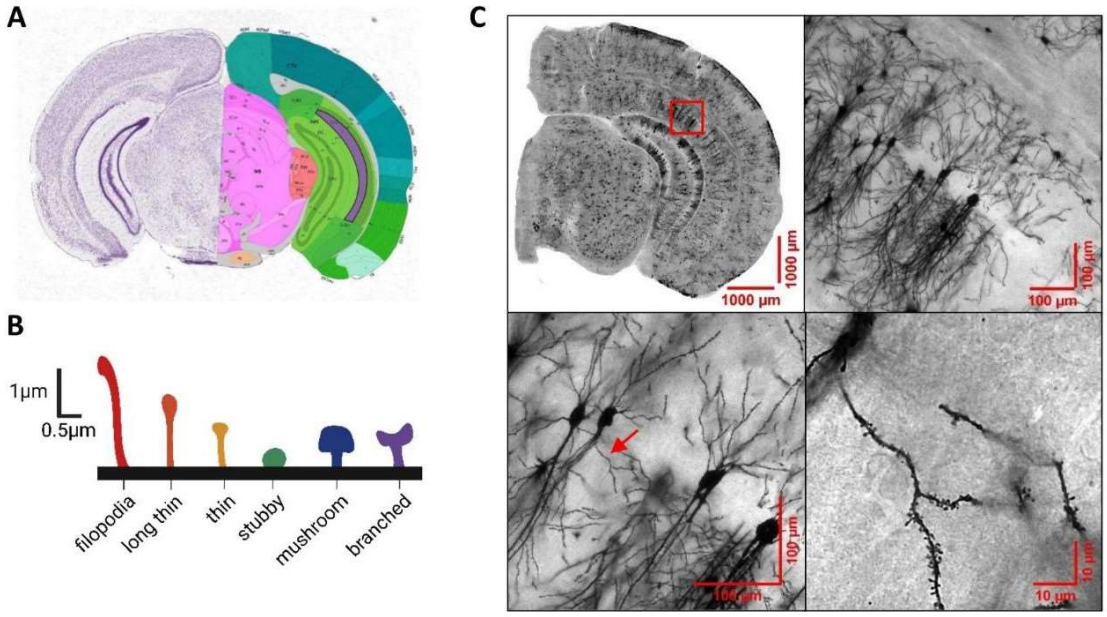

Figure 3.2. Representative images of Golgi-Cox-stained sections with CA1 pyramidal neuron isolation and dendrite selection.

(A) Reference slice from the Allen Mouse Brain Atlas and Allen Reference Atlas – Mouse Brain, anatomical annotations. The dark purple section indicates the target area, stratum radiatum of the CA1.

(B) To scale illustration of different spine types. Filopodia: longer than 2 µm; long thin spines: shorter than 2 µm and head width <0.6µm; thin spines shorter than 1 µm and head width <0.6µm; stubby spines: head width <0.6 µm and length-to-width ratio <1; mushroom spines: head width greater than 0.6µm; branched spines: containing two or more heads. Made with Biorender.com.

(C) Representative Golgi-Cox images taken with the Zeiss Axio Observer.Z1/7 microscope. Top left: Representative Golgi-Cox-stained slice using 10X magnification and tiling to encompass the entire slice. The area outlined in red represents the area of the slice shown in all images. Scale bars=1000µm (1mm). Top right: Representative image containing pyramidal neurons in the dorsal CA1 at 10X magnification. Neurons were selected if they had an intact soma and primary apical dendrite. Scale bars=100µm. Bottom left: Representative image indicating secondary and tertiary proximal apical dendrite (arrow) selected for analysis at 20X magnification. Dendrites were selected if they had a clear, unbroken origin on the primary apical dendrite and were located in the stratum radiatum. Branching patterns of the primary apical dendrite and distance from the soma were used to indicate the transition from the stratum radiatum to the stratum lacunosum-moleculare. Scale bars=100µm. Bottom right: Representative image of a secondary and tertiary segment of a proximal apical dendrite used for analysis at 100X magnification. 20-30µm was selected for analysis of spine density and morphology. Image corresponds with the area highlighted by the arrow in D. Scale bars=10µm.

3.3 Results

Spine density and morphology were analyzed from proximal apical dendrites of CA1 pyramidal neurons at P14, P21, P28, and P42 to create a spine developmental profile in the HET animals relative to WT controls. Images were taken from the dorsal and ventral hippocampus and were analyzed separately to avoid any possible confounding effects.

3.3.1 Differences in Synaptic Spine Morphology and Density in the Dorsal Hippocampus During Post-Natal Development

In the dorsal hippocampus, spine density for both WT and HET animals peaked at P21 with density in the HETs decreasing significantly again at P28, while the WT density trended downwards at P28 and P42 but did not meet significance after adjusting for multiple comparisons (One-way ANOVA; WT: $F=3.028$, $p=0.0369$; HET: $F=14.16$, $p<0.0001$; WT P14-WT P21, $p= 0.0369$, WT P21-WT P28, $p= 0.2406$, WT P21-WT P42, $p= 0.1812$, HET P21-All Het, $p<0.0001$ by Tukey's multiple comparisons test; $n=15$) (Figure 3.3A-B). Spine density was trending higher in HETs than WT at P14 (WT P14, 1.255±0.0425 spine/µm, HET P14, 1.382±0.0723 spine/µm; Unpaired t-test, $t_{28}=1.506$, $p=0.143$; $n=15$) and was significantly higher at P21 (WT P21, 1.599±0.0895 spine/µm, HET P21, 1.832±0.0671 spine/µm; Unpaired t-test, $t_{28}=2.99$, $p=0.0058$; $n=15$) (Figure 3.3C). Regarding morphology, at P14, HET slices had a significantly smaller percentage of long thin (LT) spines (WT P14 LT, 31.37%±2.31%, HET P14 LT, 18.75% ±2.27%; Unpaired t-test, $t_{28}=3.891$, $p=0.0006$; $n=15$) and a larger percentage of mushroom (mush) spines (WT P14 mushroom, 22.79%±3.22%, HET P14 stubby, 35.90% ±2.86%; Unpaired t-test, $t_{28}=3.043$, $p=0.0051$; $n=15$) relative to WT slices (Figure 3.3D). This trend switches at P21, with HETs having a higher proportion of LT (WT P21 LT, 29.68%±3.88%, HET P21 LT, 44.56%±3.19%; Unpaired t-test, $t_{28}=2.966$, $p=0.0061$; $n=15$), and a smaller proportion of mush spines (WT P21 mush, 26.41%±4.76%, HET P21 mush, 10.49%±2.44%; Unpaired t-test, $t_{28}=2.976$, $p=0.0060$; $n=15$) and branched spines (WT P21

branched, 4.03%±1.17%, HET P21 branched, 0.651%±0.291%; Unpaired t-test, t_{28}=2.805, p=0.0090; n=15) relative to WT (Figure 3.3E). The HETs maintain an elevated proportion of LT relative to WT at P28 (WT P28 LT, 26.76%±3.16%, HET P28 LT, 38.35%±3.16%; Unpaired t-test, t_{28}=2.599, p=0.0148; n=15) (Figure 3.3F), however by P42, there were no significant differences in spine types between genotypes (Figure 3.3G).

Spine length and head diameter (HD) can also provide insights into synaptic spine maturation, as spines transition from thin, elongated protrusions to shorter, bulbous structures (increased head diameter) as they mature. Following the maturation pattern observed in the spine types, the average head diameter at P14 was significantly larger in HET (WT P14 HD, 0.525µm±0.0147µm, HET P14 HD, 0.582µm±0.00876µm; Unpaired t-test, t_{28}=3.317, p=0.0025; n=15) (Figure 3.3H) but smaller at P21 relative to WT levels (WT P21 HD, 0.552µm±0.0247µm, HET P21 HD, 0.441µm±0.0138µm; Unpaired t-test, t_{28}=3.921, p=0.0005; n=15) (Figure 3.3I). No other significant differences in spine length or head diameter were observed at any age (Figure 3.3J-K). Overall, spine maturity appears to be increased in HETs at P14, followed by a dramatic increase in spine density and a decrease in immature spines at P21 relative to WT, followed by a normalization in maturation and density by P28-P42.

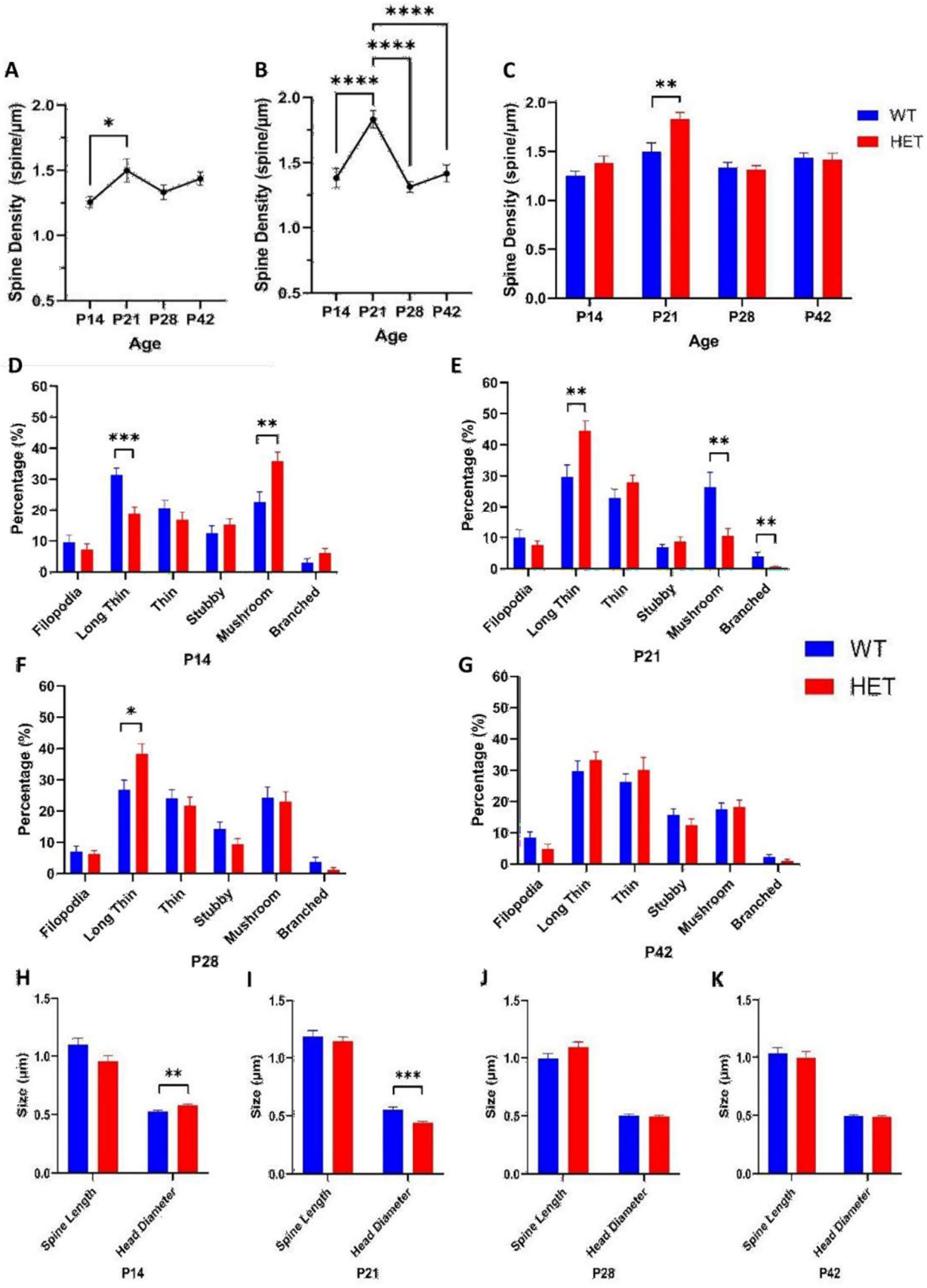
A
B
C
Spine Density (spine/µm)
Age
P14
P21
P28
P42
WT
HET
D
E
F
G
Percentage (%)
Filopodia
Long Thin
Thin
Stubby
Mushroom
Branched
H
I
J
K
Size (µm)
Spine Length
Head Diameter

Figure 3.3. Synaptic density and morphology in the *Mdga2*$^{+/+}$ (WT) and *Mdga2*$^{+/-}$ (HET) dorsal hippocampus during postnatal development.

(A-B) Synaptic density (spine/µm) of pyramidal proximal apical dendrites in the stratum radiatum within the dorsal hippocampal CA1 in (A) WT and (B) HET mice at P14, P21, P28, and P42. Synaptic density peaks in both WT and HET at P21 (One-way ANOVA; A (WT): $F=3.028$, $p=0.0369$; B (HET): $F=14.16$, $p<0.0001$; *p<0.05, ***p<0.0001 by Tukey's multiple comparisons test; n=15).

(C) Synaptic density (spine/µm) is significantly higher at P21 in HET slices compared to WT slices (WT P21, 1.599±0.0895 spine/µm, HET P21, 1.832±0.0671 spine/µm; Unpaired t-test, $t_{28}=2.99$, **p=0.0058; n=15).

(D-G) Proportion of spine types (%) in WT and HET slices at (D) P14, (E) 21, (F) 28, and (G) 42 (Unpaired T-tests with each spine type per age, *p<0.05, **p<0.01, ***p<0.001; n=15 per group)

(H-K) Average spine length and head diameter (µm) at (H) P14, (I) P21, (J) P28, and (K) P48 (Unpaired t-test, **p=0.0025, ***p=0.0005; n=15)
Error bars represent SEM.

3.3.2 Synaptic Spine Morphology and Density in the Ventral Hippocampus During Post-Natal Development

In the ventral hippocampus, there were very few to no significant differences in synaptic density and morphology – a stark contrast to the findings in the dorsal hippocampus. Across ages, neither the WT nor HET slice had a significant change in synaptic spine density from P14-P28 (One-way ANOVA; WT: F=0.4744, p=0.7014; HET: F=2.205, p=0.0976) (Figure 3.4A-B), nor were there any differences in density between genotype at any ages (Figure 3.4C). The only significant difference in morphology found was an increase in branched spines in HET slices at P21 (WT P21 branched, 0.2151%±0.2151%, HET P21 branched, 2.584%±0.840%; Unpaired t-test, t_{28}=2.732, p=0.0108; n=15), although this effect was primarily driven by the relatively low number of samples that contained branched spines, with only one sample in WT and 8 samples in HET groups out of 30 (Figure 3.4D-G). Although not reaching statistical significance, there were trends in morphology for HET samples at P28 including trends towards an increased percentage of filipodia (filo) spines (WT P28 filo, 3.406%±0.865%, HET P28 filo, 5.966%±0.921%; Unpaired t-test, t_{28}=2.030, p=0.0519; n=15) and a decreased percentage of thin spines (WT P28 thin, 34.43%±4.99%, HET P28 thin, 24.93%±2.46%; Unpaired t-test, t_{28}=1.721, p=0.0963; n=15) relative to WT controls (Figure 3.4F). However, the trend in thin spines was reversed at P42, with a trend towards HET slices having an increased percentage of thin spines relative to WT slice (WT P42 thin, 22.66%±2.76%, HET P42 thin, 29.78%±2.40%; Unpaired t-test, t_{28}=1.943, p=0.0621; n=15) (Figure 3.4G). Despite a few trends in morphological classification of spines based on maturation, the gross measures of spine maturity of spine length and head width was not significantly different between WT and HET at any age range (Unpaired t-tests, p>0.05, n=15) (Figure 3.4H-K) suggesting there was no effect of Mdga2 reduction on spine maturation, morphology, or density in the ventral hippocampus.

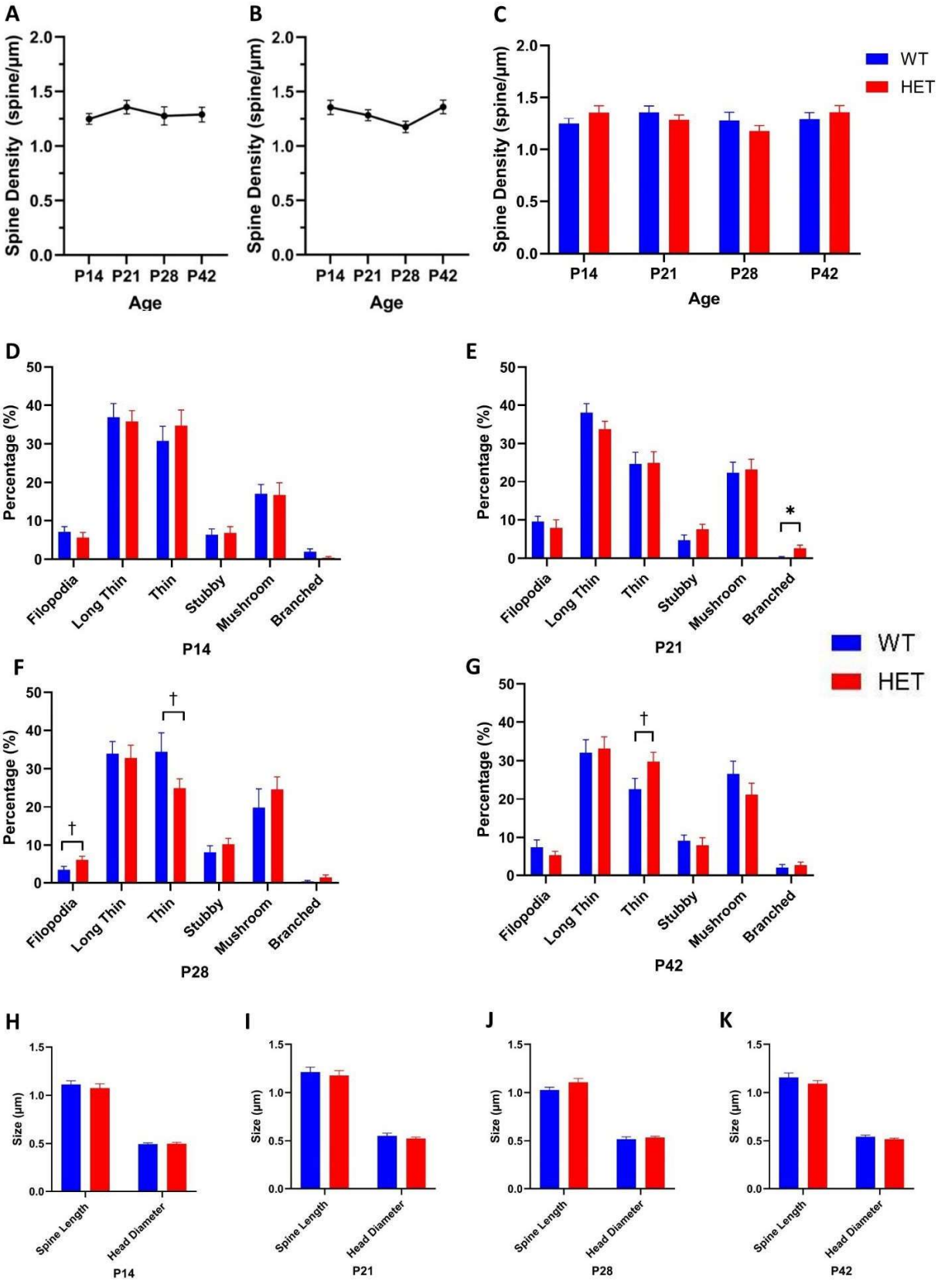
A
B
C
Spine Density (spine/µm)
2.0
1.5
1.0
0.5
0.0
P14 P21 P28 P42
Age
WT
HET
D
E
Percentage (%)
50
40
30
20
10
0
Filopodia
Long Thin
Thin
Stubby
Mushroom
Branched
P14
P21
*
F
G
†
P28
P42
H
I
J
K
Size (µm)
1.5
1.0
0.5
0.0
Spine Length
Head Diameter

Figure 3.4. Synaptic density and morphology in the *Mdga2*$^{+/+}$ (WT) and *Mdga2*$^{+/-}$ (HET) ventral hippocampus during postnatal development.

(A-B) Synaptic density (spine/µm) of pyramidal proximal apical dendrites in the stratum radiatum within the hippocampal CA1 in (A) WT and (B) HET mice at P14, P21, P28, and P42. No significant differences were found between ages, with WT slices trending towards peaking at P21. (One-way ANOVA with Tukey's multiple comparisons test; n=15).

(C) No significant differences in synaptic density (spine/µm) were found between WT and HET slices. (Unpaired t-test, n=15).

(D-G) Proportion of spine types (%) in WT and HET slices at (D) P14, (E) 21, (F) 28, and (G) 42 (Unpaired T-tests with each spine type per age; †$p<0.1$, *$p<0.05$; n=15 per group)

(H-K) No significant differences were found in average spine length and head diameter (µm) between WT and HET at (H) P14, (I) P21, (J) P28, and (K) P48 (Unpaired t-test; n=15) Error bars represent SEM.

3.4. Discussion

In the dorsal SR of the CA1, as predicted, Golgi-Cox staining revealed an increase in mature stubby spine density and a decrease in less mature long-thin spines at P14 relative to wild-type. This was accompanied by a larger head width in spines, which is also indicative of increased spine maturation (Borczyk et al., 2019). Accordingly, a reduction of Mdga2 may lead to increased spine maturity by disrupting its role as a synaptic suppressor at glutamatergic synapses. Mdga2 normally constrains excitatory synapse formation and function by inhibiting neuroligin-neurexin interactions, which are critical for synaptogenesis (Connor et al., 2019; Elegheert et al., 2017; Krueger et al., 2012; Pettem et al., 2013). When Mdga2 is deficient, this suppression is lifted, resulting in upregulated excitatory synapse density and enhanced AMPAR recruitment and currents (Connor et al., 2016; X. Wang et al., 2024, p. 20; D. Zhao et al., 2025).

The corresponding increase in synaptic activity and glutamate release may drive excessive activity-dependent maturation of spines, characterized by increased AMPAR levels and stabilization of postsynaptic components, such as PSD-95, which is a scaffolding protein known to be elevated in *Mdga2*$^{+/-}$ mice in adulthood (C.-C. Chen et al., 2014; Connor et al., 2016; X. Wang et al., 2024; D. Zhao et al., 2025). Concurrently, MDGA2 loss aberrantly activates BDNF/TrkB signaling, promoting actin cytoskeleton reorganization (via Rac1/Cdc42), which can enlarge spine heads (Costa et al., 2020), consistent with the increased head diameter seen at P14. At P21, there is a higher density of synaptic spines which suggests that synaptogenesis is disinhibited; however, unexpectedly, there is a higher proportion of immature spines in HETs relative to WT controls. This is likely due to the influence of the excessive growth of new spines that is occluding the influence of the more mature spines that began developing at P14. This effect can be explained by distinguishing two populations of spines that are differentiated by their pattern of development.

Here, it is proposed that at P14, we observe the first population of spines, which follows the expected pattern of increased maturation in HETs. Between P14 and P21, which is known to be during the period of peak synaptogenesis in the mouse hippocampus (Semple et al., 2013), there is an emergence of a second population of newly formed, immature synapses that are generated at a much higher frequency due to the reduction of Mdga2. Therefore, although the first population of more mature spines is still present, the explosion of new synaptic spines drives the overall percentage to be more immature while concurrently driving the overall synaptic density to a much higher level than observed in the WT controls at P21. Overall, increased mature spines at P14 and increased density and immature spines at P21 in HET animals can be accounted for by a reduction of Mdga2 in the hippocampus (Figure 3.5).

Following the peak density at P21, the morphology and density of spines do appear to normalize by P28-P42, countering the initial prediction that synaptic pruning would be impaired by a reduction of Mdga2 due to premature synapse maturation. However, the increase in synaptic spine density at P21 suggests that there would be an increase in glutamatergic signaling and inputs, which in turn likely drives activity-dependent recruitment of astrocytes and coordinated pruning mechanisms. Elevated synaptic activity at P21 likely increases ATP release and calcium signaling in astrocytes, prompting them to secrete transforming growth factor-beta (TGF-β), which induces neuronal C1q expression to tag excess synapses for pruning (Faust et al., 2021; Gomez-Arboledas et al., 2021; Kouser et al., 2015). This homeostatic mechanism may compensate for the excessive synapses formed at P21 to return the overall density to WT levels. This can also be connected to the hypothesis of dual spine populations; it is more likely that the excessive immature spines, previously referred to as population two, are the spines being primarily pruned (C.-C. Chen et al., 2014), as immature spines are preferentially pruned due to structural instability and higher levels of C1q/C3 complement tagging compared to mature spines

because their low synaptic activity (reduced AMPAR/NMDAR signaling) fails to suppress complement activation (Faust et al., 2021). This would allow the more mature synapses observed at P14 to continue to be strengthened in an activity-dependent manner, while the newer, less mature synapses observed at P21 are pruned at a higher rate. This is consistent with findings that stable spines formed before adolescence remain in adulthood, while newly formed spines are more likely to be eliminated (C.-C. Chen et al., 2014).

It is worth noting that the normalization of density by P42 does not align with some studies that have observed increased excitatory synaptic density in adulthood via electron microscopy and immunohistochemistry (Connor et al., 2016; D. Zhao et al., 2025). This could be due to differences in technique, where spine density on an individual dendrite was analyzed as opposed to synaptic density per square area. An increase in dendritic arborization may lead to increases in cross-sectional density as opposed to linear density, which is supported by the finding that *Mdga2* KO in cultured hippocampal neurons leads to a significant increase in dendritic branching (S. Kim et al., 2024). To confirm if this is the case in *Mdga2*$^{+/-}$ mice, Sholl analysis should be conducted to determine if there is an increase in branch intersections in the SR during development and adulthood. On the other hand, increased synaptic density has been observed in *Mdga2* condition knockout (cKO) models at 11-13 weeks, followed by cKO in excitatory CA1 neurons at 5-6 weeks (X. Wang et al., 2024). This suggests that Mdga2 reduction can cause a transient increase in synapse density following the critical periods of synaptogenesis and pruning, which may cause a re-emergence of the phenotype when microglial pruning is less active. This could be investigated by the addition of mice at ~12 weeks of age in the Golgi-Cox analysis.

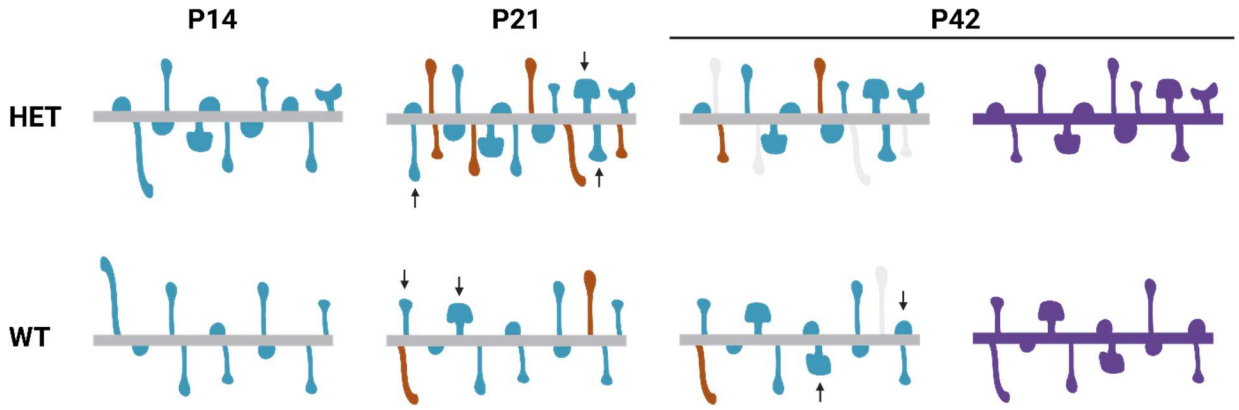

Figure 3.5. Proposed synaptic spine development model in the dorsal hippocampus of *Mdga2*$^{+/-}$ (HET) mice and *Mdga2*$^{+/+}$ (WT) controls. Orange spins represent newly formed spines, grey spines represent pruned spines, and arrows indicate maturation events of spines. Made with Biorender.com.

Unexpectedly, there were no significant differences in synaptic density or notable differences in morphology in the ventral CA1. In fact, although there was a slight trend of increased synaptic density at P14, there were no significant differences in synaptic density in the WT control group between any ages, and there was no observable trend of synaptogenesis or pruning in the *Mdga2*$^{+/-}$ SR. Although there is no literature directly comparing synaptogenesis and pruning in the dorsal and ventral hippocampus, there are some studies that can point to possible contributions to these observations. A study by Lee et al. (2017) conducted RNA-seq-based transcriptomic analysis of developing rat hippocampi at postnatal days P14, P28, and P45 and found differential expression of genes involved in synaptic function. They report that genes associated with LTP and glutamatergic synapses are more highly expressed in the dorsal hippocampus, while genes related to GABAergic and cholinergic synapses are enriched in the ventral hippocampus during these developmental stages. This implies region-specific developmental timing or mechanisms of synapse development along the dorsal-ventral axis, and that glutamatergic synapses, which are primarily located on synaptic spines, may be enriched in the dorsal hippocampus (A.-R. Lee et al., 2017). This may partly explain why the pattern of synaptogenesis is more apparent in the dorsal hippocampus.

Moreover, a related process, neurogenesis, is enhanced in the dorsal hippocampus relative to ventral in canines (Lowe et al., 2015), and is selectively impaired in the ventral and not dorsal hippocampus in *Iqsec2* KO and *Nlgn3*-R451C KI mouse models of ASD (Sun et al., 2024). Both synaptogenesis and neurogenesis share a common final signaling pathway mediated by phosphorylation of the transcription factor cyclic-AMP Response Element Binding Protein (CREB), which increases BDNF levels which is crucial for both processes (Tchantchou et al., 2009). Therefore, enhanced neurogenesis in the dorsal hippocampus may suggest enhanced synaptogenesis-linked processes as well. It is peculiar that a reduction of Mdga2 leads to such a

pronounced increase in synaptic density in the dorsal, but not the ventral hippocampus as P21, and requires additional lines of investigation. This should include elucidating dorsal-ventral expression patterns of Mdga2 in the hippocampus and comparative analysis of genes or proteins which are differentially expressed in the hippocampus of *Mdga2*$^{+/-}$ mice that are also differentially expressed across the dorsal-ventral axis. Overall, a reduction of *Mdga2*$^{+/-}$ enhances excitatory synaptogenesis and early spine maturation selectively in the dorsal hippocampus from P14-P21, which then normalizes by P42, indicating that there are transient effects of Mdga2 reduction in early postnatal neural development.

Chapter 4: Characterizing Proteomic and Phosphoproteomic Profiles of Hippocampus CA1 Synaptoneurosomes

4.1 Introduction

4.1.1. Synaptoneurosome Proteomic and Phosphoproteomic Application

Synaptoneurosome isolation and peptide mass spectrometry (MS) enable researchers to investigate the protein composition of intact pre- and postsynaptic structures from harvested brain tissues. This preparation method involves homogenizing brain tissue and separating it using a mesh filter during centrifugation to preserve sealed synaptic terminals while removing nuclei and large cellular debris (Dieterich & Kreutz, 2016). Because synaptoneurosomes contain both presynaptic boutons loaded with vesicles and postsynaptic densities anchored to dendritic membranes, they provide a comprehensive view of bidirectional communication across the synapse. It is worth noting that this preparation is derived from the whole neuropil (complete network of neurons and glial cells); therefore, there is likely inclusion of a small proportion of astrocytic and glial components that closely interact with neuronal synapses, such as astrocyte end feet, although this proportion is much less than the approximately 50% that would be included in a whole tissue homogenate (Gulyássy et al., 2020).

Mass spectrometry–based proteomics has become a valuable tool for profiling large-scale protein alterations within such synaptic fractions. Unlike targeted biochemical assays, proteomics offers an unbiased, discovery-driven approach that does not rely on pre-defined targets or candidate molecules (Dieterich & Kreutz, 2016). This is particularly valuable in ASD research, where multiple cellular and molecular pathways may converge to alter synaptic structure and function, and there have been a multitude of dysregulated processes linked to ASD pathology, including oxidative stress, protein synthesis and degradation, synaptogenesis and pruning, E/I imbalance, neuroinflammation, lipid metabolism, and more (E. Lee et al., 2017; Anashkina & Erlykina, 2021; X. Liu et al., 2022; Leisman & Melillo, 2025). By quantitatively

measuring thousands of synapse-enriched proteins simultaneously, mass spectrometry provides a systems-level map of protein expression changes that can reveal unanticipated molecular mechanisms or signaling networks disrupted in ASD models (Dieterich & Kreutz, 2016; Oostrum et al., 2023). By identifying pathways and biological processes that are consistently altered across different ASD models, this approach can highlight shared molecular mechanisms and potential therapeutic targets that extend beyond mutation-specific forms of the disorder (Carbonell et al., 2023).

Proteomics complements transcriptomic approaches such as RNA sequencing by directly measuring the translated products that ultimately carry out cellular function. While mRNA abundance can suggest transcriptional regulation, it does not necessarily reflect protein expression, stability, or turnover. Many transcripts undergo post-transcriptional regulation, local translation, or degradation that decouple mRNA levels from protein abundance (Schwanhäusser et al., 2011). Thus, proteomic data provide a more accurate picture of which molecules are present and functional at the synapse, particularly in conditions like ASD where translational control and protein degradation pathways are often dysregulated (Leisman & Melillo, 2025).

Combining global proteomic data with phosphoproteomic analyses adds another dimension by capturing dynamic post-translational modifications that regulate signaling at the synapse. Phosphorylation modulates protein activity, subcellular localization, and protein–protein interactions, making it a key regulator of synaptic plasticity and neurotransmission (Schulman, 1995; Zhong et al., 2023). Phosphoproteomic enrichment strategies enable identification of phosphorylated residues across thousands of proteins, revealing coordinated changes in kinase and phosphatase activity that may underlie altered synaptic signaling (Gerritsen & White, 2021). In eukaryotic systems, phosphorylation predominantly occurs on serine (~86%), threonine (~12%), and tyrosine (~2%) residues, owing to the hydroxyl groups in

their side chains that serve as substrates for protein kinases (Zhong et al., 2023). These three amino acids are routinely detected and quantified in mass spectrometry workflows, which can reveal activation states of pathways that may not have over- or under-expressed proteins, making it a very complementary analysis to proteomic expression level analysis.

Together, the integration of synaptoneurosome isolation with advanced mass spectrometry–based proteomics and phosphoproteomics provides a powerful, unbiased framework for dissecting the molecular architecture of the synapse. In the context of neurodevelopmental disorders such as ASD, this approach enables identification of protein- and pathway-level alterations that cannot be inferred from transcriptomic data alone, ultimately offering a clearer understanding of how synaptic signaling, structure, and plasticity become dysregulated.

4.1.2. Objective

As discussed, proteomic and phosphoproteomic analyses provide a robust data set that can indicate dysregulated proteins and pathways in neural tissue. Therefore, the purpose of this chapter is to utilize synaptoneurosome preparations in combination with liquid-chromatography and mass spectrometry to identify up- and down-regulated as well as hyper- and hypo-phosphorylated proteins in the CA1 of *Mdga2*$^{+/-}$ mice. The objective of this analysis is to use this data to identify pathways and cascades that may be dysregulated and that may contribute to the alterations in LTD (see chapter 2) and excitatory synapse development (see chapter 3), and identify other biomarkers of ASD that may be present in the *Mdga2*$^{+/-}$ mouse model.

4.2 Materials and Methods

4.2.1. CA1 Tissue Collection

P14, P21, P28, and P42 WT and HET mice were selected for CA1 tissue harvesting. Three mice per age and genotype were used, with the three mice per group from different litters to reduce litter effects and maximize genetic diversity. 400 µM transverse hippocampal slices were obtained as described in Chapter 3, methods, slice preparation. The CA1 was isolated via microdissection in a petri dish containing 4ºC aCSF. Eight ventral and eight dorsal CA1 sections were isolated per animal. Samples were flash-frozen with dry ice and ethanol in 1.5mL centrifuge tubes and stored at -80ºC. Ventral and dorsal samples were stored and processed separately.

4.2.2. Hippocampal Synaptoneurosome Isolation

The CA1 hippocampal tissue was homogenized in chilled 1X Krebs buffer (pH 7.4) using a glass homogenizer, followed by dilution and incubation on ice to facilitate gravity separation of nuclear material. The homogenate was filtered through a pre-wetted 5.0µm filter and centrifuged at 20,000g for 15 minutes at 4°C. The synaptoneurosome fraction (pellet) was then re-suspended in 6M urea/50mM Tris-HCl (pH 8). Protein reduction was performed by adding dithiothreitol to a final concentration of 5mM, followed by incubation at 37°C for 30 minutes. Alkylation was achieved by adding iodoacetamide to a final concentration of 15mM and incubating at room temperature in the dark for 30 minutes. For protease digestion, 10µL samples were diluted with Tris-HCl buffer (50mM, pH 8) and incubated overnight at 37°C in the presence of Trypsin/Lys-C mix (~25:1 protein-to-protease ratio). Digestion was terminated with 10% trifluoroacetic acid (TFA) to a final concentration of 1%, followed by centrifugation at 16,000g for 10 minutes at room temperature. The supernatant containing peptides was collected and stored at –20°C until peptide clean-up. Peptide cleanup was performed using C18 ZipTips. Tips were pre-wetted with acetonitrile, equilibrated with 0.1% TFA, and peptides were bound by repeated aspiration and

dispensing of 0.1% TFA. Bound peptides were washed and eluted with 50% acetonitrile/0.1% TFA. The eluate was diluted with LC-MS water and stored at –80°C. Peptide recovery was estimated to be 50–75%, yielding a final concentration of 0.5–1 µg/µL (Figure 4.1).

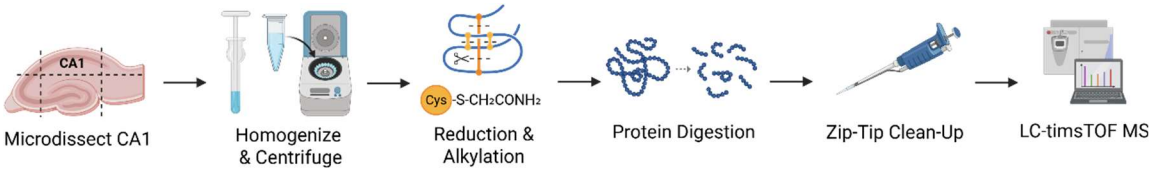

Figure 4.1. Synaptoneurosome preparation overview. Micro-dissected CA1 tissue underwent synaptosome isolation via homogenization and centrifugation. Proteins were reduced, alkylated, and digested to generate peptide fragments. Peptide cleanup was performed with C18 ZipTips. Diluted samples were sent out for liquid chromatograph-mass spec analysis.

4.2.3. TimsTOF Mass Spectrometry and Protein Detection

Samples were sent to the YSCi Core Mass Spectrometry Facility, Department of Chemistry, Faculty of Science at York University for mass spectrometry analysis. Samples underwent liquid chromatography–mass spectrometry (LC-MS) using a timsTOF Pro 2 system with a 50cm column and a 90-minute gradient. Two technical replicates were performed per sample. Peptide fragment identification was carried out in Bruker Proteoscape by matching acquired spectra against an in-house spectral library that was previously generated in the Connor lab with mouse CA1 hippocampal synaptoneurosomes. A false discovery rate of 0.05 was set for precursor, peptide, and protein detection/integration. Data reports containing protein-level outputs were received from the YSCi Core Mass Spectrometry Facility, where the numerical values for each protein were reported as integrated chromatographic peak areas inferred from the detected peptides. These peptide peak areas were aggregated to generate a single area value per protein, providing an estimate of its relative abundance in the sample. In cases where peptide origin was ambiguous (i.e., the sequence could be assigned to more than one protein), the output reported a list of all plausible protein matches for that peptide. These fragments were excluded from the analysis to avoid misidentification of up- or down-regulated proteins. Two analyses were run – one analysis identified peptide fragments regardless of post-translational modifications (proteomic analysis), and one analysis identified peptides with phosphorylated serine, threonine, and/or tyrosine (STY) residues (phosphoproteomic analysis). While the proteomics analysis provides insight into basal translation and functional protein levels, phosphoproteomic analysis can provide additional insight into the activation states of proteins and pathways, as phosphorylation is a common mechanism of protein activation and deactivation.

4.2.4. Data Analysis

The peptide peak areas per protein of the two technical replicates for each sample were averaged for analysis. Metaboanalyst 6.0 (Pang et al., 2024) was used to identify up- and down-regulated (proteomic), and increased and decreased levels of phosphorylated proteins in HET samples relative to WT in each age group, with a minimum threshold of a 1.5X fold change (FC) and p-value of 0.05. The proteomic and phosphoproteomic data were normalized using logarithmic transformation with base 10. Next, proteins unique to the phosphoproteomic dataset—those absent from the total proteome analysis—were identified, as these represent an increase in phosphorylation rather than global protein upregulation. This protein list was then used in the phosphorylation analysis, reflecting proteins that were either more commonly phosphorylated or dephosphorylated in the HET samples compared to WT controls. Gene ontology (GO) analysis was run using the Database for Annotation, Visualization, and Integrated Discovery (DAVID) (D. W. Huang et al., 2009b, 2009a) to identify biological processes associated with the up- and down-regulated proteins (proteomics analysis) and proteins with altered phosphorylation states (phosphoproteomic analysis). GO enrichment was performed for Biological Process (BP) terms using a "FAT" (filtered) GO category to remove broad, non-specific terms. The Expression Analysis Systematic Explorer (EASE) threshold was set at 0.05 (conservative modified Fisher's exact p-value) with a minimum gene (protein) count of 3 for robust enrichment with adequate representation by multiple proteins per term. Due to small protein lists, a false discovery rate correction could not be applied. To remove redundancy in the presented results and figures, for each data set, GO terms that shared identical protein lists and had high semantic similarity (ex. intracellular monoatomic ion homeostasis and monoatomic ion homeostasis) were filtered such that only the term with the strongest statistical support (lowest adjusted p-value) was retained. Moreover, as proteins have multiple functions at different developmental periods and locations in the body, GO terms that involve other areas of the body not relevant to the hippocampus (ex. spermatid development) or terms relating to prenatal time periods (ex. in utero embryonic development) were excluded from figures and the results section. The full outputs of the GO analyses, including the excluded and filtered terms, are included in Appendix C and Appendix D Horizontal bar plots to visualize GO analysis results were created in Excel.

4.3. Results

4.3.1. Differential Protein Expression and Phosphorylation in the CA1

Proteomic analysis was conducted in dorsal and ventral regions of the CA1 hippocampus from WT and HET mice across four developmental time points (P14, P21, P28, and P42) using LC-timsTOF MS. Representative images illustrate the transverse hippocampal slices used for regional analysis, with the increased size of ventral CA1 tissue highlighted (Figure 4.2A). Quantification revealed no significant differences in the number of unique protein groups detected between dorsal and ventral CA1 within each genotype at any age. However, ventral CA1 consistently exhibited a greater total number of proteins than dorsal CA1 at all ages, which likely reflects the larger tissue volume present in ventral slices (Two-way ANOVA, region $p<0.0001$, genotype $p>0.2$; Tukey's multiple comparison test, dorsal-ventral $p<0.001$, dorsal-dorsal and ventral-ventral $p>0.5$; $n=6$ per group) (Figure 4.2). Therefore, it is permissible to compare protein expression and phosphorylation between genotypes within a hippocampal region, but not across regions, due to significant differences in protein group detection between the dorsal and ventral CA1. Quantification of Mdga2 confirmed a significant reduction in expression in both dorsal and ventral CA1 from P14 to P42 in HET mice at all ages, validating the reduction in Mdga2 at the time points investigated (Table 4.1).

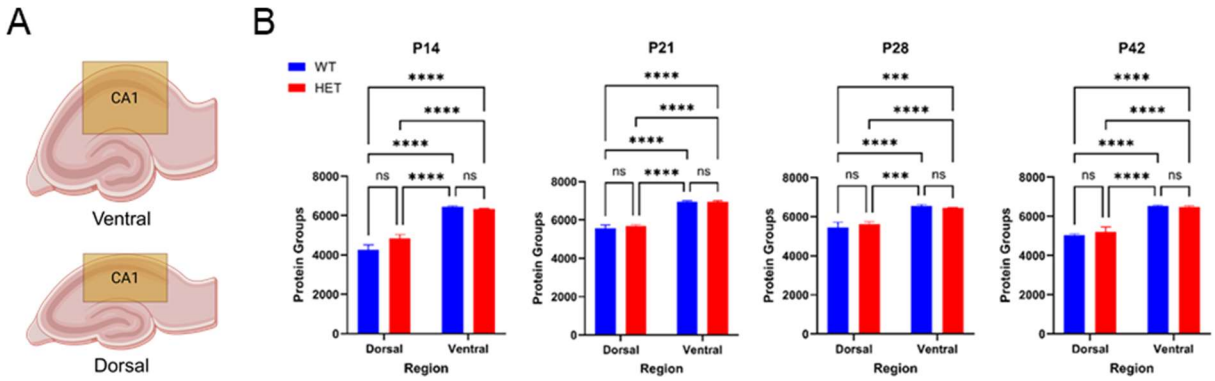

Figure 4.2. Quantity of unique protein groups detected in the ventral and dorsal CA1 by LC-timsTOF MS in the proteomic analysis in WT and HET groups at P14, P21, P28, and P42.

(A) Representative illustrations of a ventral and a dorsal transverse hippocampal slice with the CA1 highlighted in yellow to demonstrate the increased amount of CA1 tissue in ventral slices.

(B) There are no differences in the number of protein groups detected within regions (dorsal vs. ventral) at any age. There are significantly more protein groups detected in the ventral CA1 than the dorsal CA1 at all ages, likely due to an increase in CA1 size. Samples include two injections per preparation (Two-way ANOVA, region $p<0.0001$; n=6 per group, Tukey's multiple comparison test, ***$p<0.001$, ****$p<0.0001$).

Table 4.1. MDGA2 is significantly reduced in the dorsal and ventral CA1 from P14-P42 in *Mdga2*$^{+/-}$ mice when quantified by LC-timsTOF MS. Fold change is defined as expression in *Mdga2*$^{+/-}$ CA1 tissue divided by expression in *Mdga2*$^{+/+}$ CA1 tissue. Calculations ran in Metaboanalyst 6.0.

Age	CA1 Region	Fold Change	p-value
P14	Dorsal	0.564	0.00440
	Ventral	0.651	0.00689
P21	Dorsal	0.633	0.0115
	Ventral	0.673	0.0138
P28	Dorsal	0.542	0.00787
	Ventral	0.580	0.00105
P42	Dorsal	0.601	0.0260
	Ventral	0.689	8.96E-05

Quantitative analysis identified considerable changes in both protein and phosphorylation states in HET tissue relative to WT controls. The threshold for inclusion was set at a minimum fold-change of 1.5 to ensure biological relevance. Across all ages and regions, the number of down- and up-regulated proteins was variable, with ventral CA1 generally presenting a greater degree of differential expression relative to dorsal CA1, although this was again likely due to the difference in protein group detection. Interestingly, there was a general trend of more up-regulated proteins in the dorsal CA1 and more down-regulated proteins in the ventral CA1 across ages (Table 4.2). Analysis of phosphorylation states revealed distinct patterns of phosphorylation across regions and ages. Notably, ventral CA1 exhibited a more robust change in phosphorylation states of proteins than dorsal CA1, particularly at earlier timepoints (Table 4.3).

Table 4.2. Quantity of up- and down-regulated proteins in *Mdga2*$^{+/-}$ CA1 tissue relative to *Mdga2*$^{+/+}$ CA1 tissue. Proteins included have a minimum fold-change of 1.5 and a p-value ≤0.05. Analysis run in Metaboanalyst 6.0.

Proteins				
Age	Dorsal CA1		Ventral CA1	
	Down	Up	Down	Up
P14	13	37	84	36
P21	23	15	49	36
P28	9	25	25	21
P42	21	40	22	15

Table 4.3. Quantity of proteins that have an increased expression in their phosphorylated (up) and dephosphorylated (down) state in *Mdga2*$^{+/-}$ CA1 tissue relative to *Mdga2*$^{+/+}$ CA1 tissue. Proteins included have a minimum fold-change of 1.5 and a p-value ≤0.05. Proteins that were also up- or down-regulated with a fold-change of at least 1.5X are excluded. Analysis run in Metaboanalyst 6.0.

Phosphorylation				
Age	Dorsal CA1		Ventral CA1	
	Down	Up	Down	Up
P14	8	20	33	34
P21	10	15	25	32
P28	8	19	23	5
P42	12	34	14	14

4.3.2. Gene Ontology Analysis of Biological Processes

To determine the biological relevance of up- and down-regulated and changes in phosphorylation, GO analyses were run using the DAVID functional annotation tool at all ages for dorsal (Figure 4.3-4.4) and ventral tissues (Figure 4.5-4.6). Relevant GO terms are presented in Figure 4.3-4.6; for the full output of the DAVID GO analyses, see Appendix C and Appendix D. The output for these analyses provided a robust set of GO terms. For interpretation, the following themes are outlined below: (1) ion & protein transport and homeostasis, (2) cellular structure and development, (3) synaptic signaling, (4) oxidative stress and inflammation/damage response, (5) ubiquitination and protein catabolism, and (6) protein translation and modification. Please note that this list does not strictly include all GO terms presented within the figures.

Ion & protein transport homeostasis GO terms

Results of the GO analyses suggest an early onset of ion dysregulation in the dorsal hippocampus of *Mdga2*$^{+/-}$ mice. Ion-related GO terms were recurrently enriched in the dorsal CA1 (Figure 4.3). At P14 dorsal CA1, there was a significant up-regulation of proteins and phosphorylation of proteins associated with ion transport (ex. *monoatomic ion transport*, *regulation of membrane potential*, etc.) and regulation of overall *ion homeostasis* (Figure 4.3A, 4.4A). Additionally, proteins associated with protein handling processes, such as *establishment of protein localization* and *intracellular protein transport*, are down-regulated, with this effect

persisting through P21 in the dorsal CA1 (Figure 4.3A-B). Together, these results indicate that a reduction in Mdga2 may affect ion and protein-handling pathways in a regionally specific manner, with early alterations manifesting specifically in the dorsal CA1.

Cellular structure and development

Results of the GO analyses reveal progressive disruptions in cellular architecture and neuronal development across ages and regions in *Mdga2*$^{+/-}$ mice. In the dorsal CA1, increases in phosphorylated proteins were associated with *regulation of developmental growth* and *negative regulation of organelle organization* at P14 (Figure 4.4A). By P21, down-regulated proteins prominently featured structural terms within broader contexts, including *regulation of cellular component organization* and *cellular localization,* among others (Figure 4.3B), and at P28, down-regulated proteins were broadly associated with *cell development* (Figure 4.3C). At P42, the trend of changes in structural development and dysregulation continued, with increases in phosphorylated proteins associated with terms such as *regulation of neuron projection development* and *regulation of cell projection organization* (Figure 4.4D).

The ventral hippocampus exhibited sustained developmental remodeling. At P14, up-regulated proteins were associated with *neuron projection morphogenesis, cell morphogenesis involved in neuron differentiation, nervous system development*, and *regulation of cell development* (Figure 4.5A), while proteins with decreased phosphorylation levels were associated with *organelle organization* (Figure 4.6A). At P21, down-regulated proteins were associated *with cell morphogenesis involved in neuron differentiation* (Figure 4.5C), and an increase in phosphorylation of proteins associated with *microtubule cytoskeleton organization* (Figure 4.6B). At P28, up-regulated proteins were involved in *neuron development*, *neuron projection development*, *cell morphogenesis involved in neuron differentiation*, and *plasma membrane-bound cell projection organization* (Figure 4.5C). At P42, down-regulated proteins were associated with *cytoskeleton*

organization, *plasma membrane bounded cell projection organization, regulation of organelle organization*, *negative regulation of cellular component organization*, and *organelle organization* (Figure 4.5B). Together, these findings demonstrate that a reduction of Mdga2 impairs neuronal morphogenesis, organelle instability, and general dysregulation of cellular development processes.

Synaptic signaling

Results of the GO analyses reveal progressive disruptions in synaptic organization and transmission across ages and regions in *Mdga2*$^{+/-}$ mice. In the dorsal CA1, up-regulated proteins at P14 were associated with *anterograde trans-synaptic signaling*, *regulation of membrane potential, regulation of exocytosis*, and *regulation of secretion by cell* (Figure 4.3A). At P21, there is a shift to a down-regulation of proteins associated with *positive regulation of signaling* and *intracellular signaling cassette* (Figure 4.3B). At P42, additional down-regulated proteins were associated with *vesicle docking*, *anterograde trans-synaptic signaling*, *chemical synaptic transmission*, and *cell-cell signaling* (Figure 4.3D). Overall, in the dorsal hippocampus, there is a shift from an upregulation to a later downregulation of proteins involved in synaptic signaling, suggesting dynamic dysregulation of these processes across development.

The ventral hippocampus exhibited later changes in synaptic organization. At P21, down-regulated proteins were associated with *regulation of neuronal synaptic plasticity, regulation of synapse organization*, *regulation of synaptic plasticity*, *synapse organization, learning or memory,* and *circadian rhythm,* among others (Figure 4.5C). At P42, down-regulated proteins continued to show associations with *plasma membrane bounded cell projection organization* within structural contexts (Figure 4.5B). Together, these findings demonstrate that a reduction of Mdga2 compromises trans-synaptic communication through early dorsal transmission and ventral plasticity and organizational impairments.

Oxidative stress and inflammation/damage response

Results of the GO analyses reveal early activation of stress pathways that intensify across development in *Mdga2*$^{+/-}$ mice. In the dorsal CA1, there was an upregulation of proteins at P14 involved in *aerobic respiration* and an increase in phosphorylated proteins associated with *response to oxidative stress, cellular response to chemical stimulu*s, and *intracellular monoatomic cation homeostasis* (Figure 4.4A). At P21, down-regulated proteins were associated with *regulation of inflammatory response*, *cellular response to nitrogen compound*, and *response to nitrogen compound* (Figure 4.3B). The ventral hippocampus showed progressive stress engagement. At P14, up-regulated proteins were associated with *cellular response to stress,* and down-regulation of proteins associated with *programmed cell death* and *apoptotic processes* (Figure 4.5A). At P21, up-regulated proteins continued associations with *cellular response to stress* and *response to stress* (Figure 4.5C), and at P42, there was a decrease in phosphorylation of proteins associated with *cellular response to stress* (Figure 4.5B). Together, these findings demonstrate that a reduction of Mdga2 triggers acute dorsal oxidative stress and chronic dysregulation of ventral damage responses.

Ubiquitination and protein catabolism

Results of the GO analyses reveal compensatory or dysregulated protein degradation pathways across development in *Mdga2*$^{+/-}$ mice. In the dorsal CA1, down-regulated proteins at P21 were associated with *protein polyubiquitination* and *protein modification process* (Figure 4.3B). At P42, this shifted to an up-regulation of proteins associated with *protein K48-linked ubiquitination*, *protein polyubiquitination*, and *protein modification by small protein conjugation or removal* (Figure 4.3D). The ventral hippocampus activated catabolic pathways earlier and more robustly. At P14, up-regulated proteins were associated with *protein K48-linked ubiquitination,* while down-regulated proteins showed *ERAD pathway* associations (Figure 4.5A). At P21, up-regulated proteins were associated with *proteasome-mediated ubiquitin-dependent protein catabolic process*, *protein*

modification by small protein conjugation, and *protein ubiquitination* (Figure 4.5C). At P42, up-regulated proteins continued associations with *post-translational protein modification* and *protein modification process* (Figure 4.5B). Together, these findings demonstrate that a reduction of Mdga2 upregulates degradation pathways, potentially as compensation for proteome stress.

Protein translation and modification GO terms

Results of the GO analyses reveal translational and modification adjustments supporting proteome adaptation or dysregulation in *Mdga2*$^{+/-}$ mice. In the dorsal CA1, up-regulated proteins at P28 were associated with *tRNA processing*, *regulation of mRNA splicing via spliceosome*, and *regulation of mRNA metabolic process* (Figure 4.3B). At P42, up-regulated proteins showed associations with *protein modification by small protein conjugation or removal* (Figure 4.3D). The ventral hippocampus exhibited prominent translational signatures from early development. At P14, down-regulated proteins were associated with *cytoplasmic translation* and *peptidyl-tyrosine phosphorylation* (Figure 4.5A). At P21, up-regulated proteins showed *protein modification* process associations (Figure 4.5C). At P42, up-regulated proteins were strongly associated with *post-translational protein modification*, *protein modification process*, and *positive regulation of macromolecule metabolic process* (Figure 4.5B). Together, these findings demonstrate that a reduction of Mdga2 drives translational changes at synapses, potentially to compensate for disrupted protein homeostasis and maintain synaptic structure and function in the face of ongoing cellular stress, or due to aberrantly increased activation of synaptic translation pathways.

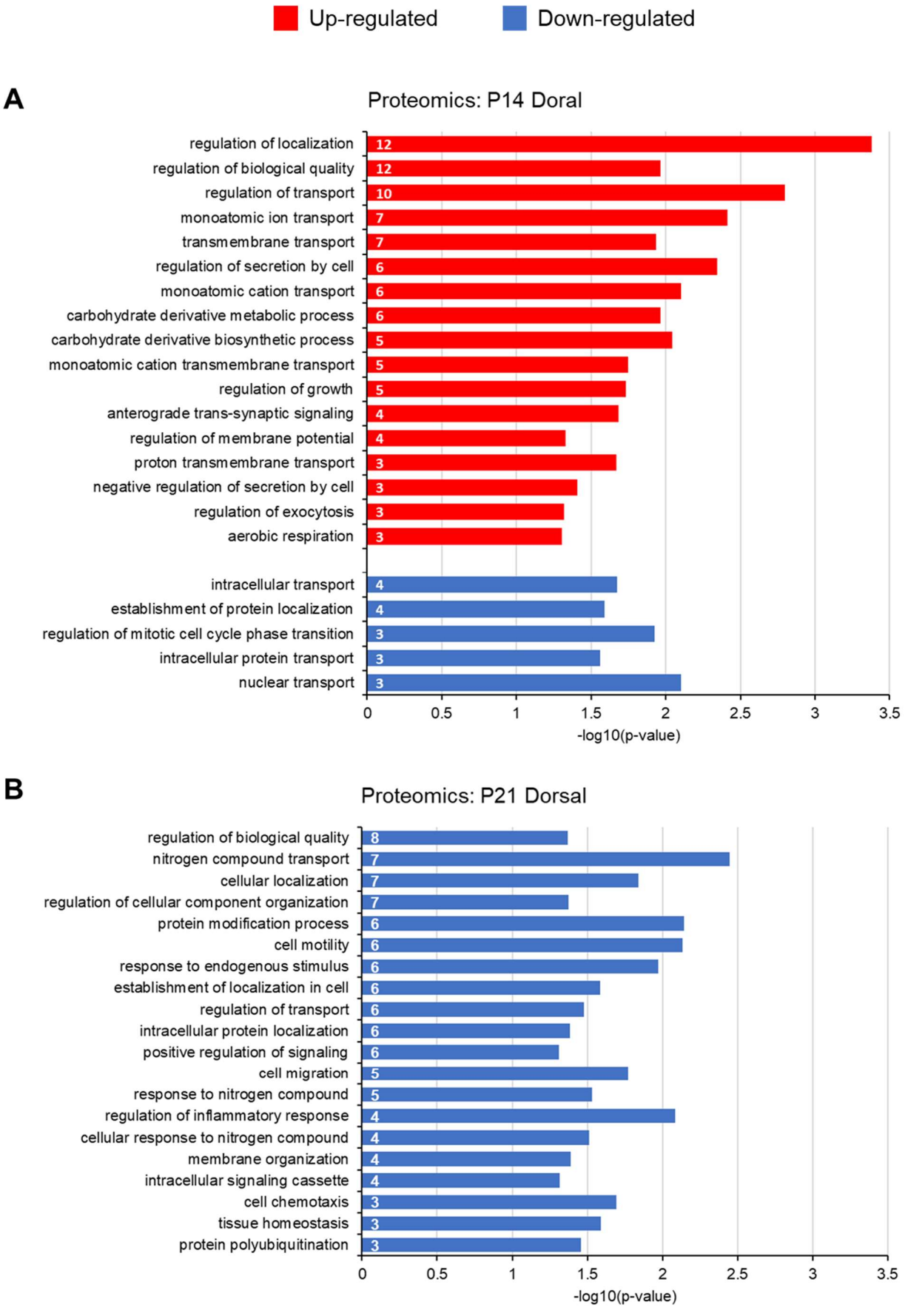
Up-regulated
Down-regulated
A
Proteomics: P14 Doral
regulation of localization
regulation of biological quality
regulation of transport
monoatomic ion transport
transmembrane transport
regulation of secretion by cell
monoatomic cation transport
carbohydrate derivative metabolic process
carbohydrate derivative biosynthetic process
monoatomic cation transmembrane transport
regulation of growth
anterograde trans-synaptic signaling
regulation of membrane potential
proton transmembrane transport
negative regulation of secretion by cell
regulation of exocytosis
aerobic respiration
intracellular transport
establishment of protein localization
regulation of mitotic cell cycle phase transition
intracellular protein transport
nuclear transport
12
12
10
7
7
6
6
6
5
5
5
4
4
3
3
3
3
4
4
3
3
3
0
0.5
1
1.5
2
2.5
3
3.5
-log10(p-value)
B
Proteomics: P21 Dorsal
regulation of biological quality
nitrogen compound transport
cellular localization
regulation of cellular component organization
protein modification process
cell motility
response to endogenous stimulus
establishment of localization in cell
regulation of transport
intracellular protein localization
positive regulation of signaling
cell migration
response to nitrogen compound
regulation of inflammatory response
cellular response to nitrogen compound
membrane organization
intracellular signaling cassette
cell chemotaxis
tissue homeostasis
protein polyubiquitination
8
7
7
7
6
6
6
6
6
6
6
5
5
4
4
4
4
3
3
3
0
0.5
1
1.5
2
2.5
3
3.5
-log10(p-value)

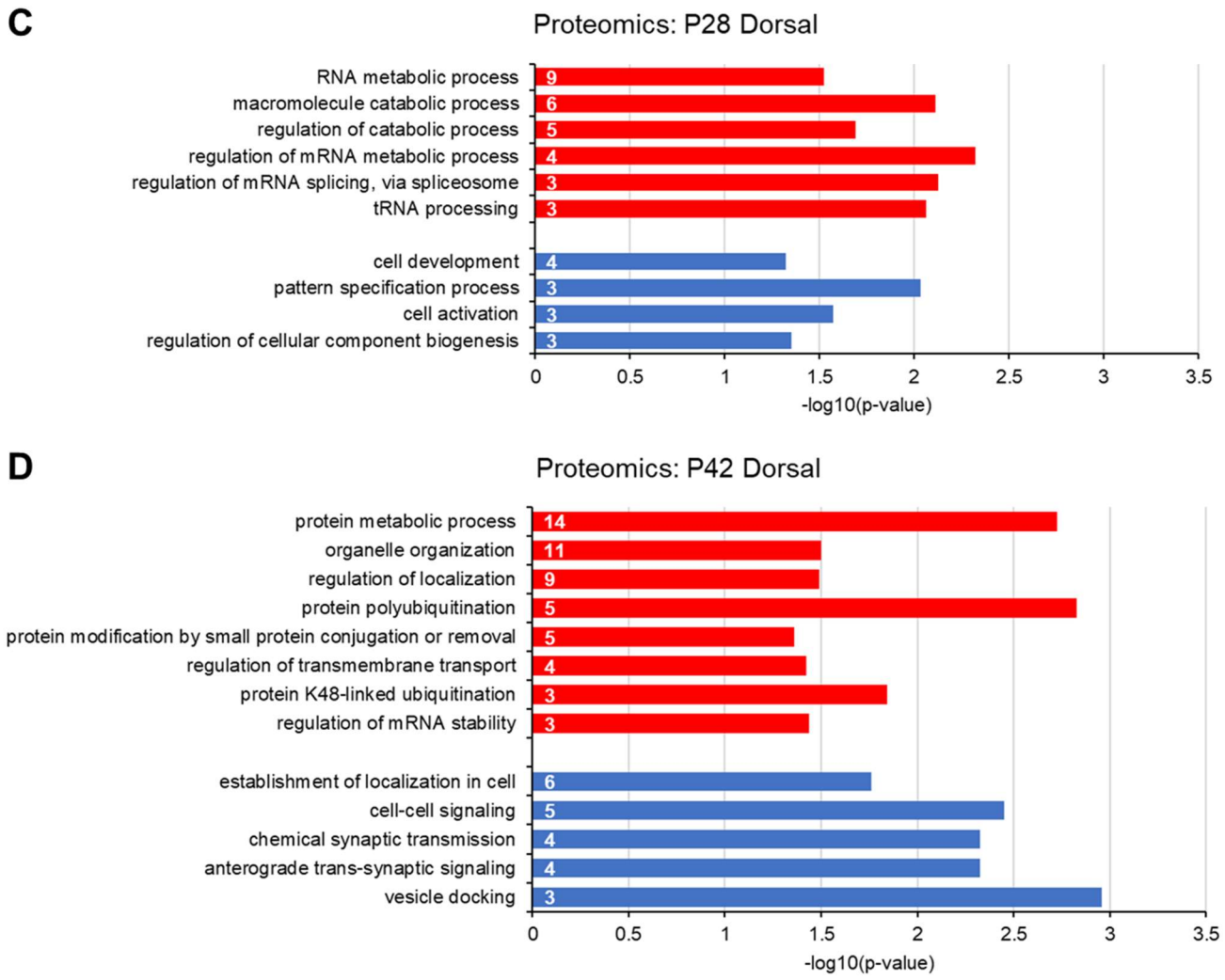

Figure 4.3. Significantly enriched gene ontology (GO) biological process associated with differentially expressed proteins in *Mdga2*$^{+/-}$ dorsal CA1 tissue relative to *Mdga2*$^{+/+}$ dorsal CA1 tissue at (A) P14, (B) P21, (C) P28, and (D) P42. Up- and down-regulated proteins were identified by Metaboanalyst 6.0, and GO analysis was run with DAVID Functional Annotation Tool. Inset numbers represent the number of proteins associated with each term. Select terms are included. For a full table of all terms in DAVID GO analysis output, see Appendix C.

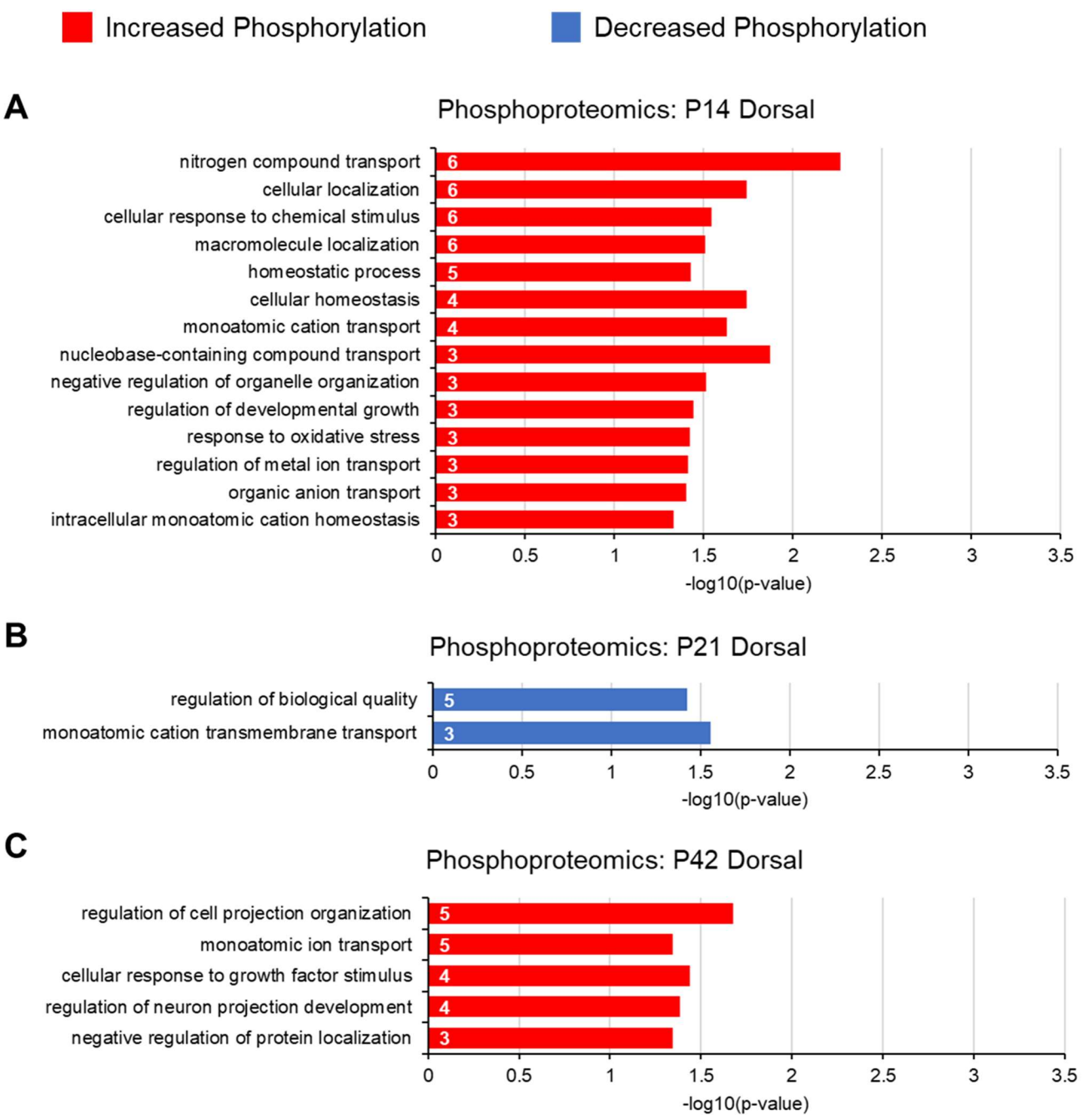

Figure 4.4. Significantly enriched gene ontology (GO) biological process associated with differentially phosphorylated proteins in *Mdga2*$^{+/-}$ dorsal CA1 tissue relative to *Mdga2*$^{+/+}$ dorsal CA1 tissue at (A) P14, (B) P21, and (C) P42. Proteins with an increase in phosphorylated states and dephosphorylated states were identified by Metaboanalyst 6.0, and GO analysis was run with DAVID Functional Annotation Tool. There were no significantly enriched terms at P28. Inset numbers represent the number of proteins associated with each term. Select terms are included. For a full table of all terms in DAVID GO analysis output, see Appendix C.

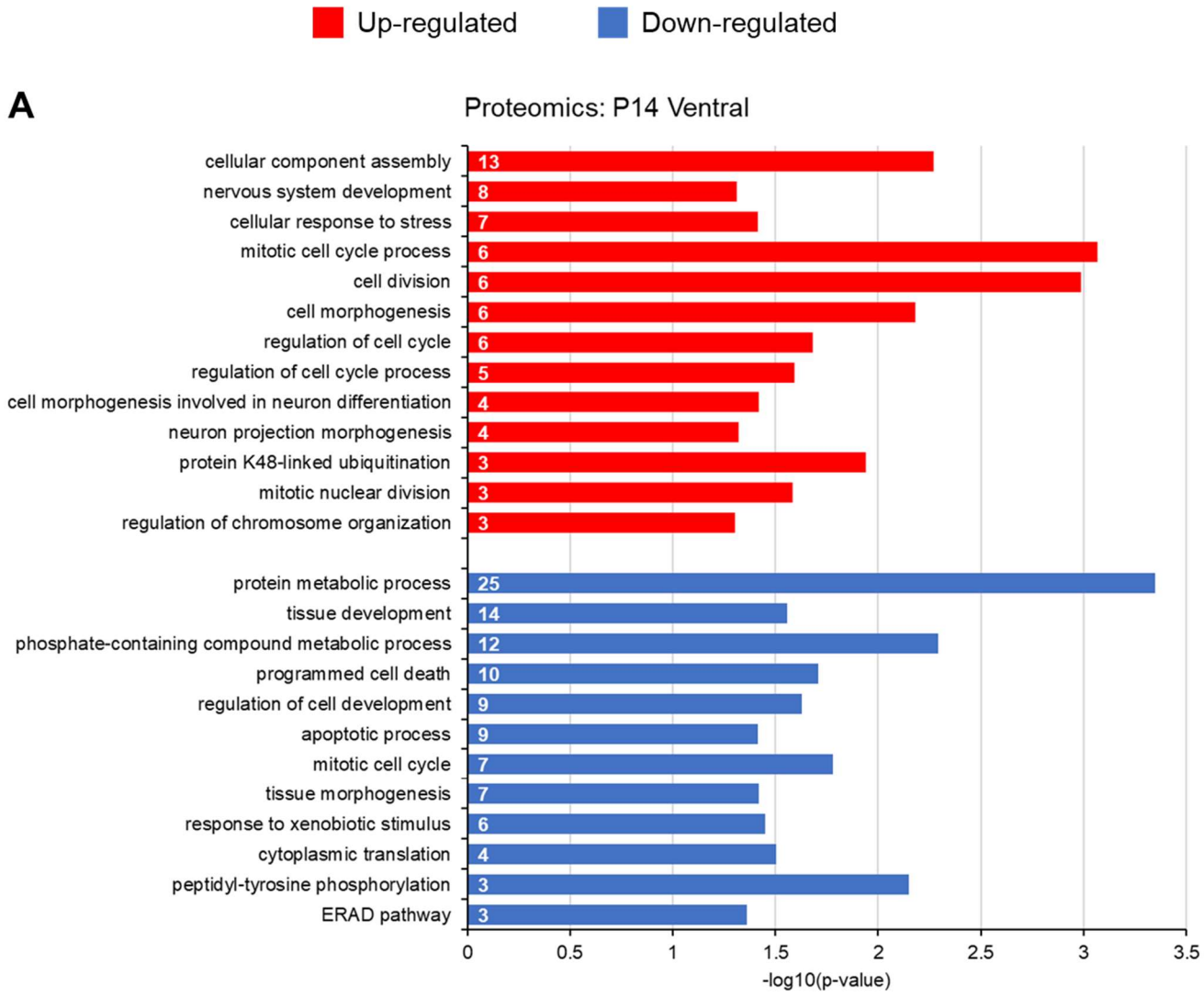
Up-regulated
Down-regulated
A
Proteomics: P14 Ventral
cellular component assembly
nervous system development
cellular response to stress
mitotic cell cycle process
cell division
cell morphogenesis
regulation of cell cycle
regulation of cell cycle process
cell morphogenesis involved in neuron differentiation
neuron projection morphogenesis
protein K48-linked ubiquitination
mitotic nuclear division
regulation of chromosome organization
protein metabolic process
tissue development
phosphate-containing compound metabolic process
programmed cell death
regulation of cell development
apoptotic process
mitotic cell cycle
tissue morphogenesis
response to xenobiotic stimulus
cytoplasmic translation
peptidyl-tyrosine phosphorylation
ERAD pathway
13
8
7
6
6
6
6
5
4
4
3
3
3
25
14
12
10
9
9
7
7
6
4
3
3
0
0.5
1
1.5
2
2.5
3
3.5
-log10(p-value)

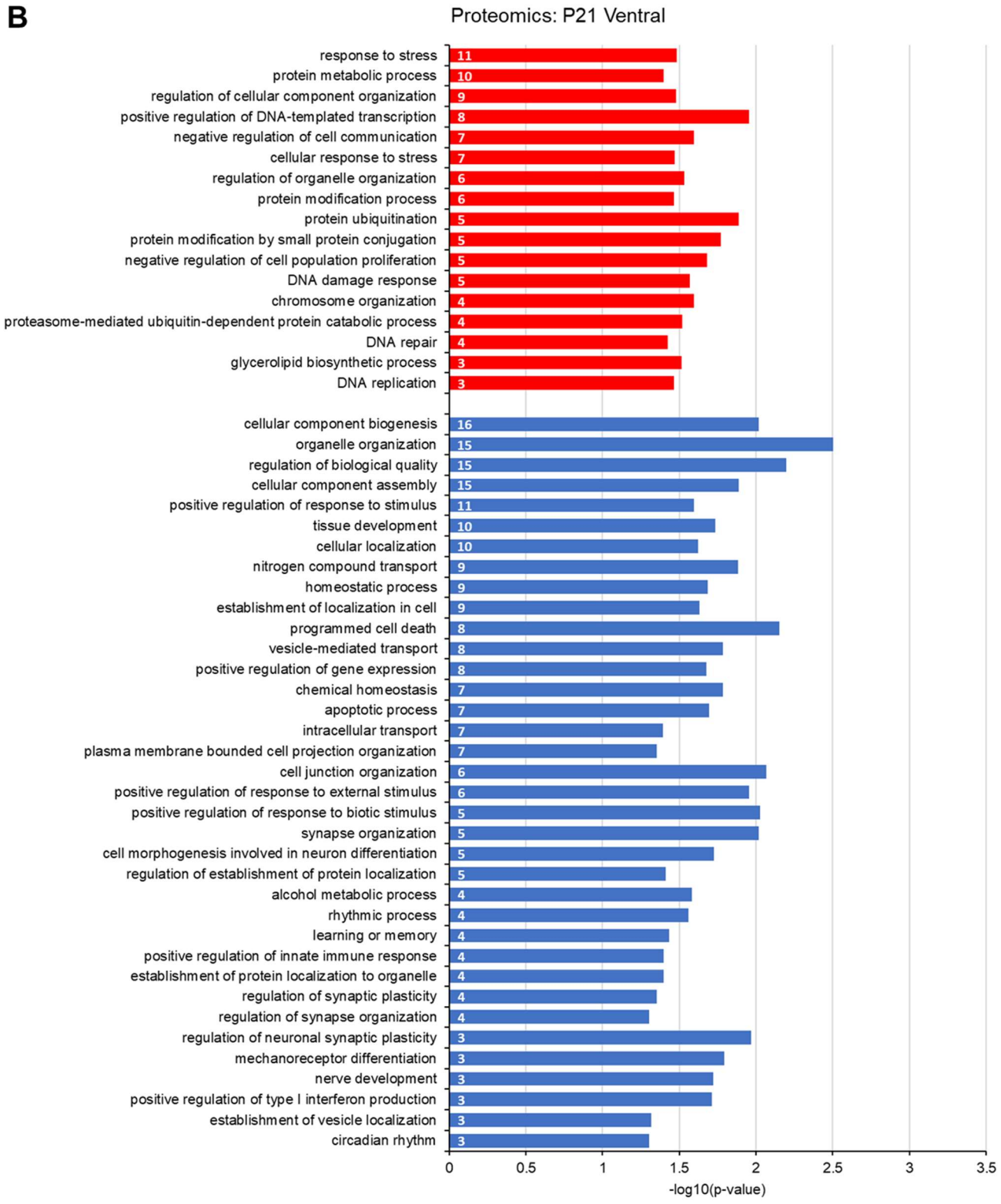
B
Proteomics: P21 Ventral
response to stress
protein metabolic process
regulation of cellular component organization
positive regulation of DNA-templated transcription
negative regulation of cell communication
cellular response to stress
regulation of organelle organization
protein modification process
protein ubiquitination
protein modification by small protein conjugation
negative regulation of cell population proliferation
DNA damage response
chromosome organization
proteasome-mediated ubiquitin-dependent protein catabolic process
DNA repair
glycerolipid biosynthetic process
DNA replication
cellular component biogenesis
organelle organization
regulation of biological quality
cellular component assembly
positive regulation of response to stimulus
tissue development
cellular localization
nitrogen compound transport
homeostatic process
establishment of localization in cell
programmed cell death
vesicle-mediated transport
positive regulation of gene expression
chemical homeostasis
apoptotic process
intracellular transport
plasma membrane bounded cell projection organization
cell junction organization
positive regulation of response to external stimulus
positive regulation of response to biotic stimulus
synapse organization
cell morphogenesis involved in neuron differentiation
regulation of establishment of protein localization
alcohol metabolic process
rhythmic process
learning or memory
positive regulation of innate immune response
establishment of protein localization to organelle
regulation of synaptic plasticity
regulation of synapse organization
regulation of neuronal synaptic plasticity
mechanoreceptor differentiation
nerve development
positive regulation of type I interferon production
establishment of vesicle localization
circadian rhythm
11
10
9
8
7
7
6
6
5
5
5
5
4
4
4
3
3
16
15
15
15
11
10
10
9
9
9
8
8
8
7
7
7
7
6
6
5
5
5
4
4
4
4
4
4
4
3
3
3
3
3
3
0
0.5
1
1.5
2
2.5
3
3.5
-log10(p-value)

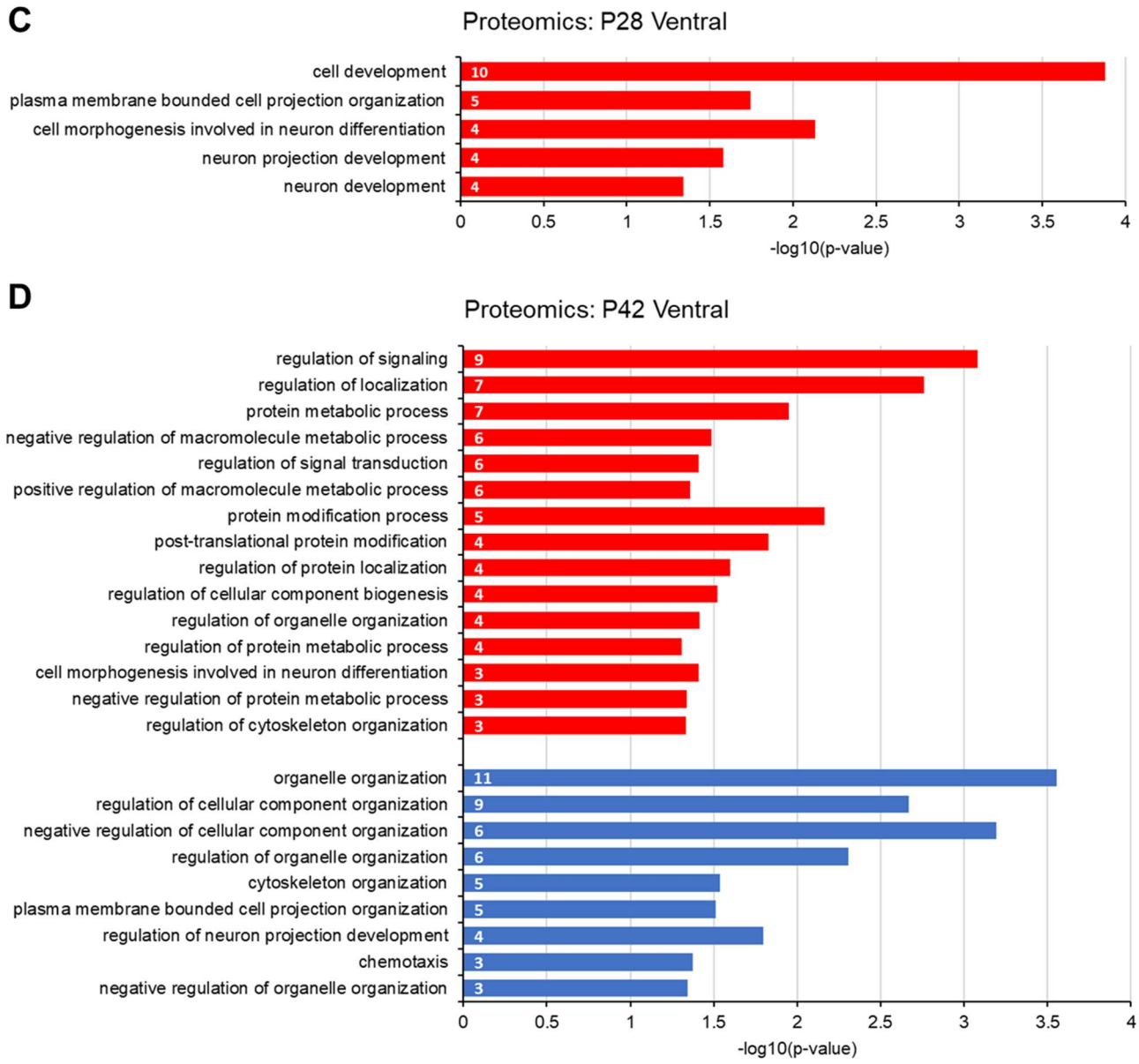

Figure 4.5. Significantly enriched gene ontology (GO) biological process associated with differentially expressed proteins in *Mdga2*$^{+/-}$ ventral CA1 tissue relative to *Mdga2*$^{+/+}$ ventral CA1 tissue at (A) P14, (B) P21, (C) P28, and (D) P42. Up- and down-regulated proteins were identified by Metaboanalyst 6.0, and GO analysis was run with DAVID Functional Annotation Tool. Inset numbers represent the number of genes/proteins associated with each term. Select terms are included. For a full table of all terms in DAVID GO analysis output, see Appendix D.

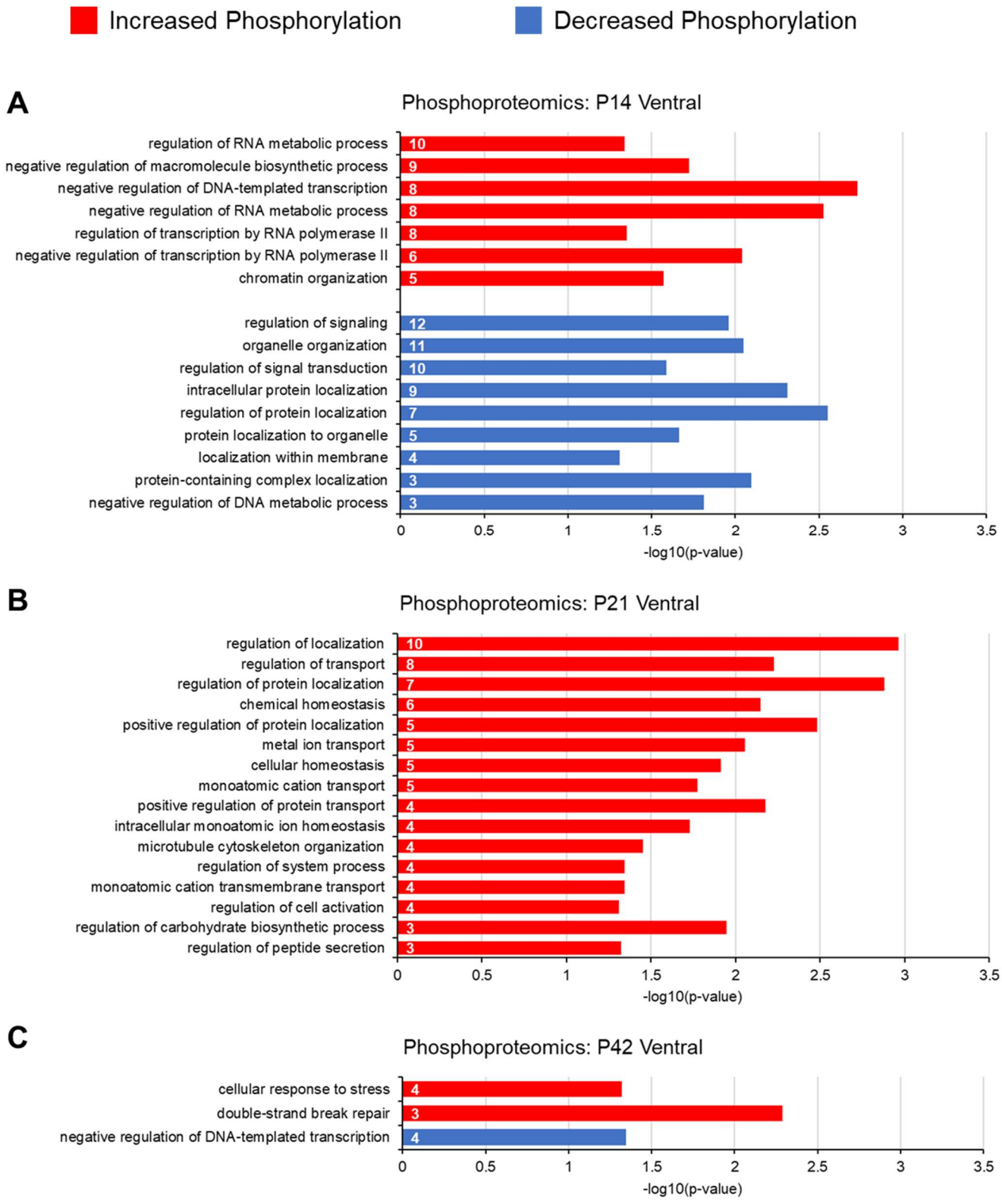

Figure 4.6. Significantly enriched gene ontology (GO) biological process associated with differentially phosphorylated proteins in *Mdga2*$^{+/-}$ ventral CA1 tissue relative to *Mdga2*$^{+/+}$ ventral CA1 tissue at (A) P14, (B) P21, and (C) P42. Proteins with an increase in

phosphorylated states and dephosphorylated states were identified by Metaboanalyst 6.0, and GO analysis was run with DAVID Functional Annotation Tool. There were no significantly enriched terms at P28. Inset numbers represent the number of genes/proteins associated with each term. Select terms are included. For a full table of all terms in DAVID GO analysis output, see Appendix D.

4.4. Discussion

Recent advances in synaptoneurosome proteomic and phosphoproteomic analysis provide an unbiased assessment of molecular alterations underpinning neurodevelopmental disorders such as ASD. Using this approach, a reduction in Mdga2 was found to cause major alterations in both the proteome and phosphoproteome at synapses within the dorsal and ventral CA1, linked to ion & protein transport and homeostasis cellular structure and development, synaptic signaling, oxidative stress and inflammation/damage response, ubiquitination and protein catabolism, and protein translation and modification. The threshold for including proteins in these analyses was set relatively stringent threshold, requiring at least a 1.5X FC to detect large and consistent differences across multiple ages. However, this means that other important biological processes or signaling pathways could still be affected in the *Mdga2*$^{+/-}$ model, even if their protein expression or phosphorylation changes do not reach this 1.5X FC cutoff. Therefore, if a biological process was not identified in this analysis, it does not necessarily mean it is unchanged or unaffected by a reduction in Mdga2. It is also noteworthy that many of the specific GO terms were limited to a gene count of 3-5, suggesting that the results should be interpreted with caution. In the future, it may be beneficial to reduce the FC threshold closer to 1.25X, which would still reflect a 25% change relative to WT levels. With a reduced threshold for protein inclusion, the threshold for GO term inclusion could be maintained or increased while being able to use the BP_direct to determine which specific biological processes are directly linked to up- and down-regulated or phosphorylated proteins without having to use more broad parent terms.

As discussed in Chapter 2, NMDAR-dependent LTD in the CA1 is impaired in *Mdga2*$^{+/-}$mice from P28-P42. This is consistent with the dysregulation of ion homeostasis and synaptic signaling in the dorsal and ventral hippocampus elucidated by the proteomic and GO analyses. These pathways are integral to NMDAR-LTD induction, where controlled calcium influx through persistent trans-synaptic signaling and NMDAR activation triggers downstream phosphatase activity leading to AMPAR

internalization (Pinar et al., 2017). For long-term maintenance of plasticity, including LTD and LTP, local synaptic translation of proteins is required; therefore disruption in the regulation of mRNAs and transcription may lead to expression impairments in these forms of plasticity, which should be investigated in future experiments. Additionally, the GO analyses revealed dysregulation of proteins in the ventral hippocampus at P21 directly related to plasticity, as reflected in terms such as *regulation of neuronal synaptic plasticity, regulation of synapse organization*, and *regulation of synaptic plasticity*. As discussed in Chapter 3, there are significant changes in spine morphology and density, specifically in the dorsal CA1 during early post-natal development. This aligns with significant changes in proteins related to the regulation of cytoskeleton organization, neuronal projection, and nerve/cell development which manifested from P14 throughout to P42, which would correspond with the increase in synaptic density at P21 and subsequent increase in pruning required to return synaptic density to WT levels. Moreover, altered pathways involved in protein ubiquitination suggest enhanced synaptic protein turnover, potentially contributing to synaptic pruning and spine shape remodeling observed during development. Taken together, these findings indicate that the loss of Mdga2 perturbs calcium signaling and cytoskeletal organization, which may influence the development of synaptic structure and the induction of NMDAR-dependent LTD in the hippocampus.

Throughout development in both regions, multiple enriched GO terms are related to oxidative stress and inflammation-related pathways. Recent evidence indicates that both oxidative stress and neuroinflammation are interconnected contributors to the pathophysiology of ASD. Children and adults with ASD frequently show elevated markers of oxidative damage (e.g., increased lipid peroxidation, lower glutathione levels) alongside signs of immune activation and elevated pro-inflammatory cytokines (Bjørklund et al., 2020; L. Chen et al., 2021; X. Liu et al., 2022). Oxidative stress can trigger inflammatory pathways, while inflammation itself can promote reactive oxygen species production and mitochondrial dysfunction, thereby creating a self-reinforcing cycle of redox/immune dysregulation

(Usui et al., 2023). These dysregulated processes appear especially relevant during neurodevelopment, for example via maternal immune activation (MIA) (Usui et al., 2023), and may disrupt synaptic development and plasticity, thus contributing to the neural connectivity and circuit abnormalities characteristic of ASD (Pangrazzi et al., 2020). Therefore, dysregulation of proteins and pathways involved in oxidative stress, neuroinflammation, and mitochondrial function may contribute to ASD-like phenotypes observed in *Mdga2*$^{+/-}$ mice, and may be a promising novel line of investigation.

Protein ubiquitination and K48-linked ubiquitination – in which a polymer of ubiquitin linked by lysine (K) residues at position 48 is attached to a protein to target it for degradation – were prevalent GO terms associated with dysregulated proteins across ages in both regions of the CA1 in *Mdga2*$^{+/-}$ tissue. This could have a couple of implications, including either excessive degradation of synaptic proteins or a compensatory mechanism for potential overproduction of synaptic proteins, both of which suggest an imbalance in the ubiquitin-proteasome system (UPS). Alterations in the UPS have also been increasingly recognized as a contributing factor to the molecular pathology of ASD (Kasherman et al., 2020; Louros & Osterweil, 2016). The UPS regulates neuronal protein homeostasis by tagging specific substrates with ubiquitin for targeted degradation or recycling, thereby maintaining the precise balance of synaptic proteins required for proper synapse development and plasticity, which is often disrupted in models of ASD (Cajigas et al., 2010; Hamilton & Zito, 2013). Human genetic studies have identified mutations and copy number variations in UPS-related genes (Glessner et al., 2009), and proteomic analyses of human ASD brain tissue have revealed enrichment of pathways involved in "ubiquitination & proteasome degradation" (Nomura et al., 2021), similar to the results seen here from *Mdga2*$^{+/-}$ tissue, reflecting altered protein turnover and synaptic maintenance. Therefore, dysregulation of the UPS may contribute to synaptic dysfunction in *Mdga2*$^{+/-}$ mice.

In summary, evidence of dysregulation of biological processes involving ion homeostasis, cellular structure and projection, cell signaling, ubiquitination and protein catabolism, oxidative stress and

inflammation, and transcription and protein modifications was found in the synaptoneurosomes from the CA1 of *Mdga2*$^{+/-}$ tissue, which provides insight into potential mechanisms by which Mdga2 reduction may contribute to synaptic dysfunction and ASD-related biomarkers. The proteomic and phosphoproteomic analyses of *Mdga2*$^{+/-}$ synaptoneurosomes provide valuable insights into synaptic protein composition and phosphorylation states, but have limitations. These include potential contamination from non-neuronal cells, reliance on fold change cutoffs that may miss subtle changes, and limited gene ontology interpretation due to low gene counts. Additionally, these analyses lack resolution to detect localized or cell-type-specific regulation, which is important to consider as Mdga2 is expressed in both parvalbumin-positive interneurons and pyramidal neurons in the hippocampus (Connor et al., 2016). Therefore, these results should be interpreted with caution, but do provide a starting point and new potential targets for investigation in the *Mdga2*$^{+/-}$ model.

Chapter 5: Concluding Remarks and Future Directions

5.1 Summary and Synthesis

This is the first study to investigate the effects of Mdga2 reduction on synapse development throughout early post-natal development and the first to investigate the effects of Mdga2 reduction on LTD. It was hypothesized that a reduction in Mdga2 would lead to impairments in LTD and synaptic pruning, and an enhancement in synaptogenesis due to the disinhibition of excitatory synapse development and premature synapse maturation (Connor et al., 2019). This would ultimately result in hyperexcitation in mature circuitry, which is consistent with the observation of increased excitatory density and glutamatergic signaling observed in adulthood in CA1 of *Mdga2*$^{+/-}$ mice (Connor et al., 2016; D. Zhao et al., 2025). The results presented here partly support this hypothesis; NMDAR-LTD, but not mGluR LTD, was impaired in the dorsal and ventral CA1 in *Mdga2*$^{+/-}$ mice aged P28-P42. This reflects pathway-specific impairments and not an overall inability for the excitatory synapses to be depressed in an activity-dependent manner to the same degree as WT individuals. Instead, this observation suggests a shift in the NMDAR-dependent LTP-LTD balance, which is supported by the observation of enhanced NMDAR-dependent E-LTP in adulthood and increased GluN2A receptors in cultured tissue with Mdga2 knockdown (Connor et al., 2016; S. Kim et al., 2024). LTP-LTD balance relies on the dynamics of calcium influx and signaling, and the proteomic analysis suggests that these processes may be dysregulated in the CA1, further supporting this interpretation (S.-N. Yang et al., 1999; Mizuno et al., 2001; Lüscher & Malenka, 2012).

In regard to the development of excitatory synaptic spines, the hypothesis was partly supported as enhancements in synaptogenesis were observed, with a significant increase in the peak synaptic density at P21 and early maturation of spines at P14, but this was limited to the dorsal hippocampus. Unexpectedly, synaptic density and morphology returned to WT levels by

P42. This suggests that synaptic pruning mechanisms remain intact, and are possibly enhanced, in order to correct the excessive production of immature spines at P21. This was unexpected, as an increase in cross-sectional excitatory density has been repeatedly reported in the SR of the CA1 in *Mdga2*$^{+/-}$ mice and cKO models (Connor et al., 2016; X. Wang et al., 2024; D. Zhao et al., 2025). As previously mentioned, this inconsistency could be due to alterations in dendritic branching, as cultured neurons with Mdga2 KO have increased dendritic arborization, which could lead to an increase in synaptic density per area (S. Kim et al., 2024). This could be confirmed by conducting Sholl analysis in CA1 tissue from *Mdga2*$^{+/-}$ mice and WT littermates. Moreover, NDMAR-LTD and synaptic pruning share molecular pathways, with weakening of synapses by LTD-like mechanisms being a first step in activity-dependent removal (Shinoda et al., 2010; Piochon et al., 2016; Faust et al., 2021); therefore, impairments in NMDAR-LTD would suggest potential deficits in synaptic pruning, but this was not observed. There are a couple of possible explanations for this observation; firstly, as the dual-population of synaptic spines hypothesis explained in Chapter 3 suggests, early maturation of spines at P14 in the dorsal CA1, followed by the emergence of excessive immature spines by P21, likely led to the selective removal of the less mature spines produced by P21 (C.-C. Chen et al., 2014).

In contrast, the more mature spines expressed at P14 continue to be strengthened and are persistent at P28 and P42. These remaining spines would have accelerated maturation and increased stability and would therefore be more resistant to NMDAR-dependent LTD. An alternative explanation is an occlusion effect: if excessive pruning occurred between P21 and P28 to restore synaptic spine density to WT levels, LTD pathways may have saturated. Overall, these results suggest that Mdga2 reduction contributes to early synapse production and maturation in the dorsal CA1 and leads to an increase in the E/I ratio that results in a shift in LTP-LTD balance across the hippocampus. In addition to synaptic development and plasticity

effects, proteomic and phosphoproteomic analyses suggest that a reduction in Mdga2 may contribute to oxidative stress and neuroinflammation, and alterations in the UPS. These are additional biomarkers of ASD and may be novel candidates for exploration in this model (Kasherman et al., 2020; Usui et al., 2023).

5.2 Limitations

There are several limitations to acknowledge in this study, including a lack of female representation due to time restrictions and the addition of confounding variables. Male mice were selected for this study as unpublished data from the Connor lab suggests that synaptic abnormalities are enhanced in males relative to females. Further experiments should explore possible sex differences in the observed results. In addition, while the present findings suggest an association between changes in synapse development and alterations in LTD, a direct causal relationship cannot be established from these data. The interpretation that abnormal spine maturation contributes to LTD impairments remains inferential. There are also limitations to each set of experiments. In the LTD experiments, it is worth noting that NMDAR-LTD and mGluR-LTD were induced in distinct ways; NMDAR-LTD was induced electrically via 1Hz LFS, and mGluR-LTD was induced chemically via bath application of DHPG. It is possible that the chemical induction of mGluR-LTD was too robust to reveal subtle group differences. Bath application DHPG activates LTD mechanisms across a broad population of synapses and can produce near-saturating depression, potentially masking mild impairments in LTD signaling. In contrast, electrically induced LTD engages activity-dependent pathways in a synapse-specific and graded manner, which may be more sensitive to detecting subtle alterations in synaptic plasticity mechanisms (Huber et al., 2001). Attempts to induce mGluR-LTD via paired-pulse

LFS in the presence of NMDAR antagonists were unsuccessful, and although this method is often used to probe mGluR-LTD, some results show that induction of LTD via this method is not inhibited by group I mGluR blockers (Volk et al., 2006). Golgi–Cox staining, while advantageous for visualizing overall density and spine morphology, has several limitations. These include potential sampling and observer bias, and the inherent restriction of 2D imaging for 3D structures, which can lead to underestimation of spine density or inaccurate categorization of spine types due to the occlusion of part of the spine by the dendrite. Moreover, this technique provides no information about the functional status of spines or dynamic changes, limiting the interpretation of how observed morphological changes relate to synaptic function. Lastly, proteomic and phosphoproteomic limitations included small sample sizes and low gene counts associated with some GO terms. Moreover, while proteomic analysis revealed several candidate pathways that may be dysregulated following Mdga2 reduction, this data does not provide directional or causal information. Increases or decreases in protein abundance or phosphorylation may represent either compensatory or pathological changes, and further functional validation is required to determine their significance.

5.3 Future Directions

Future studies should aim to build upon the present findings and address some of the limitations discussed above. One key direction will be to further dissect the cellular and molecular mechanisms underlying the selective impairment of NMDAR-LTD observed in *Mdga2*$^{+/-}$ mice. Since these effects coincided with evidence of enhanced GluN2A expression (S. Kim et al., 2024) and altered synaptic calcium signaling pathways from the proteomic analysis, it will be important to determine whether changes in NMDAR subunit composition or calcium-dependent signaling cascades directly contribute to the LTD deficit. Follow-up experiments using pharmacological tools to manipulate GluN2A and GluN2B activation in *ex vivo*

electrophysiological recordings, or utilizing patch-clamp and while simultaneously monitoring calcium dynamics during LTD and LTD induction with the use of fluorescent calcium indicators and two-photon microscopy (X.-H. Li et al., 2017), could help clarify how Mdga2 reduction shifts the LTP–LTD balance in CA1 pyramidal neurons.

Another important avenue of exploration involves the relationship between LTD and synaptic pruning. Given the role of NMDAR-dependent LTD-like processes in spine elimination (Piochon et al., 2016), a key question is why pruning appeared to normalize spine density in the dorsal CA1 despite LTD impairment. To distinguish if more mature synapses that are detected at P14 are persistent by P28-P42, contributing to LTD deficits due to increased maturation and stability, longitudinal imaging of dendritic spines across postnatal development would allow direct measurement of spine formation and elimination rates in vivo. Advancements in imaging technology have allowed researchers to conduct long-term imaging in subcortical structures, such as the hippocampus, by utilizing glass microperiscopes. This technique has been used to successfully analyze spine morphogenesis in the CA1 region and allowed for the tracking of dendritic spines over multiple days from the same dendritic arbor (Redman et al., 2022). Moreover, the recovery of normal spine density by P42 also underscores the need to examine overall dendritic structure, as increased dendritic arborization could contribute to a higher total number of excitatory contacts without altering local density. Future studies incorporating three-dimensional reconstructions or Sholl analysis of CA1 neurons will help clarify whether changes in dendritic complexity accompany the initial wave of excessive synapse formation at P21.

Lastly, there is a growing body of literature supporting molecular and functional differences across the dorsal-ventral axis of the hippocampus (A.-R. Lee et al., 2017; Dubovyk & Manahan-Vaughan, 2018; Trompoukis & Papatheodoropoulos, 2020), leading to the differentiation between the regions in the current study. Only the dorsal hippocampus displayed a

robust enhancement of synaptogenesis and enhanced synapse maturation in *Mdga2*$^{+/-}$ mice; therefore, future studies should aim to elucidate potential differences in Mdga2 expression patterns along the dorsal-ventral axis. There are currently no antibodies validated for Mdga2 binding for immunohistochemistry, which makes localization studies difficult. Alternative approaches include knocking in an epitope-flagged Mdga2 gene to express an epitope tag such as FLAG or HA, or a fluorescent protein such as GFP. This would allow for the use of highly specific and validated antibodies or direct fluorescence for the detection of Mdga2 under standard immunohistochemistry or imaging protocols while retaining native expression patterns (Z. Zhang, 2023). In addition to elucidating dorsal-ventral expression patterns, this technique would allow for the validation of synaptic localization and temporal distribution that has thus far only been accomplished with endogenous Mdga1 (Toledo et al., 2022). Together, these proposed directions will deepen our understanding of how Mdga2 regulates synaptic plasticity and circuit maturation during postnatal development, and how its dysregulation may contribute to the pathophysiology of neurodevelopmental disorders such as ASD.

References

Akinlaja, Y. O., & Nishiyama, A. (2024). Glial modulation of synapse development and plasticity: Oligodendrocyte precursor cells as a new player in the synaptic quintet. *Frontiers in Cell and Developmental Biology*, *12*, 1418100. https://doi.org/10.3389/fcell.2024.1418100

Allen Institute for Brain Science. (2004). *Allen Mouse Brain Atlas* [Dataset]. mouse.brain-map.org

Allen Institute for Brain Science. (2011). *Allen Reference Atlas – Mouse Brain* [Brain atlas]. atlas.brain-map.org

American Psychiatric Association. (2013). *Diagnostic and statistical manual of mental disorders* (5th ed.). https://doi.org/10.1176/appi.books.9780890425596

Anashkina, A. A., & Erlykina, E. I. (2021). Molecular Mechanisms of Aberrant Neuroplasticity in Autism Spectrum Disorders (Review). *Sovremennye Tekhnologii V Meditsine*, *13*(1), 78–91. https://doi.org/10.17691/stm2021.13.1.10

Anderson, G. R., Galfin, T., Xu, W., Aoto, J., Malenka, R. C., & Südhof, T. C. (2012). Candidate autism gene screen identifies critical role for cell-adhesion molecule CASPR2 in dendritic arborization and spine development. *Proceedings of the National Academy of Sciences*, *109*(44), 18120–18125. https://doi.org/10.1073/pnas.1216398109

Anderson, W. W., & Collingridge, G. L. (2007). Capabilities of the WinLTP data acquisition program extending beyond basic LTP experimental functions. *Journal of Neuroscience Methods*, *162*(1), 346–356. https://doi.org/10.1016/j.jneumeth.2006.12.018

Anggono, V., & Huganir, R. L. (2012). Regulation of AMPA receptor trafficking and synaptic plasticity. *Current Opinion in Neurobiology*, *22*(3), 461–469. https://doi.org/10.1016/j.conb.2011.12.006

Arellano, J. I., Benavides-Piccione, R., DeFelipe, J., & Yuste, R. (2007). Ultrastructure of Dendritic Spines: Correlation Between Synaptic and Spine Morphologies. *Frontiers in Neuroscience*, *1*(1), 131–143. https://doi.org/10.3389/neuro.01.1.1.010.2007

Ashby, D. M., Floresco, S. B., Phillips, A. G., McGirr, A., Seamans, J. K., & Wang, Y. T. (2021). LTD is involved in the formation and maintenance of rat hippocampal CA1 place-cell fields. *Nature Communications*, *12*(1), 100. https://doi.org/10.1038/s41467-020-20317-7

Auerbach, B. D., Osterweil, E. K., & Bear, M. F. (2011). Mutations causing syndromic autism define an axis of synaptic pathophysiology. *Nature*, *480*(7375), 63–68. https://doi.org/10.1038/nature10658

Baltaci, S. B., Mogulkoc, R., & Baltaci, A. K. (2019). Molecular Mechanisms of Early and Late LTP. *Neurochemical Research*, *44*(2), 281–296. https://doi.org/10.1007/s11064-018-2695-4

Bartlett, T. E., Bannister, N. J., Collett, V. J., Dargan, S. L., Massey, P. V., Bortolotto, Z. A., Fitzjohn, S. M., Bashir, Z. I., Collingridge, G. L., & Lodge, D. (2007). Differential roles of NR2A and NR2B-containing NMDA receptors in LTP and LTD in the CA1 region of two-week old rat hippocampus. *Neuropharmacology*, *52*(1), 60–70. https://doi.org/10.1016/j.neuropharm.2006.07.013

Basu, J., & Siegelbaum, S. A. (2015). The Corticohippocampal Circuit, Synaptic Plasticity, and Memory. *Cold Spring Harbor Perspectives in Biology*, *7*(11), a021733. https://doi.org/10.1101/cshperspect.a021733

Baudouin, S. J., Gaudias, J., Gerharz, S., Hatstatt, L., Zhou, K., Punnakkal, P., Tanaka, K. F., Spooren, W., Hen, R., De Zeeuw, C. I., Vogt, K., & Scheiffele, P. (2012). Shared Synaptic Pathophysiology in Syndromic and Nonsyndromic Rodent Models of Autism. *Science*, *338*(6103), 128–132. https://doi.org/10.1126/science.1224159

Belzung, C., & Lemoine, M. (2011). Criteria of validity for animal models of psychiatric disorders: Focus on anxiety disorders and depression. *Biology of Mood & Anxiety Disorders*, *1*, 9. https://doi.org/10.1186/2045-5380-1-9

Bemben, M. A., Sandoval, M., Le, A. A., Won, S., Chau, V. N., Lauterborn, J. C., Incontro, S., Li, K. H., Burlingame, A. L., Roche, K. W., Gall, C. M., Nicoll, R. A., & Diaz-Alonso, J. (2023). Contrastsing synaptic roles of MDGA1 and MDGA2. *bioRxiv*, 2023.05.25.542333. https://doi.org/10.1101/2023.05.25.542333

Bjørklund, G., Meguid, N. A., El-Bana, M. A., Tinkov, A. A., Saad, K., Dadar, M., Hemimi, M., Skalny, A. V., Hosnedlová, B., Kizek, R., Osredkar, J., Urbina, M. A., Fabjan, T., El-Houfey, A. A., Kałużna-Czaplińska, J., Gątarek, P., & Chirumbolo, S. (2020). Oxidative Stress in Autism Spectrum Disorder. *Molecular Neurobiology*, *57*(5), 2314–2332. https://doi.org/10.1007/s12035-019-01742-2

Bliss, T. V., & Lomo, T. (1973). Long-lasting potentiation of synaptic transmission in the dentate area of the anaesthetized rabbit following stimulation of the perforant path. *The Journal of Physiology*, *232*(2), 331–356. https://doi.org/10.1113/jphysiol.1973.sp010273

Boivin, J. R., & Nedivi, E. (2018). Functional implications of inhibitory synapse placement on signal processing in pyramidal neuron dendrites. *Current Opinion in Neurobiology*, *51*, 16–22. https://doi.org/10.1016/j.conb.2018.01.013

Bomkamp, C., Padmanabhan, N., Karimi, B., Ge, Y., Chao, J. T., Loewen, C. J. R., Siddiqui, T. J., & Craig, A. M. (2019). Mechanisms of PTPσ-Mediated Presynaptic Differentiation. *Frontiers in Synaptic Neuroscience*, *11*. https://doi.org/10.3389/fnsyn.2019.00017

Borczyk, M., Śliwińska, M. A., Caly, A., Bernas, T., & Radwanska, K. (2019). Neuronal plasticity affects correlation between the size of dendritic spine and its postsynaptic density. *Scientific Reports*, *9*(1), 1693. https://doi.org/10.1038/s41598-018-38412-7

Bourgeron, T. (2009). A synaptic trek to autism. *Current Opinion in Neurobiology*, *19*(2), 231–234. https://doi.org/10.1016/j.conb.2009.06.003

Brigman, J. L., Wright, T., Talani, G., Prasad-Mulcare, S., Jinde, S., Seabold, G. K., Mathur, P., Davis, M. I., Bock, R., Gustin, R. M., Colbran, R. J., Alvarez, V. A., Nakazawa, K., Delpire, E., Lovinger, D. M., & Holmes, A. (2010). Loss of GluN2B-Containing NMDA Receptors in CA1 Hippocampus and Cortex Impairs Long-Term Depression, Reduces Dendritic Spine Density, and Disrupts Learning. *The Journal of Neuroscience*, *30*(13), 4590–4600. https://doi.org/10.1523/JNEUROSCI.0640-10.2010

Broadbent, N. J., Squire, L. R., & Clark, R. E. (2004). Spatial memory, recognition memory, and the hippocampus. *Proceedings of the National Academy of Sciences*, *101*(40), 14515–14520. https://doi.org/10.1073/pnas.0406344101

Brown, M. R. G., Benoit, J. R. A., Juhás, M., Dametto, E., Tse, T. T., MacKay, M., Sen, B., Carroll, A. M., Hodlevskyy, O., Silverstone, P. H., Dolcos, F., Dursun, S. M., & Greenshaw, A. J. (2015). fMRI investigation of response inhibition, emotion, impulsivity, and clinical high-risk behavior in adolescents. *Frontiers in Systems Neuroscience*, *9*, 124. https://doi.org/10.3389/fnsys.2015.00124

Bryson, S. E., Clark, B. S., & Smith, I. M. (1988). First Report of a Canadian Epidemiological Study of Autistic Syndromes. *Journal of Child Psychology and Psychiatry*, *29*(4), 433–445. https://doi.org/10.1111/j.1469-7610.1988.tb00735.x

Bucan, M., Abrahams, B. S., Wang, K., Glessner, J. T., Herman, E. I., Sonnenblick, L. I., Retuerto, A. I. A., Imielinski, M., Hadley, D., Bradfield, J. P., Kim, C., Gidaya, N. B., Lindquist, I., Hutman, T., Sigman, M., Kustanovich, V., Lajonchere, C. M., Singleton, A., Kim, J., … Hakonarson, H. (2009). Genome-Wide Analyses of Exonic Copy Number Variants in a Family-Based Study Point to Novel Autism Susceptibility Genes. *PLOS Genetics*, *5*(6), e1000536. https://doi.org/10.1371/journal.pgen.1000536

Cajal, R. y. (1911). *Histologie du Système Nerveux de l'Homme et des Vertébrés*. A. Maloine.

Cajigas, I. J., Will, T., & Schuman, E. M. (2010). Protein homeostasis and synaptic plasticity. *The EMBO Journal*, *29*(16), 2746–2752. https://doi.org/10.1038/emboj.2010.173

Canitano, R., & Palumbi, R. (2021). Excitation/Inhibition Modulators in Autism Spectrum Disorder: Current Clinical Research. *Frontiers in Neuroscience*, *15*. https://doi.org/10.3389/fnins.2021.753274

Carbonell, A. U., Freire-Cobo, C., Deyneko, I. V., Dobariya, S., Erdjument-Bromage, H., Clipperton-Allen, A. E., Page, D. T., Neubert, T. A., & Jordan, B. A. (2023). Comparing synaptic proteomes across five mouse models for autism reveals converging molecular similarities including deficits in oxidative phosphorylation and Rho GTPase signaling. *Frontiers in Aging Neuroscience*, *15*, 1152562. https://doi.org/10.3389/fnagi.2023.1152562

Chen, C.-C., Lu, J., & Zuo, Y. (2014). Spatiotemporal dynamics of dendritic spines in the living brain. *Frontiers in Neuroanatomy*, *8*, 28. https://doi.org/10.3389/fnana.2014.00028

Chen, J., Yu, S., Fu, Y., & Li, X. (2014). Synaptic proteins and receptors defects in autism spectrum disorders. *Frontiers in Cellular Neuroscience*, *8*, 276. https://doi.org/10.3389/fncel.2014.00276

Chen, L., Shi, X.-J., Liu, H., Mao, X., Gui, L.-N., Wang, H., & Cheng, Y. (2021). Oxidative stress marker aberrations in children with autism spectrum disorder: A systematic review and meta-analysis of 87 studies (N = 9109). *Translational Psychiatry*, *11*(1), 15. https://doi.org/10.1038/s41398-020-01135-3

Chen, X., Levy, J. M., Hou, A., Winters, C., Azzam, R., Sousa, A. A., Leapman, R. D., Nicoll, R. A., & Reese, T. S. (2015). PSD-95 family MAGUKs are essential for anchoring AMPA and NMDA receptor complexes at the postsynaptic density. *Proceedings of the National Academy of Sciences*, *112*(50), E6983–E6992. https://doi.org/10.1073/pnas.1517045112

Chia, P. H., Li, P., & Shen, K. (2013). Cellular and molecular mechanisms underlying presynapse formation. *The Journal of Cell Biology*, *203*(1), 11–22. https://doi.org/10.1083/jcb.201307020

Collin, C., Miyaguchi, K., & Segal, M. (1997). Dendritic spine density and LTP induction in cultured hippocampal slices. *Journal of Neurophysiology*, *77*(3), 1614–1623. https://doi.org/10.1152/jn.1997.77.3.1614

Comery, T. A., Harris, J. B., Willems, P. J., Oostra, B. A., Irwin, S. A., Weiler, I. J., & Greenough, W. T. (1997). Abnormal dendritic spines in fragile X knockout mice: Maturation and pruning deficits. *Proceedings of the National Academy of Sciences*, *94*(10), 5401–5404. https://doi.org/10.1073/pnas.94.10.5401

Compans, B., Camus, C., Kallergi, E., Sposini, S., Martineau, M., Butler, C., Kechkar, A., Klaassen, R. V., Retailleau, N., Sejnowski, T. J., Smit, A. B., Sibarita, J.-B., Bartol, T. M., Perrais, D., Nikoletopoulou, V., Choquet, D., & Hosy, E. (2021). NMDAR-dependent long-term depression is associated with increased short term plasticity through autophagy mediated loss of PSD-95. *Nature Communications*, *12*(1), 2849. https://doi.org/10.1038/s41467-021-23133-9

Connor, S. A., Ammendrup-Johnsen, I., Chan, A. W., Kishimoto, Y., Murayama, C., Kurihara, N., Tada, A., Ge, Y., Lu, H., Yan, R., LeDue, J. M., Matsumoto, H., Kiyonari, H., Kirino, Y., Matsuzaki, F., Suzuki, T., Murphy, T. H., Wang, Y. T., Yamamoto, T., & Craig, A. M. (2016). Altered Cortical Dynamics and Cognitive Function upon Haploinsufficiency of the Autism-Linked Excitatory Synaptic Suppressor MDGA2. *Neuron*, *91*(5), 1052–1068. https://doi.org/10.1016/j.neuron.2016.08.016

Connor, S. A., Elegheert, J., Xie, Y., & Craig, A. M. (2019). Pumping the brakes: Suppression of synapse development by MDGA–neuroligin interactions. *Current Opinion in Neurobiology*, *57*, 71–80. https://doi.org/10.1016/j.conb.2019.01.002

Costa, J. F., Dines, M., & Lamprecht, R. (2020). The Role of Rac GTPase in Dendritic Spine Morphogenesis and Memory. *Frontiers in Synaptic Neuroscience*, *12*. https://doi.org/10.3389/fnsyn.2020.00012

Craig, A. M., & Kang, Y. (2007). Neurexin–neuroligin signaling in synapse development. *Current Opinion in Neurobiology*, *17*(1), 43. https://doi.org/10.1016/j.conb.2007.01.011

Cui, Z., Feng, R., Jacobs, S., Duan, Y., Wang, H., Cao, X., & Tsien, J. Z. (2013). Increased NR2A:NR2B ratio compresses long-term depression range and constrains long-term memory. *Scientific Reports*, *3*(1), 1036. https://doi.org/10.1038/srep01036

Cummings, J. A., Mulkey, R. M., Nicoll, R. A., & Malenka, R. C. (1996). Ca2+ Signaling Requirements for Long-Term Depression in the Hippocampus. *Neuron*, *16*(4), 825–833. https://doi.org/10.1016/S0896-6273(00)80102-6

Dang, R., Qi, J., Liu, A., Ren, Q., Lv, D., Han, L., Zhou, Z., Cao, F., Xie, W., & Jia, Z. (2018). Regulation of hippocampal long term depression by Neuroligin 1. *Neuropharmacology*, *143*, 205–216. https://doi.org/10.1016/j.neuropharm.2018.09.035

De Juan, C., Iniesta, P., González-Quevedo, R., Morán, A., Sánchez-Pernaute, A., Torres, A. J., Balibrea, J. L., Díaz-Rubio, E., Cruces, J., & Benito, M. (2002). Genomic organization of a novel glycosylphosphatidylinositol MAM gene expressed in human tissues and tumors. *Oncogene*, *21*(19), 3089–3094. https://doi.org/10.1038/sj.onc.1205383

De Roo, M., Klauser, P., & Muller, D. (2008a). LTP Promotes a Selective Long-Term Stabilization and Clustering of Dendritic Spines. *PLoS Biology*, *6*(9), e219. https://doi.org/10.1371/journal.pbio.0060219

De Roo, M., Klauser, P., & Muller, D. (2008b). LTP Promotes a Selective Long-Term Stabilization and Clustering of Dendritic Spines. *PLoS Biology*, *6*(9), e219. https://doi.org/10.1371/journal.pbio.0060219

DiCicco-Bloom, E., Lord, C., Zwaigenbaum, L., Courchesne, E., Dager, S. R., Schmitz, C., Schultz, R. T., Crawley, J., & Young, L. J. (2006). The Developmental Neurobiology of Autism Spectrum Disorder. *The Journal of Neuroscience*, *26*(26), 6897–6906. https://doi.org/10.1523/JNEUROSCI.1712-06.2006

Dieterich, D. C., & Kreutz, M. R. (2016). Proteomics of the Synapse – A Quantitative Approach to Neuronal Plasticity. *Molecular & Cellular Proteomics : MCP*, *15*(2), 368–381. https://doi.org/10.1074/mcp.R115.051482

Dubovyk, V., & Manahan-Vaughan, D. (2018). Less means more: The magnitude of synaptic plasticity along the hippocampal dorso-ventral axis is inversely related to the expression levels of plasticity-related neurotransmitter receptors. *Hippocampus*, *28*(2), 136–150. https://doi.org/10.1002/hipo.22816

Dudek, S. M., & Bear, M. F. (1992). Homosynaptic long-term depression in area CA1 of hippocampus and effects of N-methyl-D-aspartate receptor blockade. *Proceedings of the National Academy of Sciences*, *89*(10), 4363–4367. https://doi.org/10.1073/pnas.89.10.4363

Dunwiddie, T., & Lynch, G. (1978). Long-term potentiation and depression of synaptic responses in the rat hippocampus: Localization and frequency dependency. *The Journal of Physiology*, *276*, 353–367. https://doi.org/10.1113/jphysiol.1978.sp012239

Durand, G. M., Kovalchuk, Y., & Konnerth, A. (1996). Long-term potentiation and functional synapse induction in developing hippocampus. *Nature*, *381*(6577), 71–75. https://doi.org/10.1038/381071a0

Elegheert, J., Cvetkovska, V., Clayton, A. J., Heroven, C., Vennekens, K. M., Smukowski, S. N., Regan, M. C., Jia, W., Smith, A. C., Furukawa, H., Savas, J. N., de Wit, J., Begbie, J., Craig, A. M., & Aricescu, A. R. (2017). Structural Mechanism for Modulation of Synaptic Neuroligin-Neurexin Signaling by MDGA Proteins. *Neuron*, *95*(4), 896-913.e10. https://doi.org/10.1016/j.neuron.2017.07.040

El-Kordi, A., Winkler, D., Hammerschmidt, K., Kästner, A., Krueger, D., Ronnenberg, A., Ritter, C., Jatho, J., Radyushkin, K., Bourgeron, T., Fischer, J., Brose, N., & Ehrenreich, H. (2013). Development of an autism severity score for mice using *Nlgn4* null mutants as a construct-valid model of heritable monogenic autism. *Behavioural Brain Research*, *251*, 41–49. https://doi.org/10.1016/j.bbr.2012.11.016

Ethell, I. M., & Pasquale, E. B. (2005). Molecular mechanisms of dendritic spine development and remodeling. *Progress in Neurobiology*, *75*(3), 161–205. https://doi.org/10.1016/j.pneurobio.2005.02.003

Etherton, M., Földy, C., Sharma, M., Tabuchi, K., Liu, X., Shamloo, M., Malenka, R. C., & Südhof, T. C. (2011). Autism-linked neuroligin-3 R451C mutation differentially alters hippocampal and cortical synaptic function. *Proceedings of the National Academy of Sciences*, *108*(33), 13764–13769. https://doi.org/10.1073/pnas.1111093108

Faust, T. E., Gunner, G., & Schafer, D. P. (2021). Mechanisms governing activity-dependent synaptic pruning in the developing mammalian CNS. *Nature Reviews Neuroscience*, *22*(11), 657–673. https://doi.org/10.1038/s41583-021-00507-y

Fertan, E., Wong, A. A., Montbrun, T. S. G., Purdon, M. K., Roddick, K. M., Yamamoto, T., & Brown, R. E. (2023). Early postnatal development of the MDGA2+/- mouse model of synaptic dysfunction. *Behavioural Brain Research*, *452*, 114590. https://doi.org/10.1016/j.bbr.2023.114590

Fertan, E., Wong, A. A., Purdon, M. K., Weaver, I. C. G., & Brown, R. E. (2021). The effect of background strain on the behavioral phenotypes of the MDGA2+/− mouse model of autism spectrum disorder. *Genes, Brain and Behavior*, *20*(3), e12696. https://doi.org/10.1111/gbb.12696

Fiala, J. C., Feinberg, M., Popov, V., & Harris, K. M. (1998). Synaptogenesis Via Dendritic Filopodia in Developing Hippocampal Area CA1. *Journal of Neuroscience*, *18*(21), 8900–8911. https://doi.org/10.1523/JNEUROSCI.18-21-08900.1998

Fuccillo, M. V., Rothwell, P. E., Maxeiner, S., Hayton, S. J., Gokce, O., Lim, B. K., Fowler, S. C., Malenka, R. C., & Südhof, T. C. (2014). Autism-Associated Neuroligin-3 Mutations Commonly Impair Striatal Circuits to Boost Repetitive Behaviors. *Cell*, *158*(1), 198–212. https://doi.org/10.1016/j.cell.2014.04.045

García-López, P., García-Marín, V., & Freire, M. (2007). The discovery of dendritic spines by Cajal in 1888 and its relevance in the present neuroscience. *Progress in Neurobiology*, *83*(2), 110–130. https://doi.org/10.1016/j.pneurobio.2007.06.002

Gatto, C. L., & Broadie, K. (2010). Genetic Controls Balancing Excitatory and Inhibitory Synaptogenesis in Neurodevelopmental Disorder Models. *Frontiers in Synaptic Neuroscience*, *2*, 4. https://doi.org/10.3389/fnsyn.2010.00004

Ge, Y., Dong, Z., Bagot, R. C., Howland, J. G., Phillips, A. G., Wong, T. P., & Wang, Y. T. (2010). Hippocampal long-term depression is required for the consolidation of spatial memory. *Proceedings of the National Academy of Sciences*, *107*(38), 16697–16702. https://doi.org/10.1073/pnas.1008200107

Gerritsen, J. S., & White, F. M. (2021). Phosphoproteomics: A valuable tool for uncovering molecular signaling in cancer cells. *Expert Review of Proteomics*, *18*(8), 661–674. https://doi.org/10.1080/14789450.2021.1976152

Gesemann, M., Litwack, E. D., Yee, K. T., Christen, U., & O'Leary, D. D. M. (2001). Identification of Candidate Genes for Controlling Development of the Basilar Pons by Differential Display PCR. *Molecular and Cellular Neuroscience*, *18*(1), 1–12. https://doi.org/10.1006/mcne.2001.0996

Gipson, C. D., & Olive, M. F. (2017). Structural and functional plasticity of dendritic spines – root or result of behavior? *Genes, Brain, and Behavior*, *16*(1), 101–117. https://doi.org/10.1111/gbb.12324

Glessner, J. T., Wang, K., Cai, G., Korvatska, O., Kim, C. E., Wood, S., Zhang, H., Estes, A., Brune, C. W., Bradfield, J. P., Imielinski, M., Frackelton, E. C., Reichert, J., Crawford, E. L., Munson, J., Sleiman, P. M. A., Chiavacci, R., Annaiah, K., Thomas, K., … Hakonarson, H. (2009). Autism genome-wide copy number variation reveals ubiquitin and neuronal genes. *Nature*, *459*(7246), 569–573. https://doi.org/10.1038/nature07953

Goldani, A. A. S., Downs, S. R., Widjaja, F., Lawton, B., & Hendren, R. L. (2014). Biomarkers in Autism. *Frontiers in Psychiatry*, *5*, 100. https://doi.org/10.3389/fpsyt.2014.00100

Gomez-Arboledas, A., Acharya, M. M., & Tenner, A. J. (2021). The Role of Complement in Synaptic Pruning and Neurodegeneration. *ImmunoTargets and Therapy*, *10*, 373–386. https://doi.org/10.2147/ITT.S305420

Gulyássy, P., Puska, G., Györffy, B. A., Todorov-Völgyi, K., Juhász, G., Drahos, L., & Kékesi, K. A. (2020). Proteomic comparison of different synaptosome preparation procedures. *Amino Acids*, *52*(11–12), 1529–1543. https://doi.org/10.1007/s00726-020-02912-6

Hagena, H., & Manahan-Vaughan, D. (2024). Interplay of hippocampal long-term potentiation and long-term depression in enabling memory representations. *Philosophical Transactions of the Royal Society B: Biological Sciences*, *379*(1906), 20230229. https://doi.org/10.1098/rstb.2023.0229

Hamilton, A. M., & Zito, K. (2013). Breaking It Down: The Ubiquitin Proteasome System in Neuronal Morphogenesis. *Neural Plasticity*, *2013*, 196848. https://doi.org/10.1155/2013/196848

Harland, B., Contreras, M., Souder, M., & Fellous, J.-M. (2021). Dorsal CA1 hippocampal place cells form a multi-scale representation of megaspace. *Current Biology: CB*, *31*(10), 2178-2190.e6. https://doi.org/10.1016/j.cub.2021.03.003

Hebb, D. O. (1949). *Organization of Behaviour: A neuropsychological theory*. New York, NY : Wiley.

Henson, M. A., Tucker, C. J., Zhao, M., & Dudek, S. M. (2017). Long-term depression-associated signaling is required for an *in vitro* model of NMDA receptor-dependent synapse pruning. *Neurobiology of Learning and Memory*, *138*, 39–53. https://doi.org/10.1016/j.nlm.2016.10.013

Hernández-Frausto, M., & Vivar, C. (2024). Entorhinal cortex–hippocampal circuit connectivity in health and disease. *Frontiers in Human Neuroscience*, *18*, 1448791. https://doi.org/10.3389/fnhum.2024.1448791

Heynen, A. J., Yoon, B.-J., Liu, C.-H., Chung, H. J., Huganir, R. L., & Bear, M. F. (2003). Molecular mechanism for loss of visual cortical responsiveness following brief monocular deprivation. *Nature Neuroscience*, *6*(8), 854–862. https://doi.org/10.1038/nn1100

Horton, S., Mastrolia, V., Jackson, R. E., Kemlo, S., Pereira Machado, P. M., Carbajal, M. A., Hindges, R., Fleck, R. A., Aguiar, P., Neves, G., & Burrone, J. (2024). Excitatory and inhibitory synapses show a tight subcellular correlation that weakens over development. *Cell Reports*, *43*(7), 114361. https://doi.org/10.1016/j.celrep.2024.114361

Hou, L., & Klann, E. (2004). Activation of the phosphoinositide 3-kinase-Akt-mammalian target of rapamycin signaling pathway is required for metabotropic glutamate receptor-dependent long-term depression. *The Journal of Neuroscience: The Official Journal of the Society for Neuroscience*, *24*(28), 6352–6361. https://doi.org/10.1523/JNEUROSCI.0995-04.2004

Huang, C., Voglewede, M. M., Ozsen, E. N., Wang, H., & Zhang, H. (2023). SHANK3 Mutations Associated with Autism and Schizophrenia Lead to Shared and Distinct Changes in Dendritic Spine Dynamics in the Developing Mouse Brain. *Neuroscience*, *528*, 1–11. https://doi.org/10.1016/j.neuroscience.2023.07.024

Huang, D. W., Sherman, B. T., & Lempicki, R. A. (2009a). Bioinformatics enrichment tools: Paths toward the comprehensive functional analysis of large gene lists. *Nucleic Acids Research*, *37*(1), 1–13. https://doi.org/10.1093/nar/gkn923

Huang, D. W., Sherman, B. T., & Lempicki, R. A. (2009b). Systematic and integrative analysis of large gene lists using DAVID bioinformatics resources. *Nature Protocols*, *4*(1), 44–57. https://doi.org/10.1038/nprot.2008.211

Huber, K. M., Gallagher, S. M., Warren, S. T., & Bear, M. F. (2002). Altered synaptic plasticity in a mouse model of fragile X mental retardation. *Proceedings of the National Academy of Sciences*, *99*(11), 7746–7750. https://doi.org/10.1073/pnas.122205699

Huber, K. M., Kayser, M. S., & Bear, M. F. (2000). Role for rapid dendritic protein synthesis in hippocampal mGluR-dependent long-term depression. *Science (New York, N.Y.)*, *288*(5469), 1254–1257. https://doi.org/10.1126/science.288.5469.1254

Huber, K. M., Roder, J. C., & Bear, M. F. (2001). Chemical Induction of mGluR5- and Protein Synthesis–Dependent Long-Term Depression in Hippocampal Area CA1. *Journal of Neurophysiology*, *86*(1), 321–325. https://doi.org/10.1152/jn.2001.86.1.321

Humphreys, G. W., Duncan, J., Treisman, A., O'Keefe, J., Burgess, N., Donnett, J. G., Jeffery, K. J., & Maguire, E. A. (1998). Place cells, navigational accuracy, and the human

hippocampus. *Philosophical Transactions of the Royal Society of London. Series B: Biological Sciences*, *353*(1373), 1333–1340. https://doi.org/10.1098/rstb.1998.0287

Huo, Y., Zhao, D., Zhu, X., Zheng, N., Yang, D., Meng, J., Chen, Y., & Zhang, Y. (2025). RPS23RG1 inhibits SORT1-mediated lysosomal degradation of MDGA2 to protect against autism. *Theranostics*, *15*(4), 1338–1352. https://doi.org/10.7150/thno.100451

Iacobucci, G. J., & Popescu, G. K. (2018). Kinetic models for activation and modulation of NMDA receptor subtypes. *Current Opinion in Physiology*, *2*, 114–122. https://doi.org/10.1016/j.cophys.2018.02.002

Ishikawa, T., Gotoh, N., Murayama, C., Abe, T., Iwashita, M., Matsuzaki, F., Suzuki, T., & Yamamoto, T. (2011). IgSF molecule MDGA1 is involved in radial migration and positioning of a subset of cortical upper-layer neurons. *Developmental Dynamics: An Official Publication of the American Association of Anatomists*, *240*(1), 96–107. https://doi.org/10.1002/dvdy.22496

Jamain, S., Quach, H., Betancur, C., Råstam, M., Colineaux, C., Gillberg, I. C., Söderström, H., Giros, B., Leboyer, M., Gillberg, C., & Bourgeron, T. (2003). Mutations of the X-linked genes encoding neuroligins NLGN3 and NLGN4 are associated with autism. *Nature Genetics*, *34*(1), 27–29. https://doi.org/10.1038/ng1136

Jamain, S., Radyushkin, K., Hammerschmidt, K., Granon, S., Boretius, S., Varoqueaux, F., Ramanantsoa, N., Gallego, J., Ronnenberg, A., Winter, D., Frahm, J., Fischer, J., Bourgeron, T., Ehrenreich, H., & Brose, N. (2008). Reduced social interaction and ultrasonic communication in a mouse model of monogenic heritable autism. *Proceedings of the National Academy of Sciences*, *105*(5), 1710–1715. https://doi.org/10.1073/pnas.0711555105

Jin, W. (2020). Regulation of BDNF-TrkB Signaling and Potential Therapeutic Strategies for Parkinson's Disease. *Journal of Clinical Medicine*, *9*(1), Article 1. https://doi.org/10.3390/jcm9010257

Jin, Y., & Garner, C. C. (2008). Molecular mechanisms of presynaptic differentiation. *Annual Review of Cell and Developmental Biology*, *24*, 237–262. https://doi.org/10.1146/annurev.cellbio.23.090506.123417

Joset, P., Wacker, A., Babey, R., Ingold, E. A., Andermatt, I., Stoeckli, E. T., & Gesemann, M. (2011). Rostral growth of commissural axons requires the cell adhesion molecule MDGA2. *Neural Development*, *6*, 22. https://doi.org/10.1186/1749-8104-6-22

Kähler, A. K., Djurovic, S., Kulle, B., Jönsson, E. G., Agartz, I., Hall, H., Opjordsmoen, S., Jakobsen, K. D., Hansen, T., Melle, I., Werge, T., Steen, V. M., & Andreassen, O. A. (2008). Association analysis of schizophrenia on 18 genes involved in neuronal migration: MDGA1 as a new susceptibility gene. *American Journal of Medical Genetics. Part B, Neuropsychiatric Genetics: The Official Publication of the International Society of Psychiatric Genetics*, *147B*(7), 1089–1100. https://doi.org/10.1002/ajmg.b.30726

Kaizuka, T., & Takumi, T. (2024). Alteration of synaptic protein composition during developmental synapse maturation. *The European Journal of Neuroscience*, *59*(11), 2894–2914. https://doi.org/10.1111/ejn.16304

Kasherman, M. A., Premarathne, S., Burne, T. H. J., Wood, S. A., & Piper, M. (2020). The Ubiquitin System: A Regulatory Hub for Intellectual Disability and Autism Spectrum Disorder. *Molecular Neurobiology*, *57*(5), 2179–2193. https://doi.org/10.1007/s12035-020-01881-x

Kazdoba, T. M., Leach, P. T., & Crawley, J. N. (2016). Behavioral phenotypes of genetic mouse models of autism. *Genes, Brain, and Behavior*, *15*(1), 7–26. https://doi.org/10.1111/gbb.12256

Kazdoba, T. M., Leach, P. T., Yang, M., Silverman, J. L., Solomon, M., & Crawley, J. N. (2016). Translational Mouse Models of Autism: Advancing Toward Pharmacological Therapeutics. *Current Topics in Behavioral Neurosciences*, *28*, 1–52. https://doi.org/10.1007/7854_2015_5003

Kemp, A., & Manahan-Vaughan, D. (2004). Hippocampal long-term depression and long-term potentiation encode different aspects of novelty acquisition. *Proceedings of the National Academy of Sciences*, *101*(21), 8192–8197. https://doi.org/10.1073/pnas.0402650101

Kessels, R. P. C., de Haan, E. H. F., Kappelle, L. J., & Postma, A. (2001). Varieties of human spatial memory: A meta-analysis on the effects of hippocampal lesions. *Brain Research Reviews*, *35*(3), 295–303. https://doi.org/10.1016/S0165-0173(01)00058-3

Kim, H. Y., Um, J. W., & Ko, J. (2021). Proper synaptic adhesion signaling in the control of neural circuit architecture and brain function. *Progress in Neurobiology*, *200*, 101983. https://doi.org/10.1016/j.pneurobio.2020.101983

Kim, J. A., Kim, D., Won, S. Y., Han, K. A., Park, D., Cho, E., Yun, N., An, H. J., Um, J. W., Kim, E., Lee, J.-O., Ko, J., & Kim, H. M. (2017). Structural Insights into Modulation of Neurexin-Neuroligin *Trans*-synaptic Adhesion by MDGA1/Neuroligin-2 Complex. *Neuron*, *94*(6), 1121-1131.e6. https://doi.org/10.1016/j.neuron.2017.05.034

Kim, S., Jang, G., Kim, H., Lim, D., Han, K. A., Um, J. W., & Ko, J. (2024). MDGAs perform activity-dependent synapse type-specific suppression via distinct extracellular mechanisms. *Proceedings of the National Academy of Sciences*, *121*(26), e2322978121. https://doi.org/10.1073/pnas.2322978121

Knierim, J. J. (2015). The hippocampus. *Current Biology*, *25*(23), R1116–R1121. https://doi.org/10.1016/j.cub.2015.10.049

Kouser, L., Madhukaran, S. P., Shastri, A., Saraon, A., Ferluga, J., Al-Mozaini, M., & Kishore, U. (2015). Emerging and Novel Functions of Complement Protein C1q. *Frontiers in Immunology*, *6*. https://doi.org/10.3389/fimmu.2015.00317

Kouvaros, S., & Papatheodoropoulos, C. (2016). Theta burst stimulation-induced LTP: Differences and similarities between the dorsal and ventral CA1 hippocampal synapses. *Hippocampus*, *26*(12), 1542–1559. https://doi.org/10.1002/hipo.22655

Krueger, D. D., Tuffy, L. P., Papadopoulos, T., & Brose, N. (2012). The role of neurexins and neuroligins in the formation, maturation, and function of vertebrate synapses. *Current Opinion in Neurobiology*, *22*(3), 412–422. https://doi.org/10.1016/j.conb.2012.02.012

Landa, R. J. (2008). Diagnosis of autism spectrum disorders in the first 3 years of life. *Nature Clinical Practice Neurology*, *4*(3), Article 3. https://doi.org/10.1038/ncpneuro0731

Lee, A. K., Khaled, H., Chofflet, N., & Takahashi, H. (2020). Synaptic Organizers in Alzheimer's Disease: A Classification Based on Amyloid-β Sensitivity. *Frontiers in Cellular Neuroscience*, *14*. https://www.frontiersin.org/articles/10.3389/fncel.2020.00281

Lee, A.-R., Kim, J.-H., Cho, E., Kim, M., & Park, M. (2017). Dorsal and Ventral Hippocampus Differentiate in Functional Pathways and Differentially Associate with Neurological Disease-Related Genes during Postnatal Development. *Frontiers in Molecular Neuroscience*, *10*, 331. https://doi.org/10.3389/fnmol.2017.00331

Lee, E., Lee, J., & Kim, E. (2017). Excitation/Inhibition Imbalance in Animal Models of Autism Spectrum Disorders. *Biological Psychiatry*, *81*(10), 838–847. https://doi.org/10.1016/j.biopsych.2016.05.011

Lee, K., Kim, Y., Lee, S.-J., Qiang, Y., Lee, D., Lee, H. W., Kim, H., Je, H. S., Südhof, T. C., & Ko, J. (2013). MDGAs interact selectively with neuroligin-2 but not other neuroligins to regulate inhibitory synapse development. *Proceedings of the National Academy of Sciences*, *110*(1), 336–341. https://doi.org/10.1073/pnas.1219987110

Lee, K., Vyas, Y., Garner, C. C., & Montgomery, J. M. (2019). Autism-associated Shank3 mutations alter mGluR expression and mGluR-dependent but not NMDA receptor-dependent long-term depression. *Synapse*, *73*(8), e22097. https://doi.org/10.1002/syn.22097

Leisman, G., & Melillo, R. (2025). Autism Spectrum Disorder: What Do We Know and Where Do We Go? *Brain Sciences*, *15*(9), 1010. https://doi.org/10.3390/brainsci15091010

Leuner, B., & Gould, E. (2010). Structural Plasticity and Hippocampal Function. *Annual Review of Psychology*, *61*, 111-C3. https://doi.org/10.1146/annurev.psych.093008.100359

Li, J., Liu, J., Feng, G., Li, T., Zhao, Q., Li, Y., Hu, Z., Zheng, L., Zeng, Z., He, L., Wang, T., & Shi, Y. (2011). The MDGA1 gene confers risk to schizophrenia and bipolar disorder. *Schizophrenia Research*, *125*(2–3), 194–200. https://doi.org/10.1016/j.schres.2010.11.002

Li, X.-H., Song, Q., Chen, T., & Zhuo, M. (2017). Characterization of postsynaptic calcium signals in the pyramidal neurons of anterior cingulate cortex. *Molecular Pain*, *13*, 1744806917719847. https://doi.org/10.1177/1744806917719847

Limon, A., & Corona-Moreno, M. (2025). Hyperconnectivity and Disrupted Signal-to-Noise Processing in Autism. In *The Palgrave Encyclopedia of Disability* (pp. 1–9). Palgrave Macmillan, Cham. https://doi.org/10.1007/978-3-031-40858-8_179-1

Lin, B., Kramár, E. A., Bi, X., Brucher, F. A., Gall, C. M., & Lynch, G. (2005). Theta Stimulation Polymerizes Actin in Dendritic Spines of Hippocampus. *Journal of Neuroscience*, *25*(8), 2062–2069. https://doi.org/10.1523/JNEUROSCI.4283-04.2005

Litwack, E. D., Babey, R., Buser, R., Gesemann, M., & O'Leary, D. D. M. (2004). Identification and characterization of two novel brain-derived immunoglobulin superfamily members with a unique structural organization. *Molecular and Cellular Neuroscience*, *25*(2), 263–274. https://doi.org/10.1016/j.mcn.2003.10.016

Liu, L., Wong, T. P., Pozza, M. F., Lingenhoehl, K., Wang, Y., Sheng, M., Auberson, Y. P., & Wang, Y. T. (2004). Role of NMDA Receptor Subtypes in Governing the Direction of Hippocampal Synaptic Plasticity. *Science*, *304*(5673), 1021–1024. https://doi.org/10.1126/science.1096615

Liu, X., Gu, Q.-H., Duan, K., & Li, Z. (2014). NMDA Receptor-Dependent LTD Is Required for Consolidation But Not Acquisition of Fear Memory. *The Journal of Neuroscience*, *34*(26), 8741–8748. https://doi.org/10.1523/JNEUROSCI.2752-13.2014

Liu, X., Lin, J., Zhang, H., Khan, N. U., Zhang, J., Tang, X., Cao, X., & Shen, L. (2022). Oxidative Stress in Autism Spectrum Disorder—Current Progress of Mechanisms and Biomarkers. *Frontiers in Psychiatry*, *13*, 813304. https://doi.org/10.3389/fpsyt.2022.813304

Loh, K. H., Stawski, P. S., Draycott, A. S., Udeshi, N. D., Lehrman, E. K., Wilton, D. K., Svinkina, T., Deerinck, T. J., Ellisman, M. H., Stevens, B., Carr, S. A., & Ting, A. Y.

(2016). Proteomic Analysis of Unbounded Cellular Compartments: Synaptic Clefts. *Cell*, *166*(5), 1295-1307.e21. https://doi.org/10.1016/j.cell.2016.07.041
Lohmann, C., & Kessels, H. W. (2014). The developmental stages of synaptic plasticity. *The Journal of Physiology*, *592*(1), 13–31. https://doi.org/10.1113/jphysiol.2012.235119
Louros, S. R., & Osterweil, E. K. (2016). Perturbed proteostasis in autism spectrum disorders. *Journal of Neurochemistry*, *139*(6), 1081–1092. https://doi.org/10.1111/jnc.13723
Lowe, A., Dalton, M., Sidhu, K., Sachdev, P., Reynolds, B., & Valenzuela, M. (2015). Neurogenesis and precursor cell differences in the dorsal and ventral adult canine hippocampus. *Neuroscience Letters*, *593*, 107–113. https://doi.org/10.1016/j.neulet.2015.03.017
Lüscher, C., & Huber, K. M. (2010). Group 1 mGluR-dependent synaptic long-term depression (mGluR-LTD): Mechanisms and implications for circuitry & disease. *Neuron*, *65*(4), 445–459. https://doi.org/10.1016/j.neuron.2010.01.016
Lüscher, C., & Malenka, R. C. (2012). NMDA Receptor-Dependent Long-Term Potentiation and Long-Term Depression (LTP/LTD). *Cold Spring Harbor Perspectives in Biology*, *4*(6), a005710. https://doi.org/10.1101/cshperspect.a005710
Lüscher, C., Xia, H., Beattie, E. C., Carroll, R. C., Von Zastrow, M., Malenka, R. C., & Nicoll, R. A. (1999). Role of AMPA Receptor Cycling in Synaptic Transmission and Plasticity. *Neuron*, *24*(3), 649–658. https://doi.org/10.1016/S0896-6273(00)81119-8
Maguire, E. A., Burke, T., Phillips, J., & Staunton, H. (1996). Topographical disorientation following unilateral temporal lobe lesions in humans. *Neuropsychologia*, *34*(10), 993–1001. https://doi.org/10.1016/0028-3932(96)00022-x
Maguire, E. A., Frackowiak, R. S., & Frith, C. D. (1996). Learning to find your way: A role for the human hippocampal formation. *Proceedings. Biological Sciences*, *263*(1377), 1745–1750. https://doi.org/10.1098/rspb.1996.0255
Mango, D., & Ledonne, A. (2023). Updates on the Physiopathology of Group I Metabotropic Glutamate Receptors (mGluRI)-Dependent Long-Term Depression. *Cells*, *12*(12), 1588. https://doi.org/10.3390/cells12121588
Maruki, K., Izaki, Y., Nomura, M., & Yamauchi, T. (2001). Differences in paired-pulse facilitation and long-term potentiation between dorsal and ventral CA1 regions in anesthetized rats. *Hippocampus*, *11*(6), 655–661. https://doi.org/10.1002/hipo.1080
Matuskey, D., Yang, Y., Naganawa, M., Koohsari, S., Toyonaga, T., Gravel, P., Pittman, B., Torres, K., Pisani, L., Finn, C., Cramer-Benjamin, S., Herman, N., Rosenthal, L. H., Franke, C. J., Walicki, B. M., Esterlis, I., Skosnik, P., Radhakrishnan, R., Wolf, J. M., … McPartland, J. C. (2024). 11C-UCB-J PET imaging is consistent with lower synaptic density in autistic adults. *Molecular Psychiatry*, *30*(4), 1610–1616. https://doi.org/10.1038/s41380-024-02776-2
McClelland, J. L., McNaughton, B. L., & O'Reilly, R. C. (1995). Why there are complementary learning systems in the hippocampus and neocortex: Insights from the successes and failures of connectionist models of learning and memory. *Psychological Review*, *102*(3), 419–457. https://doi.org/10.1037/0033-295X.102.3.419
Megías, M., Emri, Z., Freund, T. F., & Gulyás, A. I. (2001). Total number and distribution of inhibitory and excitatory synapses on hippocampal CA1 pyramidal cells. *Neuroscience*, *102*(3), 527–540. https://doi.org/10.1016/s0306-4522(00)00496-6
Mizuno, T., Kanazawa, I., & Sakurai, M. (2001). Differential induction of LTP and LTD is not determined solely by instantaneous calcium concentration: An essential involvement of a

temporal factor. *European Journal of Neuroscience*, *14*(4), 701–708. https://doi.org/10.1046/j.0953-816x.2001.01679.x
Mulkey, R. M., Herron, C. E., & Malenka, R. C. (1993). An Essential Role for Protein Phosphatases in Hippocampal Long-Term Depression. *Science*, *261*(5124), 1051–1055. https://doi.org/10.1126/science.8394601
Müller, G. E., & Pilzecker, A. (1900). Experimentelle beiträge zur lehre vom gedächtniss. *Ja Barth*, *1*.
Nabavi, S., Fox, R., Proulx, C. D., Lin, J. Y., Tsien, R. Y., & Malinow, R. (2014). Engineering a memory with LTD and LTP. *Nature*, *511*(7509), Article 7509. https://doi.org/10.1038/nature13294
Nägerl, U. V., Eberhorn, N., Cambridge, S. B., & Bonhoeffer, T. (2004). Bidirectional Activity-Dependent Morphological Plasticity in Hippocampal Neurons. *Neuron*, *44*(5), 759–767. https://doi.org/10.1016/j.neuron.2004.11.016
Navlakha, S., Barth, A. L., & Bar-Joseph, Z. (2015). Decreasing-Rate Pruning Optimizes the Construction of Efficient and Robust Distributed Networks. *PLOS Computational Biology*, *11*(7), e1004347. https://doi.org/10.1371/journal.pcbi.1004347
Nimchinsky, E. A., Sabatini, B. L., & Svoboda, K. (2002). Structure and function of dendritic spines. *Annual Review of Physiology*, *64*, 313–353. https://doi.org/10.1146/annurev.physiol.64.081501.160008
Nobel Prize in Physiology or Medicine 1906. (n.d.). NobelPrize.Org. Retrieved October 28, 2025, from https://www.nobelprize.org/prizes/medicine/1906/summary/
Nomi, J. S., & Uddin, L. Q. (2015). Developmental changes in large-scale network connectivity in autism. *NeuroImage: Clinical*, *7*, 732–741. https://doi.org/10.1016/j.nicl.2015.02.024
Nomura, J., Mardo, M., & Takumi, T. (2021). Molecular signatures from multi-omics of autism spectrum disorders and schizophrenia. *Journal of Neurochemistry*, *159*(4), 647–659. https://doi.org/10.1111/jnc.15514
Nourbakhsh, K., & Yadav, S. (2021). Kinase Signaling in Dendritic Development and Disease. *Frontiers in Cellular Neuroscience*, *15*. https://doi.org/10.3389/fncel.2021.624648
O'Keefe, J., & Conway, D. H. (1978). Hippocampal place units in the freely moving rat: Why they fire where they fire. *Experimental Brain Research*, *31*(4), 573–590. https://doi.org/10.1007/BF00239813
O'Keefe, J., & Dostrovsky, J. (1971). The hippocampus as a spatial map. Preliminary evidence from unit activity in the freely-moving rat. *Brain Research*, *34*(1), 171–175. https://doi.org/10.1016/0006-8993(71)90358-1
Okuyama, T., Kitamura, T., Roy, D. S., Itohara, S., & Tonegawa, S. (2016). Ventral CA1 neurons store social memory. *Science*, *353*(6307), 1536–1541. https://doi.org/10.1126/science.aaf7003
Oliet, S. H. R., Malenka, R. C., & Nicoll, R. A. (1997). Two Distinct Forms of Long-Term Depression Coexist in CA1 Hippocampal Pyramidal Cells. *Neuron*, *18*(6), 969–982. https://doi.org/10.1016/S0896-6273(00)80336-0
Onay, H., Kacamak, D., Kavasoglu, A., Akgun, B., Yalcinli, M., Kose, S., & Ozbaran, B. (2016). Mutation Analysis of the NRXN1 Gene in Autism Spectrum Disorders. *Balkan Journal of Medical Genetics : BJMG*, *19*(2), 17–22. https://doi.org/10.1515/bjmg-2016-0031
Oostrum, M. van, Blok, T. M., Giandomenico, S. L., Dieck, S. tom, Tushev, G., Fürst, N., Langer, J. D., & Schuman, E. M. (2023). The proteomic landscape of synaptic diversity

across brain regions and cell types. *Cell*, *186*(24), 5411-5427.e23. https://doi.org/10.1016/j.cell.2023.09.028

Pang, Z., Lu, Y., Zhou, G., Hui, F., Xu, L., Viau, C., Spigelman, A. F., MacDonald, P. E., Wishart, D. S., Li, S., & Xia, J. (2024). MetaboAnalyst 6.0: Towards a unified platform for metabolomics data processing, analysis and interpretation. *Nucleic Acids Research*, *52*(W1), W398–W406. https://doi.org/10.1093/nar/gkae253

Pangrazzi, L., Balasco, L., & Bozzi, Y. (2020). Oxidative Stress and Immune System Dysfunction in Autism Spectrum Disorders. *International Journal of Molecular Sciences*, *21*(9), 3293. https://doi.org/10.3390/ijms21093293

Paolicelli, R. C., Bolasco, G., Pagani, F., Maggi, L., Scianni, M., Panzanelli, P., Giustetto, M., Ferreira, T. A., Guiducci, E., Dumas, L., Ragozzino, D., & Gross, C. T. (2011). Synaptic Pruning by Microglia Is Necessary for Normal Brain Development. *Science*, *333*(6048), 1456–1458. https://doi.org/10.1126/science.1202529

Papatheodoropoulos, C., & Kouvaros, S. (2016). High-frequency stimulation-induced synaptic potentiation in dorsal and ventral CA1 hippocampal synapses: The involvement of NMDA receptors, mGluR5, and (L-type) voltage-gated calcium channels. *Learning & Memory*, *23*(9), 460–464. https://doi.org/10.1101/lm.042531.116

Pearson, H. (2025, August 26). *Autism is on the rise: What's really behind the increase?* Nature. https://www.nature.com/articles/d41586-025-02636-1

Pettem, K. L., Yokomaku, D., Takahashi, H., Ge, Y., & Craig, A. M. (2013). Interaction between autism-linked MDGAs and neuroligins suppresses inhibitory synapse development. *Journal of Cell Biology*, *200*(3), 321–336. https://doi.org/10.1083/jcb.201206028

Phillips, M. L., Robinson, H. A., & Pozzo-Miller, L. (2019). Ventral hippocampal projections to the medial prefrontal cortex regulate social memory. *eLife*, *8*, e44182. https://doi.org/10.7554/eLife.44182

Pinar, C., Fontaine, C. J., Triviño-Paredes, J., Lottenberg, C. P., Gil-Mohapel, J., & Christie, B. R. (2017). Revisiting the flip side: Long-term depression of synaptic efficacy in the hippocampus. *Neuroscience & Biobehavioral Reviews*, *80*, 394–413. https://doi.org/10.1016/j.neubiorev.2017.06.001

Piochon, C., Kano, M., & Hansel, C. (2016). LTD-like molecular pathways in developmental synaptic pruning. *Nature Neuroscience*, *19*(10), Article 10. https://doi.org/10.1038/nn.4389

Posit team. (2025). *RStudio: Integrated Development Environment for R* (Version 2025.9.0.387) [R]. Posit Software, PBC. http://www.posit.co/.

Pradhan, J., Noakes, P. G., & Bellingham, M. C. (2019). The Role of Altered BDNF/TrkB Signaling in Amyotrophic Lateral Sclerosis. *Frontiers in Cellular Neuroscience*, *13*. https://doi.org/10.3389/fncel.2019.00368

Public Health Agency of Canada. (2016, January 18). *Autism: Signs and symptoms* [Education and awareness]. https://www.canada.ca/en/public-health/services/diseases/autism-spectrum-disorder-asd/signs-symptoms-autism-spectrum-disorder-asd.html

Public Health Agency of Canada. (2022). *Autism spectrum disorder: Highlights from the 2019 Canadian health survey on children and youth* [Research]. https://www.canada.ca/en/public-health/services/publications/diseases-conditions/autism-spectrum-disorder-canadian-health-survey-children-youth-2019.html

Qi, C., Luo, L.-D., Feng, I., & Ma, S. (2022). Molecular mechanisms of synaptogenesis. *Frontiers in Synaptic Neuroscience*, *14*. https://doi.org/10.3389/fnsyn.2022.939793

Redman, W. T., Wolcott, N. S., Montelisciani, L., Luna, G., Marks, T. D., Sit, K. K., Yu, C.-H., Smith, S., & Goard, M. J. (2022). Long-term transverse imaging of the hippocampus with glass microperiscopes. *eLife*, *11*, e75391. https://doi.org/10.7554/eLife.75391

Revest, J.-M., Le Roux, A., Roullot-Lacarrière, V., Kaouane, N., Vallée, M., Kasanetz, F., Rougé-Pont, F., Tronche, F., Desmedt, A., & Piazza, P. V. (2014). BDNF-TrkB signaling through Erk1/2MAPK phosphorylation mediates the enhancement of fear memory induced by glucocorticoids. *Molecular Psychiatry*, *19*(9), 1001–1009. https://doi.org/10.1038/mp.2013.134

Risher, W. C., Ustunkaya, T., Alvarado, J. S., & Eroglu, C. (2014). Rapid Golgi Analysis Method for Efficient and Unbiased Classification of Dendritic Spines. *PLOS ONE*, *9*(9), e107591. https://doi.org/10.1371/journal.pone.0107591

Rubenstein, J. L. R., & Merzenich, M. M. (2003). Model of autism: Increased ratio of excitation/inhibition in key neural systems. *Genes, Brain, and Behavior*, *2*(5), 255–267. https://doi.org/10.1034/j.1601-183x.2003.00037.x

Sakai, J. (2020). Core Concept: How synaptic pruning shapes neural wiring during development and, possibly, in disease. *Proceedings of the National Academy of Sciences of the United States of America*, *117*(28), 16096–16099. https://doi.org/10.1073/pnas.2010281117

Sauer, A. K., Stanton, J. E., Hans, S., & Grabrucker, A. M. (2021). Autism Spectrum Disorders: Etiology and Pathology. In A. M. Grabrucker (Ed.), *Autism Spectrum Disorders*. Exon Publications. http://www.ncbi.nlm.nih.gov/books/NBK573613/

Schaan Profes, M., Tiroumalechetty, A., Patel, N., Lauar, S. S., Sidoli, S., & Kurshan, P. T. (2024). Characterization of the intracellular neurexin interactome by in vivo proximity ligation suggests its involvement in presynaptic actin assembly. *PLOS Biology*, *22*(1), e3002466. https://doi.org/10.1371/journal.pbio.3002466

Schirò, G., Iacono, S., Ragonese, P., Aridon, P., Salemi, G., & Balistreri, C. R. (2022). A Brief Overview on BDNF-Trk Pathway in the Nervous System: A Potential Biomarker or Possible Target in Treatment of Multiple Sclerosis? *Frontiers in Neurology*, *13*, 917527. https://doi.org/10.3389/fneur.2022.917527

Schulman, H. (1995). Protein phosphorylation in neuronal plasticity and gene expression. *Current Opinion in Neurobiology*, *5*(3), 375–381. https://doi.org/10.1016/0959-4388(95)80051-4

Schwanhäusser, B., Busse, D., Li, N., Dittmar, G., Schuchhardt, J., Wolf, J., Chen, W., & Selbach, M. (2011). Global quantification of mammalian gene expression control. *Nature*, *473*(7347), 337–342. https://doi.org/10.1038/nature10098

Scoville, W. B., & Milner, B. (1957). LOSS OF RECENT MEMORY AFTER BILATERAL HIPPOCAMPAL LESIONS. *Journal of Neurology, Neurosurgery, and Psychiatry*, *20*(1), 11–21. https://doi.org/10.1136/jnnp.20.1.11

Semple, B. D., Blomgren, K., Gimlin, K., Ferriero, D. M., & Noble-Haeusslein, L. J. (2013). Brain development in rodents and humans: Identifying benchmarks of maturation and vulnerability to injury across species. *Progress in Neurobiology*, *0*, 1–16. https://doi.org/10.1016/j.pneurobio.2013.04.001

Shimada, T., & Yamagata, K. (2022). Spine morphogenesis and synapse formation in tubular sclerosis complex models. *Frontiers in Molecular Neuroscience*, *15*, 1019343. https://doi.org/10.3389/fnmol.2022.1019343

Shinoda, Y., Tanaka, T., Tominaga-Yoshino, K., & Ogura, A. (2010). Persistent Synapse Loss Induced by Repetitive LTD in Developing Rat Hippocampal Neurons. *PLoS ONE*, *5*(4), e10390. https://doi.org/10.1371/journal.pone.0010390

Siddiqui, T. J., & Craig, A. M. (2011). Synaptic organizing complexes. *Current Opinion in Neurobiology*, *21*(1), 132–143. https://doi.org/10.1016/j.conb.2010.08.016

Squire, L. R. (2009). The Legacy of Patient H.M. for Neuroscience. *Neuron*, *61*(1), 6–9. https://doi.org/10.1016/j.neuron.2008.12.023

Squire, L. R., Genzel, L., Wixted, J. T., & Morris, R. G. (2015). Memory Consolidation. *Cold Spring Harbor Perspectives in Biology*, *7*(8), a021766. https://doi.org/10.1101/cshperspect.a021766

Stacho, M., & Manahan-Vaughan, D. (2022). The Intriguing Contribution of Hippocampal Long-Term Depression to Spatial Learning and Long-Term Memory. *Frontiers in Behavioral Neuroscience*, *16*, 806356. https://doi.org/10.3389/fnbeh.2022.806356

Stampanoni Bassi, M., Iezzi, E., Gilio, L., Centonze, D., & Buttari, F. (2019). Synaptic Plasticity Shapes Brain Connectivity: Implications for Network Topology. *International Journal of Molecular Sciences*, *20*(24), 6193. https://doi.org/10.3390/ijms20246193

Sun, L., Ohashi, N., Mori, T., Mizuno, Y., Zang, W., Guo, Q., Kouyama-Suzuki, E., Shirai, Y., & Tabuchi, K. (2024). Adult neurogenesis in the ventral hippocampus decreased among animal models of neurodevelopmental disorders. *Frontiers in Neural Circuits*, *18*. https://doi.org/10.3389/fncir.2024.1504191

Takeuchi, A., Hamasaki, T., Litwack, E. D., & O'Leary, D. D. M. (2007). Novel IgCAM, MDGA1, expressed in unique cortical area- and layer-specific patterns and transiently by distinct forebrain populations of Cajal-Retzius neurons. *Cerebral Cortex (New York, N.Y.: 1991)*, *17*(7), 1531–1541. https://doi.org/10.1093/cercor/bhl064

Talantseva, O. I., Romanova, R. S., Shurdova, E. M., Dolgorukova, T. A., Sologub, P. S., Titova, O. S., Kleeva, D. F., & Grigorenko, E. L. (2023). The global prevalence of autism spectrum disorder: A three-level meta-analysis. *Frontiers in Psychiatry*, *14*, 1071181. https://doi.org/10.3389/fpsyt.2023.1071181

Tang, G., Gudsnuk, K., Kuo, S.-H., Cotrina, M. L., Rosoklija, G., Sosunov, A., Sonders, M. S., Kanter, E., Castagna, C., Yamamoto, A., Yue, Z., Arancio, O., Peterson, B. S., Champagne, F., Dwork, A. J., Goldman, J., & Sulzer, D. (2014). Loss of mTOR-Dependent Macroautophagy Causes Autistic-like Synaptic Pruning Deficits. *Neuron*, *83*(5), 1131–1143. https://doi.org/10.1016/j.neuron.2014.07.040

Tau, G. Z., & Peterson, B. S. (2010). Normal Development of Brain Circuits. *Neuropsychopharmacology*, *35*(1), 147–168. https://doi.org/10.1038/npp.2009.115

Tchantchou, F., Lacor, P., Cao, Z., Lao, L., Hou, Y., Cui, C., Klein, W., & Luo, Y. (2009). Stimulation of Neurogenesis and Synaptogenesis by Bilobalide and Quercetin via Common Final Pathway in Hippocampal Neurons. *Journal of Alzheimer's Disease*, *18*, 787–798. https://doi.org/10.3233/JAD-2009-1189

Tian, Y., Yang, C., Shang, S., Cai, Y., Deng, X., Zhang, J., Shao, F., Zhu, D., Liu, Y., Chen, G., Liang, J., Sun, Q., Qiu, Z., & Zhang, C. (2017). Loss of FMRP Impaired Hippocampal Long-Term Plasticity and Spatial Learning in Rats. *Frontiers in Molecular Neuroscience*, *10*. https://doi.org/10.3389/fnmol.2017.00269

Tidball, P., Burn, H. V., Teh, K. L., Volianskis, A., Collingridge, G. L., & Fitzjohn, S. M. (2017). Differential ability of the dorsal and ventral rat hippocampus to exhibit group I metabotropic glutamate receptor–dependent synaptic and intrinsic plasticity. *Brain and*

Neuroscience Advances, *1*, 2398212816689792. https://doi.org/10.1177/2398212816689792

Toledo, A., Letellier, M., Bimbi, G., Tessier, B., Daburon, S., Favereaux, A., Chamma, I., Vennekens, K., Vanderlinden, J., Sainlos, M., de Wit, J., Choquet, D., & Thoumine, O. (2022). MDGAs are fast-diffusing molecules that delay excitatory synapse development by altering neuroligin behavior. *eLife*, *11*, e75233. https://doi.org/10.7554/eLife.75233

Trompoukis, G., & Papatheodoropoulos, C. (2020). Dorsal-Ventral Differences in Modulation of Synaptic Transmission in the Hippocampus. *Frontiers in Synaptic Neuroscience*, *12*. https://doi.org/10.3389/fnsyn.2020.00024

Usui, N., Kobayashi, H., & Shimada, S. (2023). Neuroinflammation and Oxidative Stress in the Pathogenesis of Autism Spectrum Disorder. *International Journal of Molecular Sciences*, *24*(6), 5487. https://doi.org/10.3390/ijms24065487

van der Staay, F. J., Arndt, S. S., & Nordquist, R. E. (2009). Evaluation of animal models of neurobehavioral disorders. *Behavioral and Brain Functions : BBF*, *5*, 11. https://doi.org/10.1186/1744-9081-5-11

Villa, K. L., & Nedivi, E. (2016). Excitatory and Inhibitory Synaptic Placement and Functional Implications. In K. Emoto, R. Wong, E. Huang, & C. Hoogenraad (Eds.), *Dendrites: Development and Disease* (pp. 467–487). Springer Japan. https://doi.org/10.1007/978-4-431-56050-0_18

Volk, L. J., Daly, C. A., & Huber, K. M. (2006). Differential roles for group 1 mGluR subtypes in induction and expression of chemically induced hippocampal long-term depression. *Journal of Neurophysiology*, *95*(4), 2427–2438. https://doi.org/10.1152/jn.00383.2005

von Bohlen Und Halbach, O. (2009). Structure and function of dendritic spines within the hippocampus. *Annals of Anatomy = Anatomischer Anzeiger: Official Organ of the Anatomische Gesellschaft*, *191*(6), 518–531. https://doi.org/10.1016/j.aanat.2009.08.006

Wang, C. S., Kavalali, E. T., & Monteggia, L. M. (2022). BDNF signaling in context: From synaptic regulation to psychiatric disorders. *Cell*, *185*(1), 62–76. https://doi.org/10.1016/j.cell.2021.12.003

Wang, L., Wang, B., Wu, C., Wang, J., & Sun, M. (2023). Autism Spectrum Disorder: Neurodevelopmental Risk Factors, Biological Mechanism, and Precision Therapy. *International Journal of Molecular Sciences*, *24*(3), Article 3. https://doi.org/10.3390/ijms24031819

Wang, X., Lin, D., Jiang, J., Liu, Y., Dong, X., Fan, J., Gong, L., Shen, W., Zeng, L., Xu, T., Jiang, K., Connor, S. A., & Xie, Y. (2024). MDGA2 Constrains Glutamatergic Inputs Selectively onto CA1 Pyramidal Neurons to Optimize Neural Circuits for Plasticity, Memory, and Social Behavior. *Neuroscience Bulletin*. https://doi.org/10.1007/s12264-023-01171-1

Wang, X., McCoy, P. A., Rodriguiz, R. M., Pan, Y., Je, H. S., Roberts, A. C., Kim, C. J., Berrios, J., Colvin, J. S., Bousquet-Moore, D., Lorenzo, I., Wu, G., Weinberg, R. J., Ehlers, M. D., Philpot, B. D., Beaudet, A. L., Wetsel, W. C., & Jiang, Y.-H. (2011). Synaptic dysfunction and abnormal behaviors in mice lacking major isoforms of Shank3. *Human Molecular Genetics*, *20*(15), 3093–3108. https://doi.org/10.1093/hmg/ddr212

Wang, Y., Zheng, F., Zhou, X., Sun, Z., & Wang, H. (2009). Converging signal on ERK1/2 activity regulates group I mGluR-mediated Arc transcription. *Neuroscience Letters*, *460*(1), 36–40. https://doi.org/10.1016/j.neulet.2009.05.023

Watson, D. J., Ostroff, L., Cao, G., Parker, P. H., Smith, H., & Harris, K. M. (2016). LTP enhances synaptogenesis in the developing hippocampus. *Hippocampus*, *26*(5), 560–576. https://doi.org/10.1002/hipo.22536

Wright, G. J., & Washbourne, P. (2011). Neurexins, Neuroligins and LRRTMs: Synaptic adhesion getting fishy. *Journal of Neurochemistry*, *117*(5), 765–778. https://doi.org/10.1111/j.1471-4159.2010.07141.x

Yang, S.-N., Tang, Y.-G., & Zucker, R. S. (1999). Selective Induction of LTP and LTD by Postsynaptic [Ca2+]i Elevation. *Journal of Neurophysiology*, *81*(2), 781–787. https://doi.org/10.1152/jn.1999.81.2.781

Yang, Y., Sakimoto, Y., & Mitsushima, D. (2024). Postnatal Development of Synaptic Plasticity at Hippocampal CA1 Synapses: Correlation of Learning Performance with Pathway-Specific Plasticity. *Brain Sciences*, *14*(4), 382. https://doi.org/10.3390/brainsci14040382

Yang, Y., Wang, X., Frerking, M., & Zhou, Q. (2008). Spine Expansion and Stabilization Associated with Long-Term Potentiation. *The Journal of Neuroscience*, *28*(22), 5740–5751. https://doi.org/10.1523/JNEUROSCI.3998-07.2008

Yu, Z., Guindani, M., Grieco, S. F., Chen, L., Holmes, T. C., & Xu, X. (2022). Beyond t-Test and ANOVA: Applications of mixed-effects models for more rigorous statistical analysis in neuroscience research. *Neuron*, *110*(1), 21–35. https://doi.org/10.1016/j.neuron.2021.10.030

Yuste, R., & Denk, W. (1995). Dendritic spines as basic functional units of neuronal integration. *Nature*, *375*(6533), 682–684. https://doi.org/10.1038/375682a0

Zeidan, J., Fombonne, E., Scorah, J., Ibrahim, A., Durkin, M. S., Saxena, S., Yusuf, A., Shih, A., & Elsabbagh, M. (2022). Global prevalence of autism: A systematic review update. *Autism Research*, *15*(5), 778–790. https://doi.org/10.1002/aur.2696

Zhang, Y., Venkitaramani, D. V., Gladding, C. M., Zhang, Y., Kurup, P., Molnar, E., Collingridge, G. L., & Lombroso, P. J. (2008). The Tyrosine Phosphatase STEP Mediates AMPA Receptor Endocytosis after Metabotropic Glutamate Receptor Stimulation. *The Journal of Neuroscience*, *28*(42), 10561–10566. https://doi.org/10.1523/JNEUROSCI.2666-08.2008

Zhang, Z. (2023). Generation of epitope tag knock-in mice with CRISPR-Cas9 to study the function of endogenous proteins. *STAR Protocols*, *4*(3), 102518. https://doi.org/10.1016/j.xpro.2023.102518

Zhao, D., Huo, Y., Zheng, N., Zhu, X., Yang, D., Zhou, Y., Wang, S., Jiang, Y., Wu, Y., & Zhang, Y.-W. (2025). Mdga2 deficiency leads to an aberrant activation of BDNF/TrkB signaling that underlies autism-relevant synaptic and behavioral changes in mice. *PLoS Biology*, *23*(4), e3003047. https://doi.org/10.1371/journal.pbio.3003047

Zhao, X., Rosenke, R., Kronemann, D., Brim, B., Das, S. R., Dunah, A. W., & Magnusson, K. R. (2009). The Effects of Aging on NMDA Receptor Subunits in the Synaptic Membrane and Relationships to Long-term Spatial Memory. *Neuroscience*, *162*(4), 933–945. https://doi.org/10.1016/j.neuroscience.2009.05.018

Zhong, Q., Xiao, X., Qiu, Y., Xu, Z., Chen, C., Chong, B., Zhao, X., Hai, S., Li, S., An, Z., & Dai, L. (2023). Protein posttranslational modifications in health and diseases: Functions, regulatory mechanisms, and therapeutic implications. *MedComm*, *4*(3), e261. https://doi.org/10.1002/mco2.261

Zhou, Q., Homma, K. J., & Poo, M. (2004). Shrinkage of dendritic spines associated with long-term depression of hippocampal synapses. *Neuron*, *44*(5), 749–757. https://doi.org/10.1016/j.neuron.2004.11.011

Zhu, Y., Gao, H., Tong, L., Li, Z., Wang, L., Zhang, C., Yang, Q., & Yan, B. (2019). Emotion Regulation of Hippocampus Using Real-Time fMRI Neurofeedback in Healthy Human. *Frontiers in Human Neuroscience*, *13*. https://doi.org/10.3389/fnhum.2019.00242

Zito, K., Scheuss, V., Knott, G., Hill, T., & Svoboda, K. (2009). Rapid functional maturation of nascent dendritic spines. *Neuron*, *61*(2), 247–258. https://doi.org/10.1016/j.neuron.2008.10.054

Ziv, N. E., & Smith, S. J. (1996). Evidence for a role of dendritic filopodia in synaptogenesis and spine formation. *Neuron*, *17*(1), 91–102. https://doi.org/10.1016/s0896-6273(00)80283-4

Appendices

Appendix A. Full statistical analysis of the last 10 minutes of NMDAR-dependent LTD using a linear mixed effect model.

Table A1. Variance components attributed to random effects (SliceID) and residual error.

Random effects:		
Groups	Variance	Std.Dev.
SliceID	125.92	11.221
Residual	12.66	3.558

Table A2. Statistical breakdown of the fixed effects from the reference genotype (WT) and region (Dorsal).

Fixed effects:					
	Estimate	Std. Error	df	t value	Pr(>|t|)
(Intercept)	73.3217	4.0356	29.3831	18.169	<2e-16***
GenotypeHET	11.1381	5.7072	29.3831	1.952	0.0606
RegionVentral	-4.8212	5.7072	29.3831	-0.845	0.4051
Time	-0.2531	0.1385	284	-1.828	0.0687
GenotypeHET:RegionVentral	1.4994	8.0712	29.3831	0.186	0.8539
GenotypeHET:Time	0.3832	0.1959	284	1.957	0.0514
RegionVentral:Time	0.2625	0.1959	284	1.34	0.1813
GenotypeHET:RegionVentral:Time	-0.2242	0.277	284	-0.809	0.4189

Table A3. Correlation of fixed effects.

	(Intr)	GntHET	RgnVnt	Time	GnHET:RV	GHET:T	RgnV:T

GenotypeHET	-0.707						
RegionVntrl	-0.707	0.5					
Time	-0.154	0.109	0.109				
GntypHET:RV	0.5	-0.707	-0.707	-0.077			
GntypHET:Tm	0.109	-0.154	-0.077	-0.707	0.109		
RgnVntrl:Tm	0.109	-0.077	-0.154	-0.707	0.109	0.5	
GntHET:RV:T	-0.077	0.109	0.109	0.5	-0.154	-0.707	-0.707

Table A4. Full type III analysis of variance table with Satterthwaite's method.

	Sum Sq	Mean Sq	NumDF	DenDF	F value	Pr(>F)
Genotype	109.846	109.846	1	29.383	8.6772	0.006247**
Region	12.885	12.885	1	29.383	1.0179	0.321265
Time	0.495	0.495	1	284	0.0391	0.843398
Genotype:Region	0.437	0.437	1	29.383	0.0345	0.853902
Genotype:Time	48.52	48.52	1	284	3.8328	0.051237
Region:Time	14.922	14.922	1	284	1.1788	0.278523
Genotype:Region:Time	8.294	8.294	1	284	0.6552	0.418933

Table A5. Summary of post-hoc testing using Sidak's method.

contrast	estimate	SE	df	t.ratio	p.value
WT-Dorsal vs HET-Dorsal	12.9	5.64	28	2.281	0.0598
WT-Ventral vs HET-Ventral	13.4	5.64	28	2.368	0.0494*

Table A6. Summary of scaled residuals in the LMM.

Min	1Q	Median	3Q	Max
-3.1852	-0.5305	0.0719	0.5501	2.9389

Appendix B. Full statistical analysis of the last 10 minutes of mGluR-dependent LTD using a linear mixed effect model.

Table B1. Variance components attributed to random effects (SliceID) and residual error.

Random effects:		
Groups	Variance	Std.Dev.
SliceID	66.54	8.157
Residual	24.35	4.935

Table B2. Statistical breakdown of the fixed effects from the reference genotype (WT) and region (Dorsal).

Fixed effects:					
	Estimate	Std. Error	df	t value	Pr(>|t|)
(Intercept)	76.7290	3.0608	33.0385	25.068	< 2e-16 ***
GenotypeHET	-4.1676	4.3287	33.0385	-0.963	0.34265
RegionVentral	-12.8015	4.3287	33.0385	-2.957	0.00569 **
Time	0.1763	0.1921	284.0000	0.918	0.35960
GenotypeHET:RegionVentral	6.3519	6.1217	33.0385	1.038	0.30699
GenotypeHET:Time	-0.2410	0.2716	284.0000	-0.887	0.37569
RegionVentral:Time	-0.2748	0.2716	284.0000	-1.012	0.31262
GenotypeHET:RegionVentral:Time	0.1949	0.3842	284.0000	0.507	0.61225

Table B3. Correlation of fixed effects.

	(Intr)	GntHET	RgnVnt	Time	GnHET:RV	GHET:T	RgnV:T
GenotypeHET	-0.707						
RegionVntrl	-0.707	0.500					
Time	-0.282	0.200	0.200				
GntypHET:RV	0.500	-0.707	-0.707	-0.141			
GntypHET:Tm	0.200	-0.282	-0.141	-0.707	0.200		
RgnVntrl:Tm	0.200	-0.141	-0.282	-0.707	0.200	0.500	
GntHET:RV:T	-0.141	0.200	0.200	0.500	-0.282	-0.707	-0.707

Table B4. Full type III analysis of variance table with Satterthwaite's method.

	Sum Sq	Mean Sq	NumDF	DenDF	F value	Pr(>F)
Genotype	2.556	2.556	1	33.038	0.1050	0.747989
Region	240.809	240.809	1	33.038	9.8895	0.003505 **
Time	2.858	2.858	1	284.000	0.1174	0.732136
Genotype:Region	26.216	26.216	1	33.038	1.0766	0.306988
Genotype:Time	13.600	13.600	1	284.000	0.5585	0.455475
Region:Time	20.749	20.749	1	284.000	0.8521	0.356740
Genotype:Region:Time	6.270	6.270	1	284.000	0.2575	0.612254

Table B5. Summary of post-hoc testing using Sidak's method.

contrast	estimate	SE	df	t.ratio	p.value
WT_Dorsal_vs_WT_Ventral	14.04	4.15	28	3.381	0.0043**

HET_Ventral_vs_HET_Dorsal	-6.81	4.15	28	-1.640	0.2119

Table B6. Summary of scaled residuals in the LMM.

Min	1Q	Median	3Q	Max
-3.2297	-0.4991	0.0139	0.5547	4.1038

Appendix C. Full gene ontology (GO) analysis output from the DAVID functional annotation tool for dorsal CA1 tissue collected from *Mdga2*$^{+/-}$ mice and WT littermates from P14-P42 using BP_FAT (filtered biological processes) with an EASE threshold of 0.05 and protein count threshold of 3.

Table C1. Biological processes GO terms associated with up-regulated proteins in *Mdga2*$^{+/-}$ dorsal CA1 synaptoneurosomes relative to WT littermates at P14.

Term	Count	%	PValue	List Total	Fold Enrichment
regulation of localization	12	32.43243	4.17E-04	35	3.320662
regulation of biological quality	12	32.43243	0.010876	35	2.215662
regulation of transport	10	27.02703	0.001589	35	3.389373
transmembrane transport	7	18.91892	0.011613	35	3.504006
monoatomic ion transport	7	18.91892	0.003852	35	4.415728
carbohydrate derivative metabolic process	6	16.21622	0.010819	35	4.279316
monoatomic cation transport	6	16.21622	0.007924	35	4.619025
regulation of secretion	6	16.21622	0.006894	35	4.777521
regulation of secretion by cell	6	16.21622	0.004501	35	5.28963
monoatomic ion transmembrane transport	5	13.51351	0.034696	35	3.900017
regulation of growth	5	13.51351	0.018491	35	4.742649
monoatomic cation transmembrane transport	5	13.51351	0.017875	35	4.791614
carbohydrate derivative biosynthetic process	5	13.51351	0.009056	35	5.864105
regulation of membrane potential	4	10.81081	0.047108	35	4.777521
synaptic signaling	4	10.81081	0.034662	35	5.403267
trans-synaptic signaling	4	10.81081	0.024212	35	6.217635
anterograde trans-synaptic signaling	4	10.81081	0.020764	35	6.596374
chemical synaptic transmission	4	10.81081	0.020764	35	6.596374
aerobic respiration	3	8.108108	0.049884	35	8.121786
regulation of exocytosis	3	8.108108	0.048043	35	8.29459
negative regulation of secretion	3	8.108108	0.047314	35	8.365788
negative regulation of secretion by cell	3	8.108108	0.039238	35	9.282041
proton transmembrane transport	3	8.108108	0.021384	35	12.9088

Table C2. Biological processes GO terms associated with down-regulated proteins in *Mdga2*$^{+/-}$

dorsal CA1 synaptoneurosomes relative to WT littermates at P14.

Term	Count	%	PValue	List Total	Fold Enrichment
establishment of protein localization	4	30.76923	0.025721	12	5.473165
intracellular transport	4	30.76923	0.021275	12	5.880786
intracellular protein transport	3	23.07692	0.027604	12	10.37454
regulation of mitotic cell cycle	3	23.07692	0.025487	12	10.82905
regulation of cell cycle phase transition	3	23.07692	0.020227	12	12.25269
regulation of mitotic cell cycle phase transition	3	23.07692	0.011916	12	16.19729
nuclear transport	3	23.07692	0.007881	12	20.08922

Table C3. Biological processes GO terms associated with proteins with increased phosphorylation levels in *Mdga2*$^{+/-}$ dorsal CA1 synaptoneurosomes relative to WT littermates at P14.

Term	Count	%	PValue	List Total	Fold Enrichment
macromolecule localization	6	30	0.031035	18	3.055354
cellular response to chemical stimulus	6	30	0.028689	18	3.118196
cellular localization	6	30	0.018106	18	3.504546
nitrogen compound transport	6	30	0.00544	18	4.685002
homeostatic process	5	25	0.037426	18	3.597349
monoatomic ion transport	4	20	0.039187	18	4.906365
monoatomic cation transport	4	20	0.023482	18	5.987625
cellular homeostasis	4	20	0.018256	18	6.58873
intracellular monoatomic ion homeostasis	3	15	0.048876	18	7.912665
intracellular monoatomic cation homeostasis	3	15	0.046878	18	8.098647
organic anion transport	3	15	0.039719	18	8.876269
regulation of metal ion transport	3	15	0.038543	18	9.024206
response to oxidative stress	3	15	0.037712	18	9.132932
regulation of developmental growth	3	15	0.036233	18	9.335386
negative regulation of organelle organization	3	15	0.030713	18	10.21608
nucleobase-containing compound transport	3	15	0.013375	18	15.92507

Table C4. Biological processes GO terms associated with down-regulated proteins in *Mdga2*$^{+/-}$ dorsal CA1 synaptoneurosomes relative to WT littermates at P21.

Term	Count	%	PValue	List Total	Fold Enrichment
regulation of biological quality	8	34.7826087	0.042697	23	2.247773
regulation of cellular component organization	7	30.43478261	0.042016	23	2.515876
cellular localization	7	30.43478261	0.014427	23	3.199803

nitrogen compound transport	7	30.43478261	0.003557	23	4.277611
positive regulation of signaling	6	26.08695652	0.048644	23	2.791734
intracellular protein localization	6	26.08695652	0.041432	23	2.916635
regulation of transport	6	26.08695652	0.033207	23	3.094645
establishment of localization in cell	6	26.08695652	0.026008	23	3.299463
macromolecule modification	6	26.08695652	0.011869	23	4.02199
response to endogenous stimulus	6	26.08695652	0.010671	23	4.128347
cell motility	6	26.08695652	0.007351	23	4.518229
protein modification process	6	26.08695652	0.007189	23	4.542446
response to nitrogen compound	5	21.73913043	0.02931	23	3.986851
cell migration	5	21.73913043	0.016835	23	4.721772
intracellular signaling cassette	4	17.39130435	0.048477	23	4.60414
membrane organization	4	17.39130435	0.040737	23	4.937524
cellular response to nitrogen compound	4	17.39130435	0.030881	23	5.508296
regulation of inflammatory response	4	17.39130435	0.008221	23	9.071001
taxis	3	13.04347826	0.046405	23	8.285523
chemotaxis	3	13.04347826	0.04594	23	8.332071
protein polyubiquitination	3	13.04347826	0.034921	23	9.693521
tissue homeostasis	3	13.04347826	0.025693	23	11.45258
anatomical structure homeostasis	3	13.04347826	0.025693	23	11.45258
cell chemotaxis	3	13.04347826	0.020262	23	13.00973

Table C5. Biological processes GO terms associated with proteins with reduced phosphorylation levels in *Mdga2*$^{+/-}$ dorsal CA1 synaptoneurosomes relative to WT littermates at P21.

Term	Count	%	PValue	List Total	Fold Enrichment
regulation of biological quality	5	50	0.0376	10	3.231174
monoatomic cation transport	3	30	0.04165	10	8.083294
monoatomic ion transmembrane transport	3	30	0.040663	10	8.190036
metal ion transport	3	30	0.02935	10	9.774069
monoatomic cation transmembrane transport	3	30	0.027805	10	10.06239

Table C6. Biological processes GO terms associated with up-regulated proteins in *Mdga2*$^{+/-}$ dorsal CA1 synaptoneurosomes relative to WT littermates at P28.

Term	Count	%	PValue	List Total	Fold Enrichment
RNA metabolic process	9	36	0.029906	24	2.215608
macromolecule catabolic process	6	24	0.0077	24	4.490719
regulation of catabolic process	5	20	0.02047	24	4.469536
regulation of mRNA metabolic process	4	16	0.004738	24	11.11486
regulation of RNA splicing	3	12	0.017736	24	14.00308
tRNA metabolic process	3	12	0.016922	24	14.35669
regulation of mRNA processing	3	12	0.010631	24	18.33952
tRNA processing	3	12	0.008627	24	20.45054
regulation of mRNA splicing, via spliceosome	3	12	0.007472	24	22.03585

Table C7. Biological processes GO terms associated with down-regulated proteins in *Mdga2*$^{+/-}$ dorsal CA1 synaptoneurosomes relative to WT littermates at P28.

Term	Count	%	PValue	List Total	Fold Enrichment
cell development	4	44.44444	0.047406	8	3.963228
regulation of cellular component biogenesis	3	33.33333	0.044566	8	7.480592
cell activation	3	33.33333	0.026664	8	9.870226
pattern specification process	3	33.33333	0.009235	8	17.22803

Table C8. Biological processes GO terms associated with proteins with decreased phosphorylation levels in *Mdga2*$^{+/-}$ dorsal CA1 synaptoneurosomes relative to WT littermates at P28.

Term	Count	%	PValue	List Total	Fold Enrichment
cell projection organization	4	50	0.003857	7	9.437079
plasma membrane bounded cell projection organization	4	50	0.003417	7	9.844589
positive regulation of cellular component organization	3	37.5	0.044891	7	7.230076

Table C9. Biological processes GO terms associated with up-regulated proteins in *Mdga2*$^{+/-}$ dorsal CA1 synaptoneurosomes relative to WT littermates at P42.

Term	Count	%	PValue	List Total	Fold Enrichment
protein metabolic process	14	33.33333	0.001881	38	2.467097514
organelle organization	11	26.19048	0.031533	38	2.0211609
regulation of localization	9	21.42857	0.032346	38	2.293878329
protein modification by small protein conjugation or removal	5	11.90476	0.043898	38	3.631355391
protein modification by small protein conjugation	5	11.90476	0.027661	38	4.208490636
protein ubiquitination	5	11.90476	0.02123	38	4.568300522
protein polyubiquitination	5	11.90476	0.001496	38	9.778551772

regulation of transmembrane transport	4	9.52381	0.037837	38	5.238051365
regulation of RNA stability	3	7.142857	0.046147	38	8.508730357
regulation of mRNA catabolic process	3	7.142857	0.045365	38	8.590153614
regulation of mRNA stability	3	7.142857	0.03675	38	9.65237691
protein K48-linked ubiquitination	3	7.142857	0.01431	38	16.02984023

Table C10. Biological processes GO terms associated with down-regulated proteins in *Mdga2*$^{+/-}$ dorsal CA1 synaptoneurosomes relative to WT littermates at P42.

Term	Count	%	PValue	List Total	Fold Enrichment
cellular localization	6	28.57143	0.035748866	21	3.003897
establishment of localization in cell	6	28.57143	0.017458737	21	3.613698
cell-cell signaling	5	23.80952	0.003554518	21	7.316924
regulation of trans-synaptic signaling	4	19.04762	0.029176485	21	5.589186
modulation of chemical synaptic transmission	4	19.04762	0.029079777	21	5.596407
synaptic signaling	4	19.04762	0.00820199	21	9.005445
trans-synaptic signaling	4	19.04762	0.005570837	21	10.36272
anterograde trans-synaptic signaling	4	19.04762	0.004726355	21	10.99396
chemical synaptic transmission	4	19.04762	0.004726355	21	10.99396
membrane docking	3	14.28571	0.002628527	21	37.34154
organelle localization by membrane tethering	3	14.28571	0.002014117	21	42.74624
vesicle docking	3	14.28571	0.001099856	21	58.01276

Table C11. Biological processes GO terms associated with proteins with increased phosphorylation levels in *Mdga2*$^{+/-}$ dorsal CA1 synaptoneurosomes relative to WT littermates at P42.

Term	Count	%	PValue	List Total	Fold Enrichment
monoatomic ion transport	5	14.70588235	0.044974	31	3.561071
regulation of cell projection organization	5	14.70588235	0.020975	31	4.528276
regulation of plasma membrane bounded cell projection organization	5	14.70588235	0.019647	31	4.619525
response to growth factor	4	11.76470588	0.042532	31	4.948267
regulation of neuron projection development	4	11.76470588	0.041294	31	5.007376
cellular response to growth factor stimulus	4	11.76470588	0.036528	31	5.258643
negative regulation of protein localization	3	8.823529412	0.045288	31	8.530008

Appendix D. Full gene ontology (GO) analyses output from the DAVID functional annotation tool for ventral CA1 tissue collected from *Mdga2*$^{+/-}$ mice and WT littermates from P14-P42 using BP_FAT (filtered biological processes) with an EASE threshold of 0.05 and protein count threshold of 3.

Table D1. Biological processes GO terms associated with up-regulated proteins in *Mdga2*$^{+/-}$ ventral CA1 synaptoneurosomes relative to WT littermates at P14.

Term	Count	%	PValue	List Total	Fold Enrichment
cellular component biogenesis	13	36.11111	0.009284022	34	2.131149
cellular component assembly	13	36.11111	0.00538442	34	2.278587
nervous system development	8	22.22222	0.048552564	34	2.27501
cellular response to stress	7	19.44444	0.038659467	34	2.661723
sexual reproduction	7	19.44444	0.022265129	34	3.026484
mitotic cell cycle process	6	16.66667	8.57E-04	34	7.717534
cell cycle	6	16.66667	0.020901995	34	3.615421
regulation of cell cycle	6	16.66667	0.020901995	34	3.615421
cell cycle process	6	16.66667	0.010324103	34	4.319825
cell morphogenesis	6	16.66667	0.006565178	34	4.823459
mitotic cell cycle	6	16.66667	0.001415317	34	6.895391
cell division	6	16.66667	0.001031751	34	7.404276
embryo development ending in birth or egg hatching	5	13.88889	0.042666928	34	3.64299
chordate embryonic development	5	13.88889	0.04013457	34	3.71585
regulation of cell cycle process	5	13.88889	0.025534144	34	4.287519
in utero embryonic development	5	13.88889	0.009647368	34	5.746159
plasma membrane bounded cell projection morphogenesis	4	11.11111	0.049034052	34	4.693705
neuron projection morphogenesis	4	11.11111	0.047776126	34	4.743638
cell morphogenesis involved in neuron differentiation	4	11.11111	0.038311608	34	5.184907
regulation of chromosome organization	3	8.333333	0.049762828	34	8.12372
mitotic nuclear division	3	8.333333	0.026034961	34	11.59861
protein K48-linked ubiquitination	3	8.333333	0.011490287	34	17.9157

Table D2. Biological processes GO terms associated with down-regulated proteins in *Mdga2*$^{+/-}$ ventral CA1 synaptoneurosomes relative to WT littermates at P14.

Term	Count	%	PValue	List Total	Fold Enrichment
protein metabolic process	25	29.41176	4.51E-04	81	2.066792
tissue development	14	16.47059	0.027784065	81	1.901569
phosphorus metabolic process	12	14.11765	0.005220209	81	2.621819
phosphate-containing compound metabolic process	12	14.11765	0.00513064	81	2.627954
embryo development	11	12.94118	0.016740941	81	2.348505
programmed cell death	10	11.76471	0.019550386	81	2.43921
cell death	10	11.76471	0.019550386	81	2.43921
apoptotic process	9	10.58824	0.038460446	81	2.30756
regulation of cell development	9	10.58824	0.023447951	81	2.54203
embryonic organ development	8	9.411765	0.00374258	81	3.975265
tissue morphogenesis	7	8.235294	0.038060644	81	2.783671
mitotic cell cycle	7	8.235294	0.016686328	81	3.376755
response to xenobiotic stimulus	6	7.058824	0.035650753	81	3.258256
regulation of hemopoiesis	6	7.058824	0.025055524	81	3.584082
regulation of leukocyte differentiation	5	5.882353	0.044368268	81	3.713665
cytoplasmic translation	4	4.705882	0.031515374	81	5.759038
negative regulation of myeloid cell differentiation	3	3.529412	0.045055184	81	8.773534
ERAD pathway	3	3.529412	0.043381162	81	8.960205
cardiac septum morphogenesis	3	3.529412	0.038505259	81	9.571128
lung alveolus development	3	3.529412	0.025968002	81	11.86281
peptidyl-tyrosine modification	3	3.529412	0.007515233	81	22.76376
peptidyl-tyrosine phosphorylation	3	3.529412	0.007125156	81	23.39609
embryonic hemopoiesis	3	3.529412	0.004987262	81	28.07531

Table D3. Biological processes GO terms associated with proteins with increased

phosphorylation levels in *Mdga2*$^{+/-}$ ventral CA1 synaptoneurosomes relative to WT littermates at P14.

Term	Count	%	PValue	List Total	Fold Enrichment
regulation of RNA metabolic process	10	29.41176	0.045725	30	1.963308
negative regulation of macromolecule metabolic process	9	26.47059	0.036487	30	2.193666
negative regulation of biosynthetic process	9	26.47059	0.022706	30	2.396312
negative regulation of macromolecule biosynthetic process	9	26.47059	0.018971	30	2.475435
regulation of transcription by RNA polymerase II	8	23.52941	0.044368	30	2.295332
negative regulation of nucleobase-containing compound metabolic process	8	23.52941	0.004643	30	3.569315
negative regulation of RNA metabolic process	8	23.52941	0.002968	30	3.867517
negative regulation of RNA biosynthetic process	8	23.52941	0.001886	30	4.188029
negative regulation of DNA-templated transcription	8	23.52941	0.001857	30	4.199631
negative regulation of transcription by RNA polymerase II	6	17.64706	0.009129	30	4.407171
chromatin organization	5	14.70588	0.026726	30	4.192662
cellular process involved in reproduction in multicellular organism	4	11.76471	0.044822	30	4.835938
germ cell development	4	11.76471	0.038519	30	5.139209
spermatid differentiation	4	11.76471	0.013234	30	7.754817
spermatid development	4	11.76471	0.012173	30	8.000352

Table D4. Biological processes GO terms associated with proteins with reduced phosphorylation levels in *Mdga2*$^{+/-}$ ventral CA1 synaptoneurosomes relative to WT littermates at P14.

Term	Count	%	PValue	List Total	Fold Enrichment
regulation of cell communication	12	36.36363636	0.010992	32	2.186074
regulation of signaling	12	36.36363636	0.010908	32	2.188318
organelle organization	11	33.33333333	0.008955	32	2.400129
regulation of signal transduction	10	30.3030303	0.025914	32	2.182605
macromolecule localization	9	27.27272727	0.015727	32	2.577955
intracellular protein localization	9	27.27272727	0.004901	32	3.144497
regulation of protein localization	7	21.21212121	0.002798	32	4.67098
protein localization to organelle	5	15.15151515	0.021593	32	4.497824
localization within membrane	4	12.12121212	0.049137	32	4.67537
negative regulation of DNA metabolic process	3	9.090909091	0.01536	32	15.3379
protein-containing complex localization	3	9.090909091	0.008035	32	21.53504

Table D5. Biological processes GO terms associated with up-regulated proteins in *Mdga2*$^{+/-}$ ventral CA1 synaptoneurosomes relative to WT littermates at P21.

Term	Count	%	PValue	List Total	Fold Enrichment
response to stress	11	30.55556	0.032975	33	1.978166
protein metabolic process	10	27.77778	0.040169	33	2.029214
regulation of cellular component organization	9	25	0.033215	33	2.254486
positive regulation of RNA metabolic process	8	22.22222	0.016441	33	2.840273
positive regulation of RNA biosynthetic process	8	22.22222	0.011155	33	3.062761
positive regulation of DNA-templated transcription	8	22.22222	0.01109	33	3.066168
cellular response to stress	7	19.44444	0.033763	33	2.742381
negative regulation of cell communication	7	19.44444	0.02537	33	2.930649
protein modification process	6	16.66667	0.034293	33	3.165947
regulation of organelle organization	6	16.66667	0.029463	33	3.297231
post-translational protein modification	5	13.88889	0.033051	33	3.946857
protein modification by small protein conjugation or removal	5	13.88889	0.027507	33	4.181561
DNA damage response	5	13.88889	0.026975	33	4.207089
negative regulation of cell population proliferation	5	13.88889	0.020906	33	4.551659
protein modification by small protein conjugation	5	13.88889	0.01701	33	4.846141
protein ubiquitination	5	13.88889	0.012933	33	5.260467
proteasomal protein catabolic process	4	11.11111	0.046781	33	4.77727
DNA repair	4	11.11111	0.037515	33	5.220615
proteasome-mediated ubiquitin-dependent protein catabolic process	4	11.11111	0.030101	33	5.695217
chromosome organization	4	11.11111	0.0254	33	6.084956
bone development	3	8.333333	0.043378	33	8.760015
DNA replication	3	8.333333	0.034199	33	9.987264
glycerolipid biosynthetic process	3	8.333333	0.030657	33	10.60186

Table D6. Biological processes GO terms associated with down-regulated proteins in *Mdga2*$^{+/-}$ ventral CA1 synaptoneurosomes relative to WT littermates at P21.

Term	Count	%	PValue	List Total	Fold Enrichment
cellular component biogenesis	16	32.65306	0.009556	46	1.938704
cellular component assembly	15	30.61224	0.012938	46	1.943277
regulation of biological quality	15	30.61224	0.006375	46	2.107287
organelle organization	15	30.61224	0.003133	46	2.276802
positive regulation of response to stimulus	11	22.44898	0.025302	46	2.128401
cellular localization	10	20.40816	0.023924	46	2.285574
tissue development	10	20.40816	0.018325	46	2.391725

establishment of localization in cell	9	18.36735	0.023335	46	2.474597
homeostatic process	9	18.36735	0.020551	46	2.533785
nitrogen compound transport	9	18.36735	0.013089	46	2.749893
positive regulation of gene expression	8	16.32653	0.021098	46	2.771518
vesicle-mediated transport	8	16.32653	0.016506	46	2.912339
programmed cell death	8	16.32653	0.007028	46	3.436105
cell death	8	16.32653	0.007028	46	3.436105
plasma membrane bounded cell projection organization	7	14.28571	0.044481	46	2.621657
intracellular transport	7	14.28571	0.040355	46	2.684707
apoptotic process	7	14.28571	0.020129	46	3.160353
chemical homeostasis	7	14.28571	0.016498	46	3.305241
positive regulation of response to external stimulus	6	12.2449	0.011046	46	4.330244
cell junction organization	6	12.2449	0.00855	46	4.613091
regulation of response to biotic stimulus	5	10.20408	0.039883	46	3.779584
regulation of establishment of protein localization	5	10.20408	0.038764	46	3.81458
positive regulation of defense response	5	10.20408	0.022536	46	4.527194
cell morphogenesis involved in neuron differentiation	5	10.20408	0.018746	46	4.790403
synapse organization	5	10.20408	0.009639	46	5.843612
positive regulation of response to biotic stimulus	5	10.20408	0.009408	46	5.885352
regulation of synapse organization	4	8.163265	0.049885	46	4.719519
cognition	4	8.163265	0.049016	46	4.753554
regulation of synaptic plasticity	4	8.163265	0.044513	46	4.943696
establishment of protein localization to organelle	4	8.163265	0.03997	46	5.163129
positive regulation of innate immune response	4	8.163265	0.03997	46	5.163129
learning or memory	4	8.163265	0.036666	46	5.344536
sensory organ morphogenesis	4	8.163265	0.030957	46	5.715255
rhythmic process	4	8.163265	0.027435	46	5.992358
alcohol metabolic process	4	8.163265	0.026174	46	6.103328
ear development	4	8.163265	0.019635	46	6.818891
circadian rhythm	3	6.122449	0.049893	46	8.193971
establishment of vesicle localization	3	6.122449	0.047942	46	8.379145
ear morphogenesis	3	6.122449	0.040435	46	9.211855
regulation of type I interferon production	3	6.122449	0.035132	46	9.95375
positive regulation of type I interferon production	3	6.122449	0.019371	46	13.73249
nerve development	3	6.122449	0.019036	46	13.86083
mechanoreceptor differentiation	3	6.122449	0.016135	46	15.13376
regulation of neuronal synaptic plasticity	3	6.122449	0.01071	46	18.77353
neuromuscular junction development	3	6.122449	0.005132	46	27.46498

Table D7. Biological processes GO terms associated with proteins with increased phosphorylation levels in *Mdga2*$^{+/-}$ ventral CA1 synaptoneurosomes relative to WT littermates at P21.

Term	Count	%	PValue	List Total	Fold Enrichment
regulation of localization	10	32.25806	0.00109	28	3.459023
regulation of transport	8	25.80645	0.005892	28	3.389373
regulation of protein localization	7	22.58065	0.00132	28	5.338263
chemical homeostasis	6	19.35484	0.007101	28	4.654318
monoatomic ion transport	5	16.12903	0.032015	28	3.942614
monoatomic cation transport	5	16.12903	0.016753	28	4.811484
cellular homeostasis	5	16.12903	0.012152	28	5.294515
metal ion transport	5	16.12903	0.008806	28	5.817898
regulation of cellular localization	5	16.12903	0.007217	28	6.162205
regulation of establishment of protein localization	5	16.12903	0.006807	28	6.26681
regulation of protein transport	5	16.12903	0.004255	28	7.162069
positive regulation of protein localization	5	16.12903	0.0033	28	7.691085
regulation of cell activation	4	12.90323	0.048948	28	4.64766
monoatomic cation transmembrane transport	4	12.90323	0.045398	28	4.791614
regulation of system process	4	12.90323	0.045067	28	4.80579
intracellular chemical homeostasis	4	12.90323	0.040252	28	5.028969
regulation of leukocyte activation	4	12.90323	0.039786	28	5.052433
microtubule cytoskeleton organization	4	12.90323	0.035137	28	5.308357
monoatomic ion homeostasis	4	12.90323	0.029853	28	5.659781
inorganic ion homeostasis	4	12.90323	0.019394	28	6.684597
intracellular monoatomic ion homeostasis	4	12.90323	0.018669	28	6.782285
positive regulation of establishment of protein localization	4	12.90323	0.009773	28	8.640198
positive regulation of protein transport	4	12.90323	0.006673	28	9.934906
regulation of peptide transport	3	9.677419	0.047868	28	8.23154
regulation of peptide secretion	3	9.677419	0.04729	28	8.287536
regulation of peptide hormone secretion	3	9.677419	0.045857	28	8.430919
regulation of blood circulation	3	9.677419	0.045289	28	8.489671
regulation of insulin secretion	3	9.677419	0.033998	28	9.945044
regulation of carbohydrate metabolic process	3	9.677419	0.029798	28	10.68656
regulation of carbohydrate biosynthetic process	3	9.677419	0.0113	28	17.9157

Table D8. Biological processes GO terms associated with up-regulated proteins in *Mdga2*$^{+/-}$ ventral CA1 synaptoneurosomes relative to WT littermates at P28.

Term	Count	%	PValue	List Total	Fold Enrichment
cell development	10	47.61905	1.33E-04	19	4.171819
cell projection organization	5	23.80952	0.020689	19	4.346023

plasma membrane bounded cell projection organization	5	23.80952	0.017974	19	4.533692
neuron development	4	19.04762	0.045706	19	4.639127
hemopoiesis	4	19.04762	0.029738	19	5.496646
cell morphogenesis	4	19.04762	0.02642	19	5.754302
neuron projection development	4	19.04762	0.026174	19	5.775125
cell morphogenesis involved in neuron differentiation	4	19.04762	0.007353	19	9.278254
hematopoietic progenitor cell differentiation	3	14.28571	0.00699	19	22.44178

Table D9. Biological processes GO terms associated with up-regulated proteins in *Mdga2*$^{+/-}$ ventral CA1 synaptoneurosomes relative to WT littermates at P42.

Term	Count	%	PValue	List Total	Fold Enrichment
regulation of cell communication	9	60	8.36E-04	15	3.497719
regulation of signaling	9	60	8.30E-04	15	3.501309
protein metabolic process	7	46.66667	0.011257	15	3.12499
regulation of localization	7	46.66667	0.001736	15	4.51979
negative regulation of metabolic process	6	40	0.043897	15	2.710489
positive regulation of macromolecule metabolic process	6	40	0.043848	15	2.711297
regulation of signal transduction	6	40	0.039118	15	2.793735
negative regulation of macromolecule metabolic process	6	40	0.032771	15	2.924887
macromolecule modification	5	33.33333	0.010432	15	5.139209
protein modification process	5	33.33333	0.006813	15	5.804237
regulation of protein metabolic process	4	26.66667	0.049451	15	4.381696
regulation of organelle organization	4	26.66667	0.038572	15	4.835938
regulation of cellular component biogenesis	4	26.66667	0.030209	15	5.319532
regulation of protein localization	4	26.66667	0.025312	15	5.694147
post-translational protein modification	4	26.66667	0.014948	15	6.946468
cell projection morphogenesis	3	20	0.048404	15	7.828227
plasma membrane bounded cell projection morphogenesis	3	20	0.046766	15	7.979298
regulation of cytoskeleton organization	3	20	0.046619	15	7.993322
negative regulation of protein metabolic process	3	20	0.046029	15	8.049912
neuron projection morphogenesis	3	20	0.045882	15	8.064184
cell morphogenesis involved in neuron differentiation	3	20	0.039048	15	8.814341

Table D10. Biological processes GO terms associated with down-regulated proteins in *Mdga2*$^{+/-}$ ventral CA1 synaptoneurosomes relative to WT littermates at P42.

Term	Count	%	PValue	List Total	Fold Enrichment
organelle organization	11	50	2.77E-04	22	3.491096

regulation of cellular component organization	9	40.90909	0.002148	22	3.381729
negative regulation of cellular component organization	6	27.27273	6.43E-04	22	7.840823
regulation of organelle organization	6	27.27273	0.004904	22	4.945846
cell projection organization	5	22.72727	0.035059	22	3.753384
plasma membrane bounded cell projection organization	5	22.72727	0.030636	22	3.915461
cytoskeleton organization	5	22.72727	0.028954	22	3.984895
regulation of cell projection organization	4	18.18182	0.037135	22	5.104602
regulation of plasma membrane bounded cell projection organization	4	18.18182	0.035306	22	5.207465
regulation of neuron projection development	4	18.18182	0.016027	22	7.055849
negative regulation of organelle organization	3	13.63636	0.04545	22	8.358613
taxis	3	13.63636	0.04262	22	8.662138
chemotaxis	3	13.63636	0.042191	22	8.710802

Table D11. Biological processes GO terms associated with proteins with increased phosphorylation levels in *Mdga2*$^{+/-}$ ventral CA1 synaptoneurosomes relative to WT littermates at P42.

Term	Count	%	PValue	List Total	Fold Enrichment
cellular response to stress	4	28.57143	0.047642	12	4.309456
embryonic organ development	3	21.42857	0.029213	12	10.06239
DNA repair	3	21.42857	0.025759	12	10.76752
DNA recombination	3	21.42857	0.007095	12	21.21362
double-strand break repair	3	21.42857	0.005142	12	25.04515

Table D12. Biological processes GO terms associated with proteins with reduced phosphorylation levels in *Mdga2*$^{+/-}$ ventral CA1 synaptoneurosomes relative to WT littermates at P42.

Term	Count	%	PValue	List Total	Fold Enrichment
multicellular organismal reproductive process	4	28.57143	0.046361	14	4.456398
negative regulation of RNA biosynthetic process	4	28.57143	0.045565	14	4.487174
negative regulation of DNA-templated transcription	4	28.57143	0.045249	14	4.499604
developmental process involved in reproduction	4	28.57143	0.037864	14	4.827213
gamete generation	4	28.57143	0.03282	14	5.104029
male gamete generation	4	28.57143	0.011676	14	7.53762
spermatogenesis	4	28.57143	0.010883	14	7.735034
cellular process involved in reproduction in multicellular organism	4	28.57143	0.004852	14	10.36272
germ cell development	4	28.57143	0.004092	14	11.01259
spermatid differentiation	4	28.57143	0.001269	14	16.61746

spermatid development	4	28.57143	0.00116	14	17.14361